The PHILOSOPHICAL MAGAZINE

FIRST PUBLISHED IN 1798

. 43 SEVENTH SERIES No. 343 August, 1952

A Journal of Theoretical Experimental and Applied Physics

PRICE 15s. 0d.
Annual Subscription £8 0s. 0d. payable in advance

AND PUBLISHED BY TAYLOR & FRANCIS LTD., RED LION COURT, FLEET ST., LONDON, E.C.4.

ADVANCES IN PHYSICS

A QUARTERLY SUPPLEMENT OF THE PHILOSOPHICAL MAGAZINE

On 1st January, 1952, the first number of this new Quarterly Supplement to the Philosophical Magazine was published. The aim of this Supplement will be to give those interested in physics comprehensive and authoritative accounts of recent important developments. It is felt by the Editor that in view of the rapid advances in many branches of physics, scientists will welcome a journal devoted to articles of this type.

VOLUME 1 OCTOBER 1952 NUMBER 4

PRICE *per part* 15/- *plus postage* **PRICE** *per annum* £2 15s. 0d. *post free*

Printed and Published by
TAYLOR & FRANCIS, LTD., RED LION COURT, FLEET ST., LONDON, E.C.4

LXXVIII. *Simultaneous Diffusion and Reversible Chemical Reaction*

By J. Crank
Courtaulds Limited, Maidenhead, Berks.*

[Received March 21, 1952]

Abstract

The problem considered is one of diffusion in which some of the diffusing substance is immobilized by chemical reaction as diffusion proceeds. The reaction is considered to be first order and reversible, the forward reaction proceeding at a rate proportional to the concentration of solute free to diffuse, and the backward reaction at a rate proportional to the concentration of immobilized solute. Mathematical solutions are derived for the diffusion of a limited amount of solute into a plane sheet, a cylinder, and a sphere respectively. The solutions comprise two infinite series and the physical significance of the various terms is discussed briefly. Solutions involve three independent parameters ; these are the ratio of the volumes occupied by solution and sheet, cylinder or sphere respectively, the partition factor between immobilized and free solute in the final equilibrium state, and a modified rate constant expressing the relative rates of diffusion and reaction. Calculated values of M_t/M_∞, where M_t is the total amount of solute present in the sheet, cylinder or sphere at time t and M_∞ the corresponding quantity after infinite time, are tabulated for the case of an infinite amount of solute and for a range of values of the other two parameters. Characteristic features of diffusion-with-reaction are shown graphically. An important general conclusion is that if the diffusion is more than a thousand times faster than the reaction, expressed in terms of the respective half-times of the two processes, the behaviour of the joint diffusion-reaction process is almost the same as if diffusion were infinitely rapid. If on the other hand the half-times for diffusion and reaction are comparable the behaviour approximates to that for an infinitely rapid reaction. It is shown that the mathematical solutions derived for absorption also describe the course of desorption under comparable conditions. Solutions for an irreversible reaction are deduced as special cases of those for a reversible reaction.

§1. Introduction

The problem to be discussed is that of the absorption of one substance by another through which it can diffuse and with which it can also react chemically. This can be regarded as a problem in diffusion, in which some

* Communicated by the Author.

of the diffusing substance becomes immobilized as diffusion proceeds, or as a problem in chemical kinetics in which the rate of reaction depends on the rate of supply of one of the reactants by diffusion. There are numerous practical examples of processes involving simultaneous diffusion and chemical reaction of one sort or another. Thus diffusion may take place within the pores of a solid body which can absorb some of the diffusing substance ; or we may have diffusion occurring through a gel and an immobile product resulting from the attraction of the diffusing molecules to fixed sites within the medium. This occurs, for example, when substantive dye molecules diffuse into water-swollen cellulose. Similar processes may be involved in the swelling of a high polymer substance by a solvent. In other cases, the diffusing substance may be immobilized by the formation of a new compound between itself and the medium. Examples involving diffusion into living cells and micro-organisms can be cited from biology and biochemistry. One example from physiology which has been considered in detail recently by Nicolson and Roughton (1951) is the uptake of oxygen by red blood corpuscles. Chemical reactions in high polymer substances are often considerably dependent on the mobility of the reactants as well as on the kinetics of the reaction itself.

It this paper we confine attention to cases in which the process by which the diffusing substance is immobilized is first order and reversible. This appears to be the most general case for which formal mathematical solutions can be obtained at the present time. Although of course in practice not all processes will be strictly first order, nevertheless it is thought that the number for which it will be a useful approximation is large enough to justify extensive mathematical treatment. Subject to this condition the treatment is quite general, irrespective of the precise nature and mechanism of the diffusion or of the formation of immobilized product. The aim of this paper is not to examine any one practical example in detail. It is rather to establish quantitatively the characteristic features of the diffusion-with-reaction system, and to provide theoretical curves which the experimentalist can use in attempting to assess his practical measurements.

The behaviour to be expected when the reaction is reversible clearly depends on the relative rates of diffusion and reaction. Several authors (Hill 1929 ; Wilson 1948 ; Crank 1948) have discussed problems in which the product is formed so rapidly compared with the diffusion that it is always effectively in equilibrium with the diffusing substance. At the other extreme is the case of diffusion being so rapid compared with the reaction that the concentrations of diffusing substance and product are effectively uniform throughout the medium and the behaviour is controlled solely by the reversible reaction. So far as is known only one mathematical solution has been obtained (Wilson 1948) for the more general case in which the rates of diffusion and reaction are comparable. In attempting to evaluate Wilson's series solution numerically some interesting features concerning its physical significance, and also some unexpected difficulties in evaluation emerged, and this led to the problem being taken up anew.

§2. Statement of the Problem

The general problem considered in this paper can conveniently be stated in terms of a solute diffusing from a solution into a plane sheet of material. The modifications necessary for corresponding, alternative problems, such as those of a sphere or cylinder suspended in a vapour, will be obvious.

Suppose an infinite sheet of uniform material of thickness $2a$ is placed in a solution and that the solute is allowed to diffuse into the sheet. As diffusion proceeds, a first order, reversible reaction occurs and a product, which is non-diffusing, is formed. The sheet occupies the space $-a \leqslant x \leqslant a$, and there is a restricted amount of solution which occupies the space $-l-a \leqslant x \leqslant -a$, $a \leqslant x \leqslant l+a$. The concentration of solute in the solution is always uniform and is initially C_0, while initially the sheet is free from solute. Let c be the concentration of solute free to diffuse within the sheet and s that of the immobilized solute, each being expressed as amount per unit volume of sheet.

The diffusion is governed by the equation

$$\frac{\partial c}{\partial t} = D\frac{\partial^2 c}{\partial x^2} - \frac{\partial s}{\partial t}, \quad . \quad . \quad . \quad . \quad . \quad . \quad . \quad . \quad (2.1)$$

and we consider the simultaneous reaction to be of the type

$$\partial s/\partial t = \lambda c - \mu s. \quad . \quad . \quad . \quad . \quad . \quad . \quad . \quad . \quad (2.2)$$

Here D is the diffusion coefficient and λ and μ are the rate constants of the forward and backward reactions respectively. Thus the immobilized solute is formed at a rate proportional to the concentration of solute free to diffuse, and disappears at a rate proportional to its own concentration. We require solutions of (2.1) and (2.2) with the initial condition

$$s = c = 0, \quad -a < x < a, \quad t = 0, \quad . \quad . \quad . \quad . \quad . \quad . \quad . \quad (2.3)$$

and with a boundary condition expressing the fact that the rate at which solute leaves the solution is equal to that at which it enters the sheet over the surfaces $x = \pm a$. This condition is

$$l\partial c/\partial t = -D\partial c/\partial x, \quad x = \pm a, \quad t > 0. \quad . \quad . \quad . \quad . \quad . \quad . \quad (2.4)$$

We here assume that the concentration of solute free to diffuse just within the surface of the sheet is the same as that in the solution. This may not be so and there may be a distribution factor K, which is not unity, such that the concentration just within the sheet is K times that in the solution. This can clearly be allowed for by using a modified length of solution, l/K, in place of l in (2.4) and elsewhere. Mathematical solutions follow for these equations and for corresponding equations for the cylinder and sphere.

§3. Mathematical Solutions

(*a*) *Plane Sheet*

Solutions of the equations of § 2 can be obtained by the method of Laplace transforms (Carslaw and Jaeger 1941). Writing $\bar{c}$ and $\bar{s}$ for the Laplace transforms of c and s respectively, so that

$$\bar{c} = \int_0^\infty c \exp(-pt)\, dt, \quad \bar{s} = \int_0^\infty s \exp(-pt)\, dt, \quad . \quad . \quad . \quad (3.1)$$

we have the following equations for $\bar{c}$ and $\bar{s}$:

$$p\bar{c}=-p\bar{s}+D\partial^2\bar{c}/\partial x^2\,, \quad . \quad . \quad . \quad . \quad . \quad . \quad . \quad (3.2)$$

$$p\bar{s}=\lambda\bar{c}-\mu\bar{s}\,, \quad . \quad . \quad . \quad . \quad . \quad . \quad . \quad . \quad . \quad (3.3)$$

$$-lC_0+pl\bar{c}=-D\partial\bar{c}/\partial x,\ x=a\,. \quad . \quad . \quad . \quad . \quad . \quad . \quad . \quad (3.4)$$

On eliminating $\bar{s}$ from (3.2) and (3.3) and replacing the partial derivative by an ordinary derivative since t does not appear, we find

$$\frac{d^2\bar{c}}{dx^2}+k^2\bar{c}=0,\ k^2=-\frac{p}{D}\frac{p+\lambda+\mu}{p+\mu}, \quad . \quad . \quad . \quad . \quad . \quad . \quad (3.5)$$

of which the solution that gives $\bar{c}$ an even function of x is

$$\bar{c}=F(p)\cos kx. \quad . \quad . \quad . \quad . \quad . \quad . \quad . \quad . \quad . \quad (3.6)$$

The function $F(p)$ is determined by the boundary condition (3.4) and it follows immediately that

$$\bar{c}=\frac{lC_0\cos kx}{pl\cos ka-kD\sin ka}. \quad . \quad . \quad . \quad . \quad . \quad . \quad . \quad (3.7)$$

The application of the Inversion Theorem (Carslaw and Jaeger 1941) is straightforward and after some reduction gives

$$c=\frac{lC_0}{l+(R+1)a}+\sum_1^\infty \frac{C_0\exp(p_nt)}{1+\left\{1+\frac{\lambda\mu}{(p_n+\mu)^2}\right\}\left\{\frac{a}{2l}+\frac{p_n}{2Dk_n^2}+\frac{p_n^2la}{2D^2k_n^2}\right\}}\frac{\cos k_nx}{\cos k_na}, \quad . \quad . \quad . \quad (3.8)$$

where the p_n's are the non-zero roots of

$$\frac{lp_n}{D}=k_n\tan k_na,\quad k_n^2=-\frac{p_n}{D}\frac{p_n+\lambda+\mu}{p_n+\mu}, \quad . \quad . \quad . \quad (3.9)$$

and $R=\lambda/\mu$ is the partition factor between immobilized and free solute. The expression for s differs from (3.8) only by having an extra factor $\lambda/(p_n+\mu)$ multiplying the nth term, including the term $p_n=0$. Writing M_t for the total amount of solute, both free to diffuse and immobilized, in half the sheet at time t, and M_∞ for the corresponding quantity in the final equilibrium state attained theoretically after infinite time, we have

$$\frac{M_t}{M_\infty}=1-\sum_1^\infty \frac{(1+\alpha)\exp(p_nt)}{1+\left\{1+\frac{\lambda\mu}{(p_n+\mu)^2}\right\}\left\{\frac{a}{2l}+\frac{p_n}{2Dk_n^2}+\frac{p_n^2la}{2D^2k_n^2}\right\}}, \quad . \quad (3.10)$$

where the p_n's are given by (3.9) and where

$$\alpha=l/(R+1)a,\quad M_\infty=lC_0/(1+\alpha). \quad . \quad . \quad . \quad . \quad (3.11)$$

(*b*) *Cylinder*

The case of the cylinder has previously been considered by Wilson (1948), using a slightly different method. The final result for a cylinder of radius, a, in a solution occupying a region of cross-sectional area, A, is

$$\frac{M_t}{M_\infty}=1-\sum_1^\infty \frac{(1+\alpha)\exp(p_nt)}{1+\left\{1+\frac{\lambda\mu}{(p_n+\mu)^2}\right\}\left\{\frac{\pi a^2}{A}+\frac{Ap_n^2}{4\pi D^2k_n^2}\right\}}, \quad . \quad (3.12)$$

where

$$\alpha=A/\pi a^2(R+1),\ M_\infty=AC_0/(1+\alpha) \quad . \quad . \quad . \quad . \quad . \quad (3.13)$$

and the p_n's and k_n's are given by

$$\frac{Ap_n}{2\pi Da}=k_n\frac{J_1(k_na)}{J_0(k_na)},\qquad k_n^2=-\frac{p_n}{D}\frac{p_n+\lambda+\mu}{p_n+\mu}. \quad . \quad . \quad (3.14)$$

The expression for the concentration of free solute is

$$c=\frac{AC_0}{A+(R+1)\pi a^2}+\sum_1^\infty\frac{C_0\exp(p_nt)}{1+\left\{1+\dfrac{\lambda\mu}{(p_n+\mu)^2}\right\}\left\{\dfrac{\pi a^2}{A}+\dfrac{Ap_n^2}{4\pi D^2k_n^2}\right\}}\frac{J_0(k_nr)}{J_0(k_na)}. \quad (3.15)$$

The expression for s differs from (3.15) only by having an extra factor $\lambda/(p_n+\mu)$ multiplying the nth term, including the term $p_n=0$.

(*c*) *Sphere*

On introducing new variables rc and rs the equations for the spherical case take essentially the same form as those for the plane case, and the same method of solution leads to

$$\frac{M_t}{M_\infty}=1-\sum_1^\infty\frac{(1+\alpha)\exp(p_nt)}{1+\left\{1+\dfrac{\lambda\mu}{(p_n+\mu)^2}\right\}\left\{\dfrac{2\pi a^3}{V}-\dfrac{p_n}{2Dk_n^2}+\dfrac{Vp_n^2}{8\pi aD^2k_n^2}\right\}}, \quad . \quad (3.16)$$

where the p_n's and k_n's are given by

$$\frac{V}{4\pi Da}p_n-1=-k_na\cot k_na,\quad k_n^2=-\frac{p_n}{D}\frac{p_n+\lambda+\mu}{p_n+\mu}, \quad . \quad (3.17)$$

and

$$\alpha=\frac{3V}{4\pi a^3(R+1)},\qquad M_\infty=\frac{VC_0}{1+\alpha}. \quad . \quad . \quad . \quad . \quad (3.18)$$

The expression for c is

$$c=\frac{3VC_0}{3V+4\pi a^3(R+1)}+\sum_1^\infty\frac{C_0\exp(p_nt)}{1+\left\{1+\dfrac{\lambda\mu}{(p_n+\mu)^2}\right\}\left\{\dfrac{2\pi a^3}{V}-\dfrac{p_n}{2Dk_n^2}+\dfrac{Vp_n^2}{8\pi aD^2k_n^2}\right\}}\frac{a}{r}\frac{\sin k_nr}{\sin k_na}, \quad . \quad (3.19)$$

and that for s differs from (3.19) only by having an extra factor $\lambda/(p_n+\mu)$ multiplying the nth term, including the term $p_n=0$.

§4. Physical Significance of the Mathematical Solutions

When mathematical solutions are as complicated in form as those in § 3, their physical significance is not immediately obvious. Consider eqns. (3.9) and put

$$x=k^2a^2,\ y=pa^2/D,\ \xi=a^2(\lambda+\mu)/D,\ \eta=a^2\mu/D. \quad . \quad . \quad . \quad (4.1)$$

Then

$$ly/a=\sqrt{x}\tan\sqrt{x}, \quad . \quad . \quad . \quad . \quad . \quad . \quad . \quad (4.2)$$

$$x=-\frac{y(y+\xi)}{y+\eta}, \quad . \quad . \quad . \quad . \quad . \quad . \quad . \quad . \quad (4.3)$$

are the equations to be solved for the roots. Graphs of (4.2) and (4.3) are sketched in fig. 1 to show the general location of the roots. The graph of (4.2) is the same for all ξ and η, and from the figure it is easy to see qualitatively how the roots vary with ξ and η. When corresponding transformations to those of (4.1) are applied to eqns. (3.14) for the cylinder and (3.17) for the sphere, the resulting equations are of the same form as (4.2) and (4.3), so that fig. 1 can be taken as showing qualitatively the location of the roots for all three cases. There is a root for which $k_n a$ is imaginary given by

$$ly/a = \sqrt{(-x)} \tanh \sqrt{(-x)} . \quad . \quad . \quad . \quad . \quad (4.2\,a)$$

Fig. 1

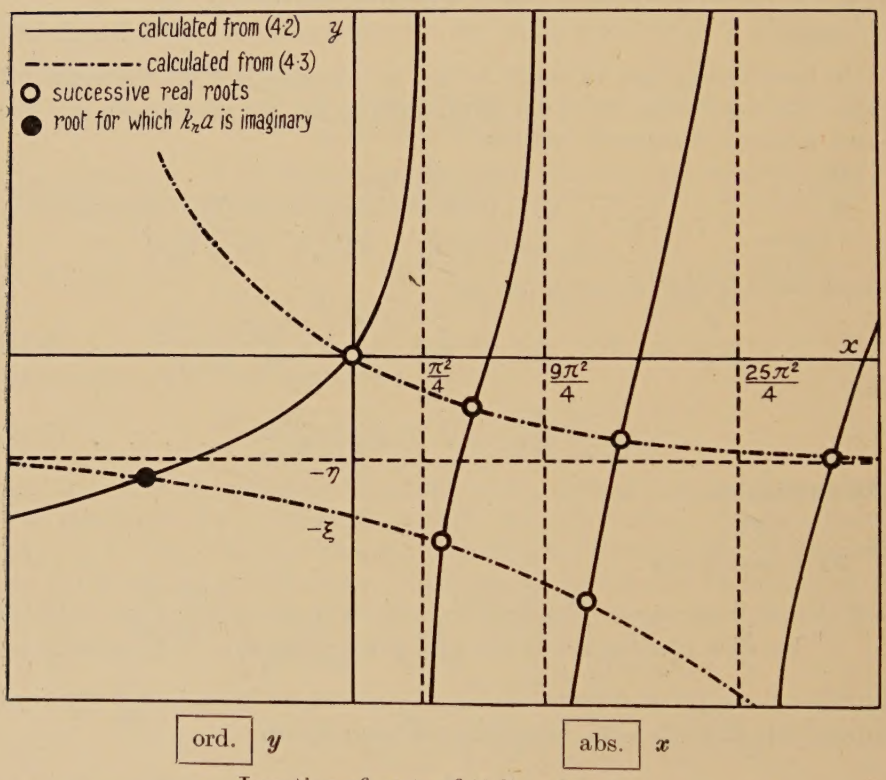

Location of roots of (4.2) and (4.3).

The general expression for M_t/M_∞ therefore comprises a unit term from $p_n=0$, a term for which $k_n a$ is imaginary, and two infinite series of terms corresponding to the intersections of the two branches of (4.3) with successive branches of (4.2).

The relative importance of the various terms depends on the parameter η. It is interesting to see quantitatively what happens to the general solution for the extreme values of this parameter which correspond to very fast and very slow reactions. The roots of (4.3) are given by

$$2y = -(x+\xi) \pm \sqrt{\{(x+\xi)^2 - 4x\eta\}}, \quad . \quad . \quad . \quad . \quad . \quad (4.4)$$

the two infinite series arising from the alternative sign. For extreme values of η the roots are readily obtained by using the appropriate binomial expansion of the term under the square root sign in (4.4). Proceeding in this way with the aid of fig. 1 it is not difficult to show that if η is very large, that is the reaction is very rapid compared with diffusion, the terms in the general solution for M_t/M_∞ which arise by taking the negative sign in (4.4) vanish, as does also the term from the imaginary root. The terms from the positive sign lead to

$$\frac{M_t}{M_\infty} = 1 - \Sigma \frac{2\alpha(1+\alpha)\exp(-\beta k_n^2 a^2 t)}{1+\alpha+\alpha^2 k_n^2 a^2}, \quad \ldots \quad (4.5)$$

where the $k_n a$'s approach the roots of

$$\tan k_n a = -\alpha k_n a, \quad \ldots \quad (4.6)$$

and

$$\beta = D/(R+1)a^2. \quad \ldots \quad (4.7)$$

This is the solution obtained by Wilson (1948) for the case of an immobilizing reaction which is rapid compared with diffusion.

If, however, η is small because the reaction is infinitely slow ($\mu=0$) we find that the terms arising from the positive sign in (4.4) vanish provided a/l is not zero, which case is treated separately in § 5. The terms from the negative sign combine with that from the imaginary root to give

$$\frac{M_t}{M_\infty} = \left(1 - \frac{R}{R+1}\frac{l}{l+a}\right)\left\{1 - \sum_1^\infty \frac{2(l/a)(1+l/a)\exp(-Dk_n^2 t)}{1+l/a+(l/a)^2 k_n^2 a^2}\right\}, \quad (4.8)$$

where the k_n's are given by

$$\tan k_n a = -(l/a)\, k_n a. \quad \ldots \quad (4.9)$$

The whole term in the second bracket in (4.8) is to be recognized as the expression for simple diffusion from a finite bath i.e. diffusion in the absence of any immobilized component. Equation (4.8) also describes a simple diffusion process, therefore, and M_t/M_∞ changes from zero at $t=0$ to $1-Rl/(R+1)(l+a)$ at $t=\infty$, which is easily shown to be the fractional uptake of solute to be expected in the absence of immobilized solute. Thus (4.8) indicates the behaviour to be expected on general argument, namely that for an infinitely slow reaction the sheet takes up, by simple diffusion, only the fraction of solute which it can accommodate in the freely diffusing state and none in the immobilized state.

If on the other hand $\mu a^2/D$ is small because D is very large, all terms in the general solution vanish except the one associated with the imaginary root and we are left with

$$\frac{M_t}{M_\infty} = 1 - \frac{R}{R+1}\frac{l}{l+a}\exp\left\{-\left(1+\frac{Ra}{l+a}\right)\mu t\right\}. \quad \ldots \quad (4.10)$$

This expression is readily deduced from elementary considerations when diffusion is so rapid that the concentration of solute is effectively uniform through the sheet at all times.

The type of behaviour observed in a practical system for which $\mu a^2/D$ is very small depends on the time scale of the experiment. If this is such that the reaction occurs very slowly compared with the duration of the experiment the simple diffusion behaviour of (4.8) is observed. If on the other hand diffusion is very rapid compared with the time scale of the experiment the simple first-order reaction of (4.10) is observed.

§5. Evaluation of Numerical Values

When eqns. (3.9) and (3.10) are written in terms of p_n/μ and $k_n a$ we see that M_t/M_∞ can be calculated as a function of Dt/a^2 if three parameters are known. The parameters are l/a, that is the ratio of the volumes occupied by solution and sheet respectively, the partition factor R, and the modified rate constant for the reaction, $\mu a^2/D$. Alternatively, since $R=\lambda/\mu$, a solution is defined by l/a and the two rate constants $\mu a^2/D$ and $\lambda a^2/D$. In some cases it is more useful to relate R to the fraction of the total amount of solute which is in the sheet finally, i.e. to M_∞/lC_0, by the relations (3.11). For the cylinder the corresponding parameters are $\pi a^2/A$, R and $\mu a^2/D$, and for the sphere $4\pi a^3/3V$, R and $\mu a^2/D$.

Once the roots p_n, $k_n a$ are obtained, the evaluation of each of the expressions for M_t/M_∞ for the plane sheet, cylinder, and sphere is straightforward provided l, A and V are finite. The cases of l, A and V infinite, however, need further consideration because the convergence of terms for which p_n approaches $-\mu$ can be very slow and numerical evaluation becomes awkward and laborious, particularly for small $\mu a^2/D$. For the plane sheet when $\alpha=\infty$, (3.10) reduces to

$$\frac{M_t}{M_\infty}=1-\sum_1^\infty \frac{2D^2k_n^2(1+p_n/\mu)^2\exp(p_nt)}{(R+1)p_n^2a^2\{(1+p_n/\mu)^2+R\}}, \quad \ldots \quad (5.1)$$

where now $k_n a=(n+\frac{1}{2})\pi$. As we saw in § 4 there are two infinite series in the general expression for M_t/M_∞. We shall confine attention for the moment to the series associated with the positive square root in (4.4) since these are the terms for which p_n approaches $-\mu$ when $Dk_n^2a^2/\mu a^2$ is large. Substituting for $1+p_n/\mu$ from the second of (3.9) we find

$$\frac{M_t}{M_\infty}=1-\sum_1^\infty \frac{2(R+1+p_n/\mu)^2\exp(p_nt)}{(R+1)\{(1+p_n/\mu)^2+R\}k_n^2a^2}. \quad \ldots \quad (5.2)$$

If $p_n=-\mu$ to the order of accuracy required, after the first r non-zero roots, we have

$$\frac{M_t}{M_\infty}=1-\sum_1^r \frac{2(R+1+p_n/\mu)^2\exp(p_nt)}{(R+1)\{(1+p_n/\mu)^2+R\}k_n^2a^2}-\frac{R}{R+1}\left\{1-\sum_1^r\frac{2}{k_n^2a^2}\right\}\exp(-\mu t) \quad \ldots \quad (5.3)$$

approximately since

$$\sum_1^\infty \frac{2}{k_n^2a^2}=1. \quad \ldots \quad (5.4)$$

The relationship (5.4) follows, for example, from (4.5) when $\alpha=\infty$, since $M_t/M_\infty=0$ when $t=0$. The error involved in use of the approximate form (5.3) is less than

$$\left[\frac{(R+1+p_{r+1}/\mu)^2\exp(p_{r+1}t)}{(R+1)\{(1+p_{r+1}/\mu)^2+R\}}-\frac{R}{R+1}\exp(-\mu t)\right]\left[1-\sum_1^r\frac{2}{k_n{}^2a^2}\right], \quad . \quad (5.5)$$

and can be made as small as desired by choice of r. We may note in passing that since in (5.2) p_n/μ and $1+p_n/\mu$ occur only with R, this is a more convenient form of expression for computation than (5.1) when p_n/μ is small or near -1, particularly for large R, since it is less sensitive to the accuracy of the roots p_n/μ.

When $l/a=\infty$, it follows from (4.2 a) that there is no root for which k_na is imaginary. The complete expression for M_t/M_∞ is therefore that of (5.3) together with terms arising from the negative sign in the roots of (4.4). On using (5.3) numerical evaluation of M_t/M_∞ for l/a infinite is straightforward. The corresponding formulae for the plane sheet and the sphere are easily derived.

§6. Irreversible Reaction

A special case of the above solutions of particular interest is that of an irreversible reaction, when the rate of formation of immobilized solute is directly proportional to the concentration of free solute. In this case $\mu=0$, but λ is non-zero so that $R=\infty$, $\alpha=0$, $M_\infty=lC_0$. The solution for the plane sheet, for example, for these values follows immediately from (3.9) and (3.10) provided l is finite.

The solution for the case of $l=\infty$ is less obvious. When $\mu=0$, the imaginary root (p_i, k_i) is given by

$$lp_i=-Dk_i'\tanh k_i'a, \quad k_i'^2=(p_i+\lambda)/D, \quad . \quad . \quad . \quad . \quad (6.1)$$

where $k_i=ik_i'$, and so when $l=\infty$,

$$p_i=0, \quad k'_i{}^2=\lambda/D. \quad . \quad . \quad . \quad . \quad . \quad . \quad . \quad (6.2)$$

When $\alpha=0$, $\mu=0$ and p_i is small, we can expand $\exp(p_it)$ in powers of p_it and write (3.10) as

$$M_t=lC_0-\frac{lC_0(1+p_it)}{1+\dfrac{a}{2l}-\dfrac{p_i}{2Dk_i'^2}-\dfrac{p_i{}^2la}{2D^2k_i'^2}}-\sum\frac{lC_0\exp(p_nt)}{1+\dfrac{a}{2l}+\dfrac{p_n}{2Dk_n{}^2}+\dfrac{p_n{}^2la}{2D^2k_n{}^2}}, \quad (6.3)$$

from which, when $l=\infty$, so that lp_i is given by (6.1) and (6.2), we have finally

$$\frac{M_t}{aC_0}=\frac{Dt}{a^2}q\tanh q+\tfrac{1}{2}\operatorname{sech}^2 q+\frac{1}{2q}\tanh q-\sum\frac{2D^2k_n{}^2\exp(p_nt)}{a^2p_n{}^2}, \quad . \quad . \quad (6.4)$$

where

$$k_na=(n+\tfrac{1}{2})\pi, \quad k_n{}^2=-(p_n+\lambda)/D, \quad q=\sqrt{(\lambda a^2/D)}. \quad . \quad . \quad (6.5)$$

The first term on the right-hand side of (6.4) gives the rate of uptake of solute due to the chemical reaction in the final steady state.

The forms of (3.12) and (3.14) for the cylinder, and of (3.16) and (3.17) for the sphere when $\mu=0$, $\alpha=0$, are obvious. When $A=\infty$ we have for the cylinder

$$\frac{M_t}{\pi a^2 C_0}=1+\frac{2Dt}{a^2}q\frac{I_1(q)}{I_0(q)}-\frac{I_1^2(q)}{I_0^2(q)}-\Sigma\frac{4D^2k_n^2\exp(p_nt)}{p_n^2}. \quad . \quad (6.6)$$

where

$$J_0(k_na)=0,\ k_n^2=-(p_n+\lambda)/D,\ q=\sqrt{(\lambda a^2/D)}. \quad . \quad . \quad (6.7)$$

When $V=\infty$ we have for the sphere

$$\frac{3M_t}{4\pi a^3C_0}=\frac{3Dt}{a^2}(q\coth q-1)-\tfrac{3}{2}\operatorname{cosech}^2 q+\frac{3}{2q}\coth q-\Sigma\frac{6D^2k_n^2\exp(p_nt)}{a^2p_n^2}, \quad . \quad . \quad . \quad (6.8)$$

where

$$k_na=n\pi,\ k_n^2=-(p_n+\lambda)/D,\ q=\sqrt{(\lambda a^2/D)}. \quad . \quad . \quad . \quad (6.9)$$

The solutions (6.4), (6.6), (6.8) can of course by obtained directly by use of the Laplace transform or otherwise. Danckwerts (1951) has shown that solutions for diffusion and simultaneous irreversible reaction can sometimes be obtained by a simple transformation of the expressions for the corresponding diffusion problem without reaction.

§ 7. Desorption

We have considered diffusion into a plane sheet initially free of solute. There is the complementary problem in which all the solute is initially uniformly distributed through the sheet and subsequently diffuses out into the solution. If free and immobilized solute are considered to be initially in equilibrium everywhere in the sheet, it is easily seen that the mathematical solutions presented above for absorption also describe desorption, provided M_t is taken to mean the amount of solute leaving the sheet up to time t, and M_∞ the corresponding amount after infinite time. For desorption from a plane sheet, for example, we want solutions of the eqns. (2.1) and (2.2) satisfying the condition (2.4) but with (2.3) replaced by

$$c=C_0,\ s=S_0,\ -a<x<a,\ t=0. \quad . \quad . \quad . \quad . \quad . \quad . \quad (7.1)$$

Writing

$$c_1=C_0-c,\quad s_1=S_0-s, \quad . \quad . \quad . \quad . \quad . \quad . \quad . \quad (7.2)$$

it is easy to see that (7.1) and the other equations for desorption are identical with (2.1), (2.2), (2.3) and (2.4) with c_1, s_1 written for c, s respectively, remembering only that $\lambda C_0-\mu S_0=0$, if we have equilibrium throughout the sheet at $t=0$. Hence the equations and solutions for desorption are identical with those for absorption.

§ 8. Calculated Results

Evaluation of the expressions of § 6 for the irreversible reaction and any particular set of parameters is comparatively simple and straightforward. On the other hand a considerable amount of painstaking labour is involved in the evaluation of the formulae for the reversible reaction even when

there is an infinite amount of solute, and it is therefore worth while to present some numerical values. In tables 1, 2, 3 and 4 calculated values of M_t/M_∞ are tabulated for the plane sheet, cylinder, and sphere. The arrangement of the tables was decided by ease of presentation. Three values of the partition factor R are included and for each R three rates of reaction. All tabulated solutions refer to an infinite amount of diffusing substance. The values of M_t/M_∞ are believed to be correct to within ± 1 in the third decimal place.

Table 1. Values of M_t/M_∞ for $\mu a^2/D=0{\cdot}01$

$Dt/(R+1)a^2$ \ R	plane sheet		cylinder		sphere	
	10	100	10	100	10	100
0·005	0·024	0·009	0·043	0·012	0·057	0·013
0·01	0·034	0·013	0·058	0·017	0·073	0·018
0·02	0·048	0·021	0·074	0·026	0·086	0·027
0·04	0·067	0·036	0·088	0·043	0·093	0·046
0·06	0·079	0·051	0·093	0·060	0·096	0·064
0·08	0·086	0·065	0·096	0·077	0·098	0·081
0·10	0·091	0·079	0·099	0·094	0·100	0·099
0·15	0·099	0·114	0·104	0·133	0·105	0·140
0·2	0·104	0·147	0·108	0·172	0·109	0·180
0·3	0·114	0·210	0·118	0·243	0·119	0·254
0·4	0·123	0·268	0·128	0·308	0·129	0·322
0·5	0·133	0·322	0·137	0·368	0·138	0·383
1·0	0·178	0·537	0·183	0·597	0·184	0·616
1·5	0·220	0·683	0·226	0·743	0·227	0·761
2·0	0·261	0·782	0·267	0·836	0·269	0·851
2·5	0·299	0·850	0·306	0·895	0·307	0·907
5·0	0·463	0·977	0·471	0·989	0·473	0·991
7·5	0·588	0·996	0·597	0·999	0·599	0·999
10	0·685	0·999	0·693	1·000	0·695	1·000
15	0·815	1·000	0·822		0·823	
20	0·891		0·896		0·898	
40	0·987		0·988		0·989	
60	0·998		0·999		0·999	
80	1·000		1·000		1·000	

Solutions for the plane sheet are illustrated in figs. 2, 3 and 4. Those for the cylinder and sphere show the same general features, differing only in detail. Figure 2 shows how the absorption curves change in shape and position as $\mu a^2/D$ is varied between the two extremes given by $\mu=\infty$ (infinitely rapid reaction) and $\mu=0$ (simple diffusion with no reaction). By plotting against $(\mu t)^{1/2}$ as in fig. 3 we can show the approach to the curve for $D=\infty$ (purely reaction controlled) as $\mu a^2/D$ tends to zero because of D becoming large. We see also in fig. 3 that the discontinuity in the gradient of the curve for D infinite appears as a 'shoulder' when

Table 2. Values of M_t/M_∞ for $\mu a^2/D=0{\cdot}1$

$Dt/(R+1)a^2$ \ R	plane sheet			cylinder			sphere		
	1	10	100	1	10	100	1	10	100
0·005	0·057	0·025	0·017	0·108	0·044	0·029	0·155	0·059	0·037
0·01	0·080	0·035	0·032	0·149	0·060	0·054	0·210	0·076	0·068
0·02	0·113	0·052	0·062	0·205	0·081	0·101	0·279	0·095	0·127
0·04	0·160	0·076	0·116	0·277	0·106	0·188	0·361	0·117	0·232
0·06	0·197	0·095	0·166	0·327	0·125	0·265	0·409	0·136	0·324
0·08	0·227	0·112	0·211	0·365	0·143	0·333	0·441	0·153	0·404
0·10	0·254	0·128	0·253	0·395	0·159	0·394	0·463	0·171	0·474
0·15	0·310	0·164	0·343	0·445	0·200	0·519	0·494	0·212	0·613
0·2	0·354	0·198	0·418	0·476	0·238	0·615	0·508	0·252	0·712
0·3	0·418	0·261	0·536	0·507	0·309	0·748	0·522	0·325	0·838
0·4	0·459	0·320	0·626	0·524	0·373	0·832	0·532	0·391	0·907
0·5	0·488	0·374	0·696	0·535	0·432	0·887	0·542	0·451	0·946
1·0	0·559	0·585	0·889	0·579	0·652	0·983	0·585	0·672	0·996
1·5	0·601	0·724	0·959	0·619	0·786	0·997	0·624	0·804	1·000
2·0	0·638	0·816	0·985	0·655	0·868	1·000	0·660	0·883	
2·5	0·671	0·877	0·994	0·687	0·919		0·692	0·930	
5·0	0·797	0·983	1·000	0·809	0·993		0·813	0·995	
7·5	0·875	0·998		0·884	0·999		0·886	1·000	
10	0·923	1·000		0·929	1·000		0·931		
15	0·971			0·974			0·974		
20	0·989			0·990			0·990		
40	1·000			1·000			1·000		

Table 3. Values of M_t/M_∞ for $\mu a^2/D=1{\cdot}0$

$Dt/(R+1)a^2$ \ R	plane sheet			cylinder			sphere		
	1	10	100	1	10	100	1	10	100
0·005	0·057	0·028	0·045	0·109	0·051	0·085	0·155	0·070	0·120
0·01	0·081	0·045	0·081	0·151	0·079	0·151	0·211	0·105	0·212
0·02	0·115	0·075	0·136	0·208	0·129	0·250	0·283	0·166	0·346
0·04	0·164	0·131	0·210	0·285	0·217	0·378	0·371	0·273	0·510
0·06	0·203	0·181	0·264	0·341	0·295	0·465	0·429	0·366	0·613
0·08	0·237	0·226	0·309	0·385	0·363	0·531	0·471	0·445	0·687
0·10	0·267	0·268	0·348	0·423	0·423	0·587	0·504	0·514	0·743
0·15	0·334	0·358	0·430	0·495	0·547	0·692	0·564	0·648	0·840
0·2	0·390	0·432	0·497	0·549	0·638	0·767	0·608	0·743	0·899
0·3	0·481	0·549	0·607	0·630	0·768	0·866	0·676	0·860	0·959
0·4	0·553	0·637	0·691	0·691	0·848	0·923	0·732	0·922	0·983
0·5	0·613	0·707	0·758	0·741	0·898	0·955	0·777	0·956	0·993
1·0	0·804	0·895	0·927	0·891	0·986	0·997	0·912	0·997	1·000
1·5	0·900	0·962	0·978	0·954	0·998	1·000	0·965	1·000	
2·0	0·948	0·986	0·994	0·980	1·000		0·986		
2·5	0·973	0·993	0·998	0·992			0·995		
5·0	0·999	1·000	1·000	1·000			1·000		
7·5	1·000								

Table 4. Values of M_t/M_∞ for $\mu a^2/D=10$

$Dt/(R+1)a^2$ \ R	plane sheet	cylinder	sphere
	1	1	1
0·005	0·059	0·112	0·160
0·01	0·085	0·159	0·224
0·02	0·126	0·230	0·316
0·04	0·190	0·336	0·448
0·06	0·242	0·420	0·546
0·08	0·288	0·489	0·623
0·10	0·329	0·547	0·686
0·15	0·414	0·660	0·796
0·2	0·484	0·740	0·865
0·3	0·595	0·845	0·939
0·4	0·680	0·906	0·972
0·5	0·746	0·943	0·987
1·0	0·920	0·995	1·000
1·5	0·975	1·000	
2·0	0·992		
2·5	0·998		
5·0	1·000		

Fig. 2

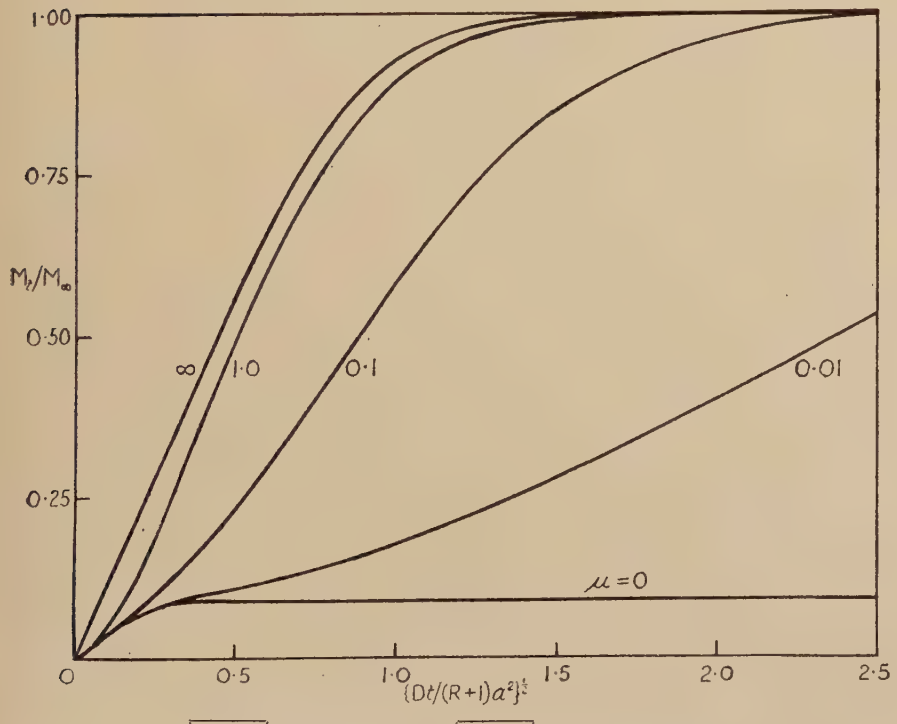

Flanc sheet, $R=10$. Curves are labelled with values of $\mu a^2/D$.

$\mu a^2/D=0{\cdot}01$. As $\mu a^2/D$ is increased further the shoulder disappears leaving an absorption curve with a point of inflexion. At still higher $\mu a^2/D$ the inflexion becomes less noticeable as in fig. 2 and the curves have the simple shape commonly associated with diffusion. Figure 4 shows the influence of the parameter R, the partition factor between immobilized and free solute. As R is increased the height of the shoulder decreases and if curves for $R=100$ were plotted on the present scale no shoulder would be detected for any value of $\mu a^2/D$.

Fig. 3

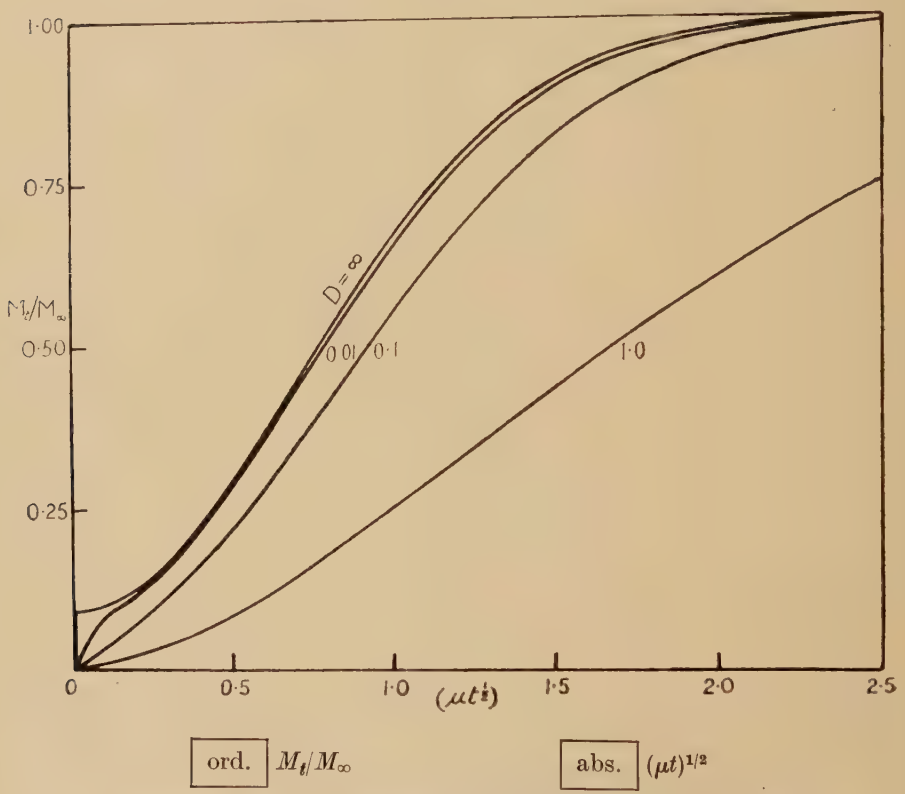

Plane sheet, $R=10$. Curves are labelled with values of $\mu a^2/D$.

One interesting feature of these results is that they indicate limits to the relative rates of diffusion and reaction outside of which the reaction is effectively infinitely rapid or infinitely slow as the case might be. Thus for the plane sheet the values of M_t/M_∞ for $\mu a^2/D=10$ differ by only a few per cent from those for an infinitely rapid reaction. The differences are greatest for $R=1$ where they are about 5%. At the other extreme the solution for $\mu a^2/D=0{\cdot}01$, $R=1$ is the same as that for an infinitely slow reaction to the same degree of accuracy except at small times (see fig. 4 for example). The differences increase in this case as R increases, being about 20% for $R=100$.

The significance of these limits is perhaps easier to appreciate when they are expressed in terms of the half-times of the simple diffusion and simple reaction processes respectively. For simple diffusion into the plane sheet from an infinite amount of solution it is easy to show that the half-time, t_d, that is the time at which $M_t/M_\infty=\frac{1}{2}$, is given by

$$Dt_d/a^2=-(4/\pi^2)\ln \pi^2/16=0{\cdot}2 \quad . \quad . \quad . \quad . \quad . \quad . \quad (8.1)$$

approximately. On the other hand if immobilized solute is formed from a uniform constant, concentration, C_0, of free solute according to the equation

$$\partial s/\partial t=\lambda C_0-\mu s \quad . \quad . \quad . \quad . \quad . \quad . \quad . \quad . \quad (8.2)$$

Fig. 4

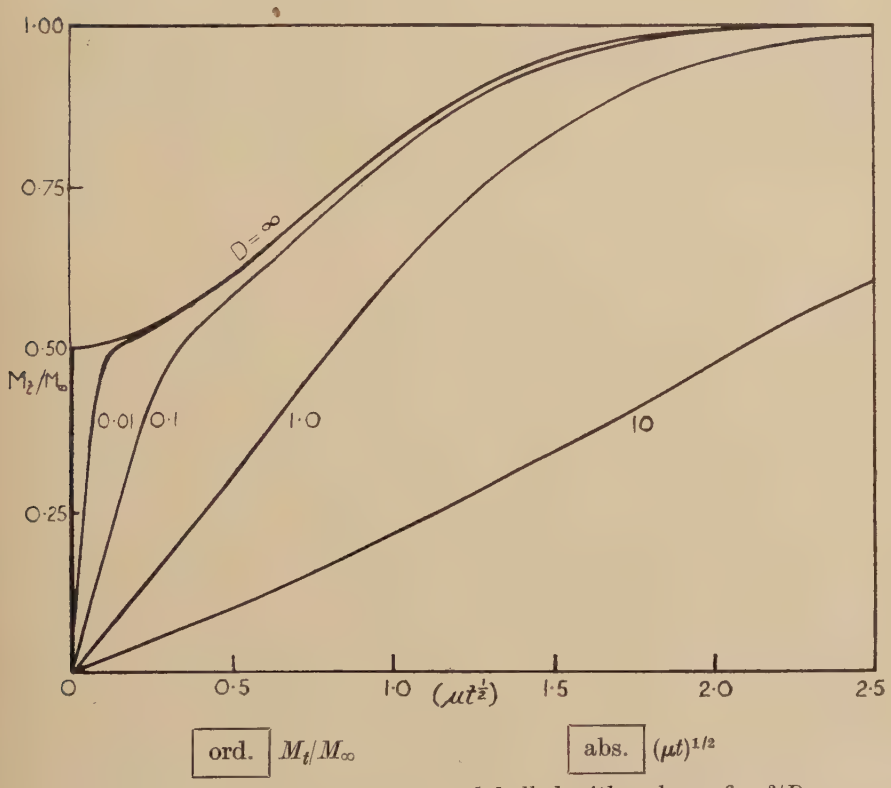

Plane sheet, $R=1$. Curves are labelled with values of $\mu a^2/D$.

this reaction has a half-time, t_r, given bv

$$\mu t_r=\ln 2=0{\cdot}7 \quad . \quad . \quad . \quad . \quad . \quad . \quad . \quad . \quad (8.3)$$

approximately, and combining (8.1) and (8.2) we have for the ratio of the half-times,

$$t_r/t_d=3{\cdot}5D/\mu a^2 \quad . \quad . \quad . \quad . \quad . \quad . \quad . \quad . \quad (8.4)$$

Thus we can say roughly that if the diffusion is more than a thousand times faster than the reaction, the behaviour of the diffusion-reaction process

is roughly the same as it would be if diffusion were infinitely rapid. On the other hand if the half-times for diffusion and reaction are comparable, the behaviour approximates to that for any infinitely rapid reaction. These statements indicate orders of magnitude only. They apply also to the cylinder and sphere.

In conclusion the author wishes to acknowledge the computational assistance of Mrs. D. M. Lambert to whom the tabulated numerical values are due.

References

Carslaw, H. S., and Jaeger, J. C., 1941, *Operational Methods in Applied Mathematics*, Chap. 6 (Oxford University Press).
Crank, J., 1948, *Phil. Mag.*, **39,** 140, 362.
Danckwerts, P. V., 1951, *Trans. Faraday Soc.*, **47,** 1014.
Hill, A. V., 1929, *Proc. Roy. Soc.* B, **104,** 39.
Nicolson, P., and Roughton, F. J. W., 1951, *Proc. Roy. Soc.* B, **138,** 241.
Wilson, A. H., 1948, *Phil. Mag.*, **39,** 48.

LXXIX. *Microscopic Studies on Beryl Crystals.—III. The Movement of Dislocations*

By L. J. Griffin
H. H. Wills Physical Laboratory, University of Bristol*

[Received May 8, 1952]

Abstract

It is shown that slight anomalies in the layer pattern near a dislocation can often be interpreted only as due to movement of the dislocation over a short distance. Examples are also shown in which a single dislocation has moved and cut across neighbouring layers.

Characteristic types of dislocation groups, termed limited slip-zones, which are often observed, are shown to be explicable, in all details, in terms of the 'generation' of dislocations by Frank–Read sources. The type of layer structure to be observed while such a source is still active, or has just ceased to be active, is deduced and some of the cases observed are shown.

§ 1. Introduction

The patterns of unimolecular layers observed on beryl crystals are static and necessarily display the situation extant when the layers finally come to rest, whether the final stage was growth or dissolution. The purpose of this paper is to present evidence that some of the dislocations present have moved in some stage of the history of the crystal; this is deduced from the static picture through the observations of anomalies in the layer structure near the dislocations which are inexplicable in terms of either growth or dissolution; alternatively, certain precisely defined types of dislocation groups are observed which give evidence for the existence of Frank–Read sources. Evidence is presented below to show that on the various crystals observed deformation has occurred, including both the movement of single dislocations over very small distances, and large-scale production of dislocations from sources in the interior, resulting in the displacement of considerable sections of the crystal.

If any movement of a dislocation over a short distance is to be detected it is necessary to know

(*a*) the dependence of growth rate upon orientation for the particular crystal face;

(*b*) the normal type of cross-linking which takes place between a dislocation and advancing layers.

The examples cited in § 2 were all observed on the prism faces of one beryl crystal. These faces had a rate of growth parallel to the *c*-axis of the crystal, which was usually some two to four times greater than the

* Communicated by the Author.

rate of growth perpendicular to this axis. The normal type of cross-linking with a single dislocation (Griffin 1951) is shown for a layer edge running perpendicular to the *c*-axis in figs. 1*a* and 1*b*, where the shading denotes the low side of the steps.

The type of cross-linking is precisely similar for right- and left-handed screw dislocations. Propagation of layers past single dislocations is, in all cases, a simple repeat of stages (i) to (iv) in fig. 1. Inspection of this

Fig. 1

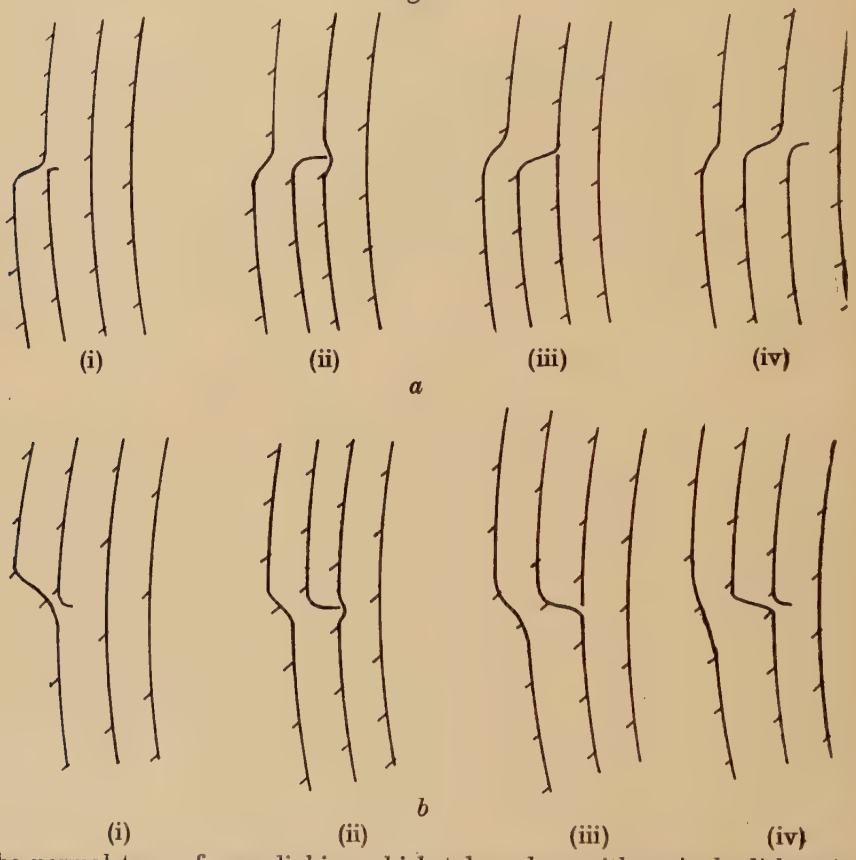

The normal type of cross-linking which takes place with a single dislocation. Both a right-handed and a left-handed screw dislocation are shown, the layer topography in the one case merely being a mirror image of the other.

figure also shows that for the layer which passes on after cross-linking, the ' bump ' or kink in the edge accurately locates the previous position of the dislocation.

A case of cross-linking which may appear identical to fig. 1 in its early stages is shown in figs. 2*a* and 2*b*. Here cross-linking results in

(*a*) the formation of a depression which will be filled in rapidly;

(*b*) attachment of the dislocation to the type of layer edge shown in fig. 1.

It is obvious that layers of the stage (i) type of fig. 2 cannot persist after the first cross-linking, and that the second, and all subsequent cross-linkings, will be of the type shown in fig. 1, the dislocation being attached to a normal type of layer.

This can be generalized, and any complicated type of layer running from a dislocation can be considered. This is shown in fig. 3.

We are led to the following general rule. No matter what the shape of the original layer attached to the dislocation, this layer will conform to the layer type of the incident system after the first cross-linking. This will also be true for all subsequent cross-linkings.

Fig. 2

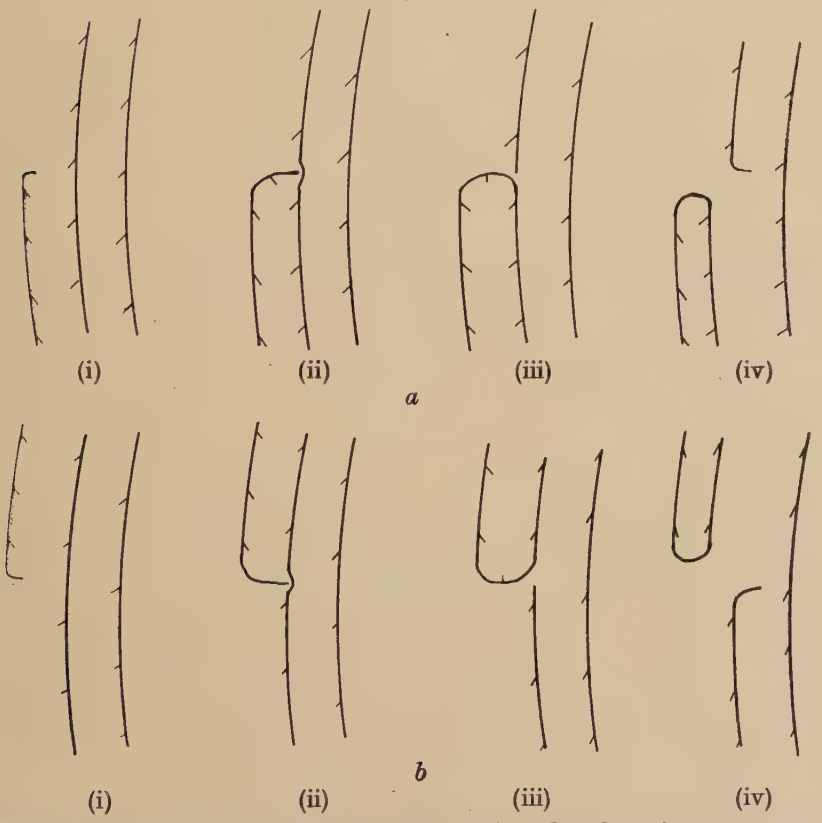

Stage (i) of both *a* and *b* shows a situation which under the microscope appears to be identical with that shown in fig. 1. However, as the steps attached to the dislocations are facing in the opposite direction in this case, the result of cross-linking is quite different.

Alternatively this rule can be stated as follows: provided that the dislocation remains stationary, and that the conditions are not fluctuating markedly, all cross-linkings after the first will be of the types shown in fig. 1.

We shall now consider some experimental observations.

§ 2. Movement of a Dislocation over a Short Distance

Example 1

This is shown in fig. 4, Plate LIV. Two such events occur on the plate; they are isolated and shown in figs. 5*a* and 5*c*. (In all figures the *c*-axis is approximately horizontal unless otherwise specified.) In fig. 5*a* note (i) the re-entrant in the layer edge numbered 1, (ii) the position of the dislocation.

Fig. 3

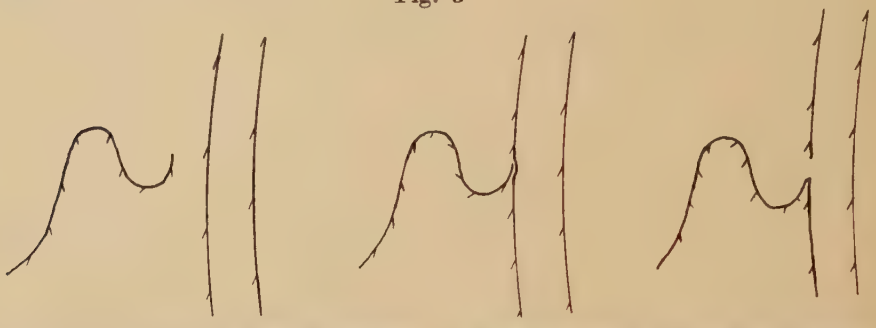

An arbitrarily shaped layer is attached to the dislocation in the first instance, but the result of cross-linking is to attach the dislocation to a normal type of layer.

Fig. 5

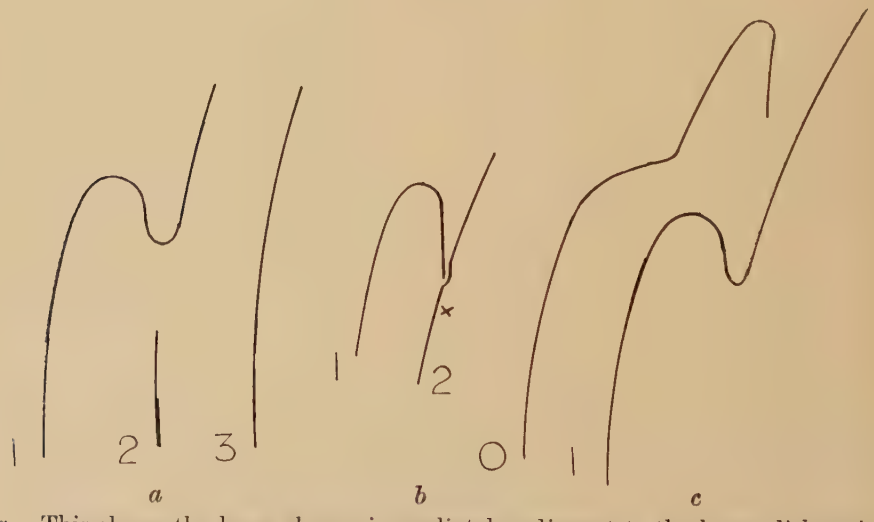

a. This shows the layer shapes immediately adjacent to the lower dislocation which is indicated on fig. 4, Plate LIV, and will help to identify this area.

b. The assumed layer shapes at the moment of cross-linking. The cross marks the position of the dislocation which is actually observed.

c. This shows the layer shapes close to the higher dislocation indicated in fig. 4, Plate LIV. Layer 1 is also common to fig. 5*a*.

It is known that sharp re-entrants are eliminated at a speed considerably greater than the normal growth rate, probably for a re-entrant of this curvature about twice as fast. However, in the case of fig. 5 the direction

of elimination of the re-entrant corresponds to a minimum growth rate, and in this region the rate of growth parallel to the *c*-axis is some four times greater than the minimum growth rate. Consequently a re-entrant reaching the dislocation is unlikely to have been eliminated to the extent apparent in this figure.

The observed shapes of the layer edges can be satisfactorily explained if it is assumed that at the moment of cross-linking of edges 1 and 2 the position was as shown in fig. 5 *b*. Here the cross marks the observed position of the dislocation. It is shown above that such an edge-shape could not persist. Therefore this deviation from a normal shape could only have been produced between the penultimate and final cross-linkings of this dislocation before growth ceased. Thus the motion must have taken place just before growth ceased.

In fig. 4, immediately above the layers just considered, is the situation shown in fig. 5 *c*. Applying similar arguments, it is obvious that layer O must have taken this outline just before growth ceased. This layer can have undergone no cross-linking. Note also that the bump on the lower part of layer O is entirely consistent with normal cross-linking of the dislocation, now attaching layer 2 of fig. 5 *a* with layer O : this was the second cross-linking before growth ceased. Moreover, the position of this bump is such that the dislocation must have been near the top of the right-hand straight portion of layer 1 as seen in fig. 5 *b*. The short straight sections of the layer edges running up to the dislocations in figs. 5 *b* and 5 *c* are not consistent with the normal growth rates. These normal growth rates are observed to hold for the layers immediately adjacent to those under consideration.

The only explanation which can satisfactorily account for this behaviour is that the two dislocations have moved a short distance along a line perpendicular to the *c*-axis. Thus it appears that these two dislocations of the same hand which are 10 microns apart have each moved a distance of approximately 5 microns.

Example 2

This case is shown in fig. 6, Plate LIV. This could correspond to either fig. 7 *a* or 7 *b*. In fact the shape of layer 1 shows that cross-linking took place just before growth ceased and, therefore, the right-hand upper part of layer 1 and the right-hand part of layer 2 must correspond. Therefore the situation shown in fig. 7 *b* must be that observed.

The shape of layer 2 could not possibly be due to cross-linking, and, in fact, this shape would disappear at the first cross-linking. This shape is also entirely at variance with the observed growth rates and growth behaviour. The sharpness of the right-hand corner of the bump on layer 1 indicates that cross-linking can only just have taken place before growth ceased. Thus the only feasible explanation is a movement of the dislocation perpendicular to the *c*-axis, as shown in fig. 7 *c*. The sharp corner resulting from this movement would soon be rounded off by

dissolution to the kind of shape observed. In this case the distance moved was probably some 6 microns, part of this movement possibly taking place after growth had ceased.

Examples 3 *and* 4

These examples are shown in figs. 8 and 9, Plate LIV. In this case interest is centred in the hook-shaped layer edges. In principle these examples are similar to example 2. In detail they differ in that the 'hook' in these two examples is facing the advancing layer system. Both hook-shapes must have been produced since the last cross-linking took place. In fact in both cases the position of the bump on the last layer to be propagated past the dislocation suggests that the dislocation was located at the lowest point of the hook at the moment of cross-linking.

Once again these examples can only be satisfactorily explained if, since the last cross-linking, the dislocations have moved a distance perpendicular to the *c*-axis of 6 microns and 8 microns respectively.

Fig. 7

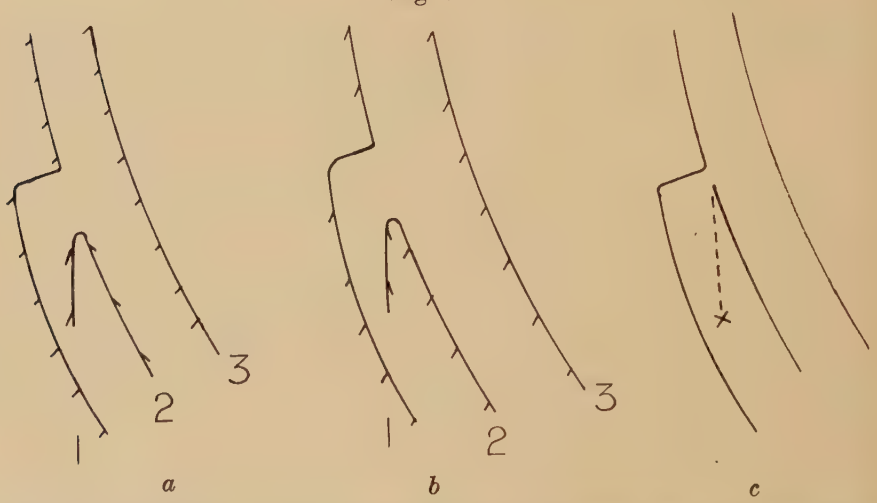

a and *b* The shading here denotes the low side of the steps, and the layer shapes indicated in fig. 6, Plate LIV, could correspond to either of these two cases.

c. The full lines represent the original and typical layer shapes, while the dotted line indicates the path of movement of the dislocation to its observed position at the point indicated by a cross.

Some layers shown in fig. 9 are isolated in fig. 10. It is necessary to decide whether the dislocation is attached to layer 1 or layer 2. If the dislocation is attached to layer 1, it means that cross-linking has still to take place, but if the dislocation is attached to layer 2 then cross-linking must have taken place.

It appears that cross-linking has taken place because

(*a*) the bump on edge 1 is the normal type produced by a little growth subsequent to cross-linking: bumps of this type do not result from normal growth of a layer attached to a dislocation;

(*b*) layer 1 as far as the start of the bump, and layer 2 above this level appear to be co-linear.

Further support for this view was obtained from observations with an objective of N.A. 1.32. The dislocation and layer 1 were then almost resolved and appeared to be separate.

The bump on layer 1 indicates the approximate position of the dislocation when cross-linking took place. At some time after cross-linking, therefore, the dislocation must have moved 10 microns to its observed position. The layer edge running from the assumed position of the dislocation at the moment of cross-linking to the position observed in fig. 9 is only perpendicular to the axis in its lower part. This could be due to a small amount of growth taking place after the dislocation had moved an initial short distance perpendicular to the *c*-axis, further movement in the same direction taking place after growth had ceased. It is probably coincidental that the dislocation has come to rest when almost in contact with layer 1.

Fig. 10

The observed layer shapes in the area marked by the left-hand pair of vertical and horizontal arrows in fig. 9, Plate LIV.

Example 5

The layers indicated in fig. 11, Plate LV, show three 'hooks' which are very similar to the examples shown in figs. 8 and 9. The layer system is advancing from left to right, so that the 'hooks' are again facing the incident layers.

Again these cases can only be satisfactorily explained if the three dislocations which are all of the same hand, have moved distances of approximately 6 microns, all in the same direction.

Example 6

This is shown in fig. 12, Plate LV. The events leading to the observed layer shapes can be represented as in fig. 13. Once again the only satisfactory explanation of these shapes is the type of movement shown in the figure. Figure 13 (i) shows in full line what may be assumed

to be the original shape of the layers, while the dotted lines show the path of movement of the dislocations. Very slight growth subsequent to such movement will produce the layer shapes shown in fig. 13 (ii), these being identical with the observed shapes. This movement over a distance of 2 microns and 3 microns respectively is normal to the *c*-axis, as usual. In this case movement probably occurred only a very short time before growth ceased.

Example 7

This is shown in fig. 14, Plate LV, and the processes involved are shown in fig. 15. (This latter figure may be more readily comprehensible if it is remembered that although the eye moves from left to right for the successive stages the direction of advance of the layer system is from right to left.)

Fig. 13

The area of interest in fig. 12, Plate LV, is shown on the right. On the left the full lines represent assumed typical layer shapes, while the dotted lines represent the path of movement of the dislocations. Slight growth on the new layer edges so produced would then result in layer shapes as shown on the right.

It is assumed that the original situation was as shown in fig. 15 (i), and that the two dislocations moved just in front of the incident layers, causing the latter to retreat a little (e.g. because of the heat liberated in dislocation motion) as indicated in figs. 15 (ii) and (iii). Eventually, after an abnormally large kink had been formed, cross-linking took place, producing the final configuration shown in fig. 15 (iv), which corresponds to that observed. The layer edges running from the main bumps down to the dislocations must represent the paths of the latter. These paths make an angle with the main part of the layer edge and are approximately perpendicular to the *c*-axis.

Example 8

This is shown in fig. 16, Plate LV. The two twin-dislocation loops indicated are of quite anomalous shapes. These shapes are totally inconsistent with the observed growth rates on this face, and can only be satisfactorily explained in terms of movement of the lower dislocation of each loop.

Example 9

See fig. 17, Plate LVI. This area is very close to that shown in fig. 16. There are two layer edges, indicated in the centre of the figure, which have short straight sections before the dislocation. The shape of these sections is inconsistent with the generally applicable growth rates and can only be explained, once again, by movement of the dislocations perpendicular to the *c*-axis. This movement probably took place after

Fig. 15

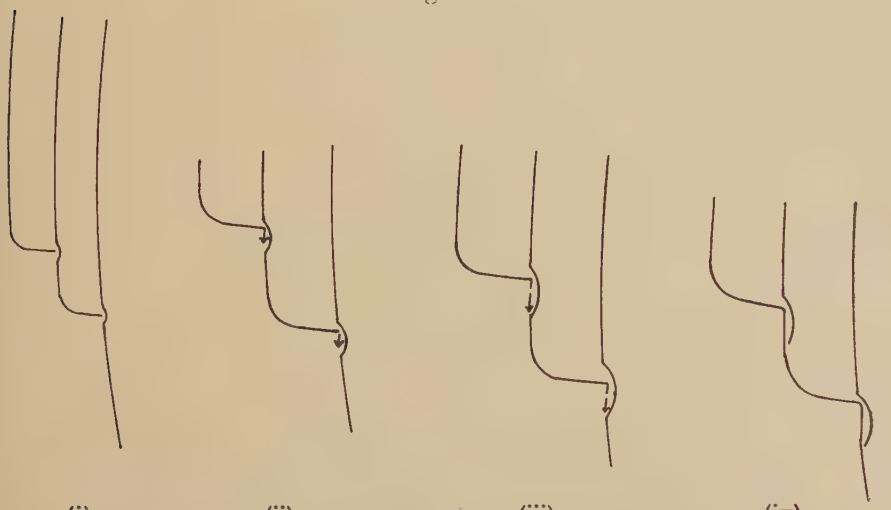

In this figure although the successive stages are drawn from left to right the layers are advancing from right to left. Stage (iv) shows layer shapes corresponding to those indicated in fig. 14, Plate LV. The situation shown in stage (i) is entirely typical, but in (ii) and (iii) the moving dislocations cause an ever-increasing length of kink, until cross-linking produces the layer shapes shown in (iv).

growth had ceased. The dislocation at the termination of the upper arrowed layer edge must also have moved upwards. The way in which further growth would have resulted in these layer edges acquiring normal shapes has already been fully discussed (Griffin 1951).

Example 10

In this example, shown in fig. 18, Plate LVI, all three of the dislocations shown appear to have moved. The previous positions of the dislocations can be located from the ' bumps ' on the last edges to

have undergone cross-linking. In each case the distance moved is about 4 microns. The sections of the layer edges marking this movement are approximately perpendicular to the *c*-axis, the deviation from true perpendicularity probably being due to a slight amount of growth taking place after the dislocations had moved.

General

The examples given above comprise only some of the cases of this type of movement which have been observed. Movement along a line perpendicular to the *c*-axis of the crystal corresponds to the trace of a (0001) plane in the face, and this plane may well be one of the characteristic slip planes of the crystal. The other family of slip planes which one might expect are the first order prism faces $\{10\bar{1}0\}$. These planes would, of course, have a trace parallel to the *c*-axis in this case.

Fig. 20

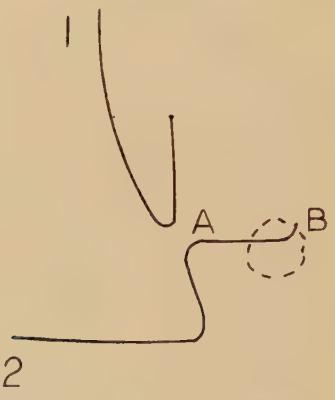

The area of fig. 19, Plate LVII, which is of interest.

The straight edge produced by such a movement is parallel to a close-packed direction (i.e. it is perpendicular to a direction of minimum growth rate) and the types of edge produced by slight dislocation movements and by normal growth processes are normally almost indistinguishable. It is therefore difficult to find examples which can be ascribed with certainty to dislocation movement. However, two cases have been observed in which, because of the local topography, it appeared probable that movement parallel to the *c*-axis had taken place.

§ 3. Movement of a Dislocation across One or more Layer Edges

Example 11

See fig. 19, Plate LVII. In this case interest is centred on the two layer edges isolated in fig. 20. Note that: (*a*) the right-hand part of layer 2 continues across a patch which partially obscures it; there is no doubt, however, that layer 2 is attached to the dislocation as shown in the

figure ; (*b*) that section AB of layer 2, when produced, very nearly touches the lowest point of edge 1. The observed layer shapes can then be explained in terms of the processes shown in (i) to (iii) of fig. 21.

In fig. 21 (i) layer edges 1 and 2 are of typical shape. Movement of the dislocation attached to layer 2, as shown in (ii), will produce the situation shown in (iii). It should be noted that because the steps in (ii) appear to cross this does not mean that the height of the steps is multi-valued at this point. The steps are, in fact, still distinct, although not resolved at Q. This can be explained as follows.

At stage (i) of fig. 21 the levels on opposite sides of the steps differ in height by one unit cell, and the layer enclosed by edge 1 is one unit cell higher than the higher level bounded by layer edge 2. If the

Fig. 21

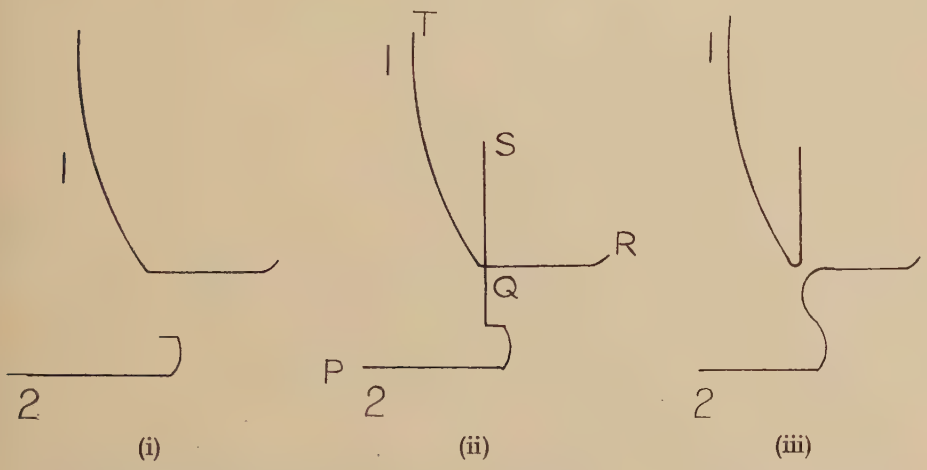

Starting from typical spiral layer shapes, as shown in (i), movement of the lower dislocation, as in (ii), can produce the layer shapes shown in (iii), which correspond closely to those observed in fig. 19, Plate LVII.

dislocation of layer 2 moves towards layer edge 1, as in (ii), then the increasing length of edge attached to the dislocation still marks a difference in height of one molecule. This applies to an area in which, previous to the movement of the dislocation, no such difference in height had existed. The movement of the dislocation, in fact, has caused a depression of the lattice on one side of the step. As soon as the dislocation crosses edge 1 the lattice to the right of the dislocation, and hence the step QR, is depressed by one lattice spacing. Therefore PQ of layer 2 and QR of layer 1 (see (ii)) are at the same level, mark steps of the same height, and meet at a point. Similarly, TQ of layer 2 and QS of layer 1 are now at the same level, mark steps of the same height, and meet at a point. In other words, PQR and TQS are now distinct steps which touch at a point Q.

If, after the situation shown in (ii) has been reached, a slight amount of growth or dissolution takes place, then the two layer edges will move apart. Dissolution will take place at these very sharp corners at Q, so as to round these corners off to a curvature not greater than that of the critical nucleus, and this, followed by a slight amount of growth, would produce the situation shown in (iii), which can be compared with fig. 19.

It is possible for layer shapes of the type of 1 and 2 to be produced by dissolution alone. Such a mechanism cannot have been responsible in this case because of (*a*) slight, but important, differences of edge shape very close to the dislocations, (*b*) the closeness of other layers, which show no signs of dissolution themselves, and which would also prevent the ideal conditions necessary for the production by dissolution of layer shapes of this type.

Fig. 22

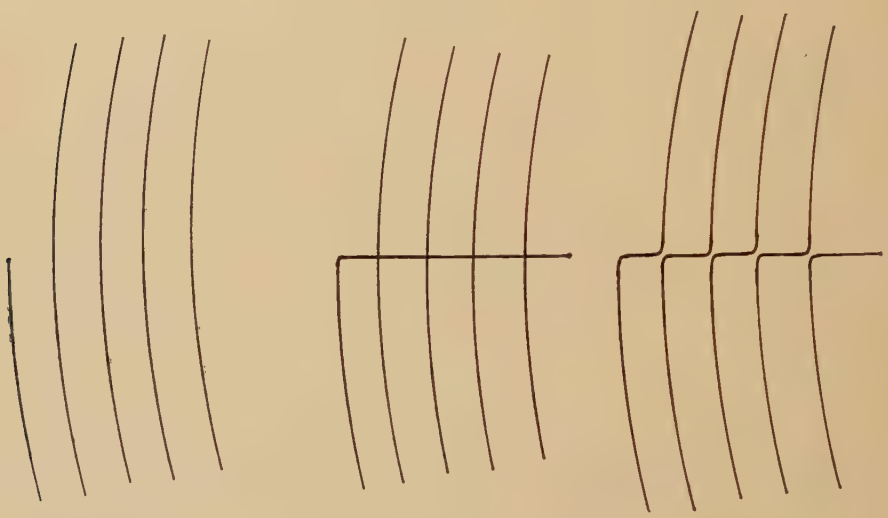

The type of layer shapes produced by movement of a single dislocation across a number of layers.

The distance moved by the dislocation was approximately 24 microns. The direction of movement has been partially masked by slight subsequent growth, but was almost perpendicular to the *c*-axis.

Example 12

Consider first the movement of a dislocation across a number of layers (fig. 22). This is merely an extension of the case considered immediately above. If the original position be as in (i) of fig. 22, with the levels of the layers as marked, movement of the dislocation downwards will give (ii), and subsequent slight dissolution at the sharp corners will produce (iii). Thus such circumstances will typically produce

(*a*) a series of kinked layer edges in which the short sections of the kinked edge are roughly co-linear for all the layers, and

(*b*) layer-edge shapes such that the right- and left-hand sides of any kinked edge are respectively co-linear with one of the branches of either the upper or lower neighbouring kinked edges.

These two conditions will become less obviously applicable as growth proceeds after movement of the dislocation, as the abrupt kinking will tend to be grown out, while the co-linearity of the now different layers will also gradually be destroyed.

A situation almost identical with the single case of fig. 22 is shown in fig. 23, Plate LVII. Unfortunately the visibility is low in the area of interest which is contained by the arrows. Within this area the situation corresponds very closely to fig. 22 (iii), except that the layers have a decreasing spacing. One point of note is that the short kinks, which are strictly co-linear, lie perpendicular to the *c*-axis, and would normally be rapidly eliminated by growth. The dislocation therefore probably moved after growth had ceased. Although the significant features are of too poor visibility to show well in reproduction, it is possible to decide from the layer shapes that the dislocation probably moved upwards in fig. 16. The point where the dislocation came to rest cannot be decided with any certainty.

§ 4. Limited Slip-Zones

Some examples of limited slip-zones have already been shown (Griffin 1951). Another typical example is shown in fig. 24, Plate LVII. As observed on a crystal surface these features consist of a line of dislocations which is divided about the centre into two equal groups of opposite hand.

Limited slip-zones may conceivably be formed from the perfect lattice by slip taking place over part of a crystal plane. If the initial three-dimensional nucleus of a crystal is composed of perfect lattice it may be that processes of this kind result in the formation of dislocations in the lattice, thereby enabling the seed to continue to grow steadily at low supersaturations. However, the stresses necessary to produce slip in a perfect lattice are very high, and limited slip-zones are sufficiently common on some crystals of beryl for it to be obvious that most of them must have been formed when the lattice was no longer perfect, by some mechanism requiring much smaller stresses for the creation of dislocations. A mechanism admirably suited to account for all aspects of these features is provided by the multiplication process of Frank and Read (1950).

In this process it is assumed that a dislocation line is anchored at two points. Under a sufficient stress this line will move outwards in the slip plane to encompass a larger area, and in doing so will eventually touch itself and so create a series of closed dislocation loops, in a way precisely similar to the behaviour of a double dislocation loop in the dislocation theory of growth. In this way a large number of dislocations can be generated from a single dislocation line.

The shape and spacing of the loops so produced will be dependent on the stress, the elastic constants of the material, and the length of dislocation line which is acting as a source. If we consider a number of loops spreading out from a source and expanding in the slip-plane it is obvious that we have precisely the conditions for limited slip-zone formation. The dislocation loops will normally be compound in form (i.e. neither true edge nor true screw), so that intersection of a loop and a face will result in two points of emergence of dislocations with screw components of opposite hand (except in special cases). The two ' dislocations ' (or, strictly speaking, the two points of emergence of the same dislocation line) will continue to move outwards from the original point of contact while the ' source ' continues to be active. (Stages in this development are shown diagrammatically in fig. 25.) When the

Fig. 25

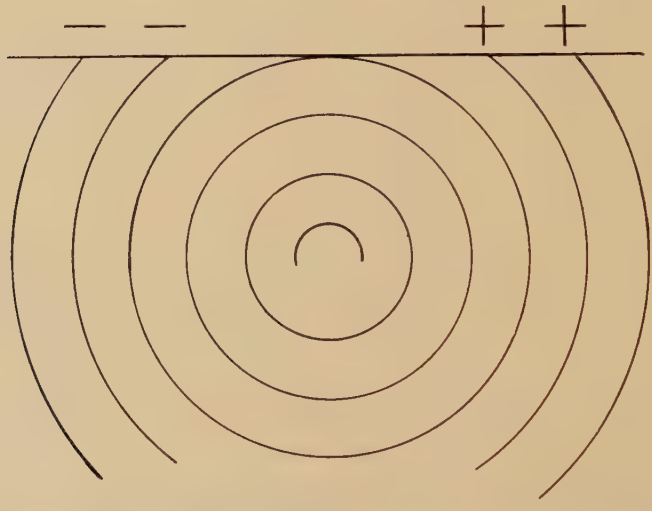

A section in the slip plane representing the action of a Frank–Read source in an isotropic material. The central arc represents the expanding ' source ' dislocation line which produces the closed dislocation loops shown. Each of these loops expands to cut the crystal face in two points, the screw components at the two points of intersection of each loop being of opposite hand.

dislocation lines come to a halt, either because of removal of the stress or other reasons, the ideal situation to be seen will consist of a movement step one unit high at the left- and right-hand extremities and steadily increasing in height towards the centre.

The presence on the face of a closely spaced layer system before the source was active can result in a more complex situation. The various stages which would be observed on the face of the development of the slip-zone are shown diagrammatically in fig. 26. (Stages (i) to (iv) of

this figure are drawn, for the sake of clarity, as if dissolution was taking place simultaneously with the movement of the dislocations. This allows the connections between different layers to be shown, although in practice it would be impossible to resolve them.) Figure 26 (i) shows the situation when the first loop has just intersected the surface and the two dislocations are moving away from the point of contact. In fig. 26 (ii) the dislocations have cut the first two-layer edges, producing unit kinking. The original pair of dislocations are continuing to move outwards in fig. 26 (iii), leaving a series of layers behind them showing unit kinking, and meanwhile another dislocation loop has intersected the surface, the

Fig. 26

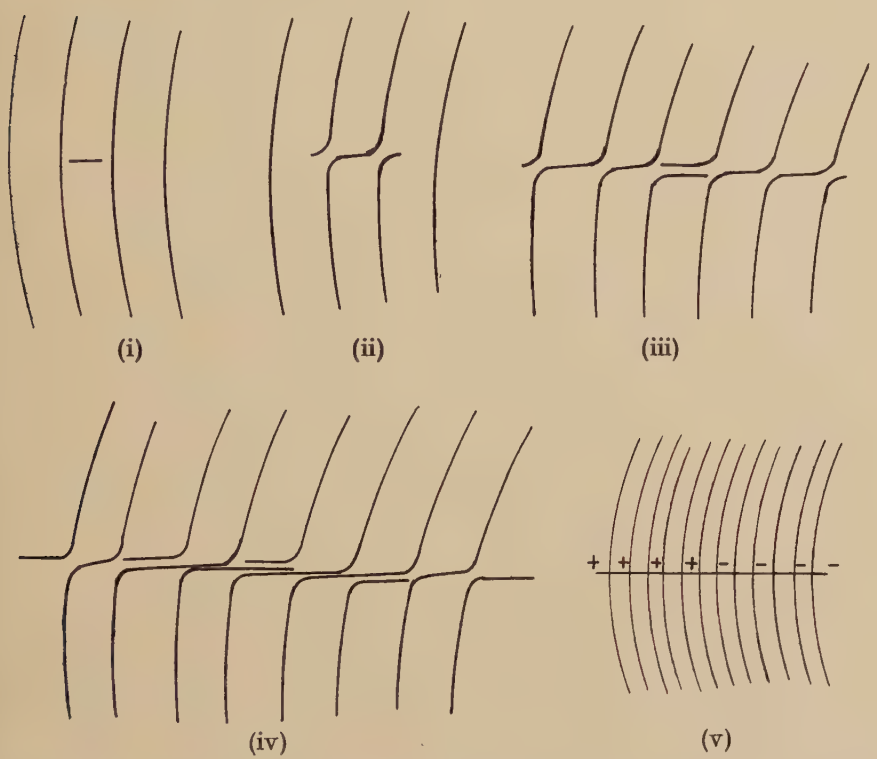

The development of a limited slip-zone as observed on a crystal face with a layer system already present.

two dislocations attaching edges as shown. These two dislocations are just about to cut other layer edges, and so produce two doubly kinked layers. In fig. 26 (iv) the slip-zone is limited on left and right by dislocations which are moving outward and contain a series of layers showing unit kinking until the second pair of dislocations are met with. Between this pair all layers show double kinking as far as the centre of the

system, where the third pair of dislocations is now moving outwards and the left-hand dislocation of the pair is about to cut a layer edge and so produce triple kinking. (The asymmetry of attachment of this central dislocation pair is due to the asymmetrical nature of the kinking process.) The next pair of dislocations to be produced will be attached, in the same way, to a singly kinked and a triply kinked layer edge, producing quadruple kinking on intersection with other layer edges and so on. The type of layer structure which would normally be seen in practice after processes of this kind is shown in fig. 26 (v), where the plus and minus signs indicate the presence of dislocations.

Further growth on this face will result in the advance of the main layer system, so that layers not attached to dislocations would have the kinks grown out by cross-linking and growth together, these layers eventually passing through the dislocation group, while at the same time linking of dislocations of opposite hand will take place (in the way discussed in a previous paper). Eventually, a layer system will be centred on the dislocation group as shown, for example, in fig. 24. (It is, of course, possible for the dislocation group to be completely 'dominated' by the incident layer system, but this is not normally observed.)

Thus it can be seen that the examples of limited slip-zones so far shown are derived from sources which were active before growth ceased. The processes shown in fig. 26 can only be observed if sources have been active either just before, or after, growth ceased. Examples of this kind are shown in figs. 27 and 28, Plate LVIII and fig. 29, Plate LVII.

In fig. 27 the source appears to have been active along the line indicated, and in the original it is possible to trace the kinking of some of the layers. A layer count above and below the zone from the last dislocation on the left, to show definite evidence of layer kinking, gives a difference in count of two layers, although it is possible to distinguish a number of dislocations.

The same type of behaviour is shown in fig. 28. On the right of the light patch which blocks out part of the zone it is again possible to trace the kinking between layers. (Unfortunately, in the general area in which figs. 27, 28 and 29 were observed the visibility of the layer edges was poor. Largely because of this no additional information could be obtained from observation with a 2 mm oil immersion objective, as compared with the 4 mm objective of N.A. 0.95 with which these pictures were taken.) A layer count of this zone gives an equal number of layers above and below, so that the development is presumably of the ideal kind.

A well-developed slip-zone is shown in fig. 29. At either end of the zone, where the degree of kinking is less, it is again possible to trace out the kinking between layers, and some dislocations can be seen.

In all three cases the zones are approximately parallel to the c-axis of the crystal. Other features similar to these have been observed, but only in these cases was it possible to trace the connection between some of the layers in the zone.

On another crystal features were observed which may correspond to limited slip-zones of considerable extent, in some cases extending from edge to edge of the face, and having been developed either just before, or after, the cessation of growth. The orientation of these features corresponded approximately to the trace of pyramidal planes in the face. However, there were always certain aspects of these features which could not be explained purely in terms of the movement of dislocations, so that similar evidence from other crystals is needed before any definite decision can be made about them.

The number of dislocations present in limited slip-zones would be expected to vary widely, and this is found to be the case. The spacing of the dislocations will be largely governed by the factors influencing the shape and spacing of the dislocation groups, and is found to vary considerably.

The distance apart of the two dislocation groups will also depend on the distance of the source from the face. If the source lies very close to the crystal face (and the other conditions are appropriate) the spacing between the two groups will be very small. On the other hand, if the source is far from the face the loop will be large by the time that it touches the face, so that a considerable section of the loop may be almost tangential to the face. This will result in the two groups being widely separated even if the original loops were closely spaced. When sufficiently far apart each group will be identical with, and act as, a lineage boundary. The table below gives approximate figures of the number of dislocations and their average spacing between dislocation groups for a number of the smaller limited slip-zones which have been observed.

Total number of dislocations	Average spacing of dislocations (microns)	Distance between two groups (microns)	Orientation relative to *c*-axis
12	1·7	12	parallel
12	4·0	15	parallel
22	1·6	8	parallel
24	4·1	20	parallel
34	1·8	1·5	perpendicular
64	1·5	27	perpendicular
100	0·9	50	parallel

Features which have long closely packed lines of dislocations, almost certainly in the form of limited slip-zones, are not uncommon, but these are not listed in the table as it is difficult to obtain accurate information from them. These features are marked by lines of ' rods ', a short stubby type of projection which will be discussed fully in a later paper in this series. For our present purpose it is only necessary to know that these rods only occur in areas which have a steep gradient parallel to the *c*-axis.

The size of the rods in any one area is directly related to the steepness of the gradient, or, in this case, the difference in height at a discontinuity in level. These features are typically observed as a long line of ' rods ' producing a sudden break in the layer system, and in the simplest cases the rods increase steadily in size towards the centre of the feature, tailing off gradually towards each end. This indicates that the sudden change of level is greatest at the centre, and this can often be confirmed by examination of the layer topography. Many dislocations can often be observed lying along the bases of the ' rods ', but it is often not possible to determine the sign of these dislocations. However, after the line of ' rods ' ceases the line of the feature is sometimes continued by a row of dislocations, all of the same hand. Thus the evidence is entirely in favour of these features consisting of either large single slip-zones or, in some cases, of series of contiguous slip-zones resulting from the simultaneous activity of several sources in the same, or neighbouring, planes.

Features of this kind are too large for reproduction if the layers are to be satisfactorily resolved, but a feature which is in some ways similar is shown in fig. 30, Plate LIX. In this figure the magnification is too low for the layers to be satisfactorily resolved, but the main features can be distinguished.

In this case two boundaries contain a strip, these boundaries being marked over most of their length by ' rod ' structures which eventually end at the top of the figure in a more easily observed layer system. The right hand of the two boundaries starts first at the bottom of the figure and is distinguished by a line of small rods. It can be observed from the general nature of the layer structure that there is a steady decrease in height from the bottom to the top of the figure. Thus the sudden appearance of a line of rods can only be due to the commencement of a discontinuity in level due to the presence of a number of dislocations. (At higher magnifications it is possible to see that below this line of rods the boundary is marked by a line of thirty or more dislocations, all of the same hand.) When the right-hand boundary is roughly level with the start of the left-hand boundary the rods decrease in size and then disappear, indicating an approximate equality in level between this boundary and the layer system to the right. The boundary is blank for a considerable length and the rods then again increase to a maximum size and then decrease again, indicating equivalent variations in level. After another short blank stretch the rods again appear and build up rapidly to become very large, showing that in this region the central strip must be much higher than the layer system on the right.

At the lower end of the left-hand boundary the rods again point to the right, indicating that the layer system on the left is above the level of the strip. As one moves upwards this rod structure increases rapidly in size until it soon fills the whole of the central strip. The rods then decrease and eventually become very small before a blank section of the

boundary is reached. Another rod system then increases and decreases in size until another blank section of the boundary is reached. Above this point a rod structure commences which points to the *left* and gradually increases in size. This means that the central strip is now above the level of the layer system on the left (as it is also on the right).

Figure 31 shows diagrammatically cross-sections of this area along the lines indicated in fig. 30. It can be seen that these variations in level of the strip cannot be correlated with layer spacing inside and outside the strip, as the layer spacing inside the strip is consistently larger and bears no relation to the layer systems on either side. Such variations in level can therefore only be due to the presence of groups of dislocations, and it seems probable that some form of slip process (presumably due to

Fig. 31

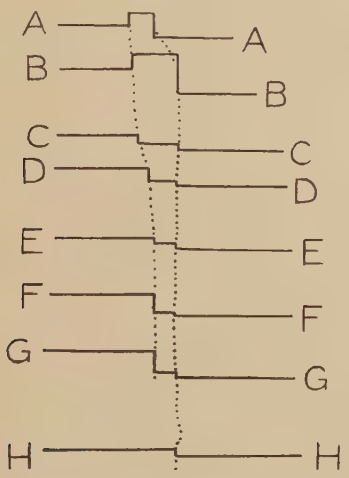

Approximate cross-sections across the feature shown in fig. 30, Plate LIX.

the simultaneous action of a number of different sources) has produced this curious ' buckled ' strip. Although the boundaries of the strip are mainly approximately perpendicular to the *c*-axis, there is one section where the deviation is considerable.

§ 5. Conclusions

The many slight movements of single dislocations which have been observed do not show, except over very small areas, any correlation between the sign of the dislocation and the direction of movement. As the energy of a dislocation is high, probably being several electron volts per atomic layer in beryl, there will be a considerable effective line tension on each dislocation. Consequently many of these slight movements probably correspond to a straightening and shortening of the dislocation lines, the movement possibly being aided by local internal stresses.

The various stages, and degrees, of development of limited slip-zones which have been observed provide evidence in favour of the action of Frank–Read ' sources ' which is almost as direct and conclusive as one could expect to obtain from static surface studies. As dislocation ' sources ' of this type produce considerable amounts of slip in a material as strongly bound as beryl, it appears probable that this process is of application to a wide variety of substances.

Particularly in the case of the movement of single dislocations, it is possible in some cases to fix a time scale, for, as has been shown, the movement must have taken place in the time interval between two cross-linkings. Unfortunately the rate of advance of a layer, which necessarily governs this time scale, must be assumed, and could vary between very wide limits, so that the time scale for any one crystal must remain entirely arbitrary.

The basal plane (0001) and the first-order prism planes $\{10\bar{1}0\}$ appear to be the common slip planes in beryl. Observations on (0001) faces of beryl have provided independent evidence of the $\{10\bar{1}0\}$ family of slip planes.

Acknowledgments

I should like to thank the Department of Scientific and Industrial Research for a grant which has made this work possible. I am also grateful to the Keeper and staff of the Mineralogy Department, British Museum, for the loan of specimens of beryl.

References

Frank, F. C., and Read, W. T., 1950, *Phys. Rev.*, **79**, 722.
Griffin, L. J., 1951, *Phil. Mag.*, **42**, 1337.

LXXX. *On the Possible Relation of Galactic Radio Noise to Cosmic Rays*

By G. W. Hutchinson
Cavendish Laboratory, Cambridge*

[Received May 6, 1952]

Abstract

The possibility is considered that cosmic rays are accelerated in regions of the galaxy of intermediate particle density ($\approx 10^9$ cm^{-3}). It is found that a conservative estimate of the magnetic fields in such regions would lead to a radio noise flux of the observed order of magnitude, and that the observed spectrum could easily be produced. A possible cause is suggested for the low energy cut-off in the cosmic-ray spectrum. If the proposed mechanism accounts for any large proportion of the cosmic rays, these should be accompanied by a small flux of γ quanta which should show the same anisotropy as the galactic radio noise.

The observed energy flux falling on the earth's atmosphere as galactic radio noise of frequency between 2×10^7 and 10^8 c/sec is of the order of 3×10^{-7} that of cosmic rays. This disparity has led several authors to seek to explain radio noise as an interaction of cosmic-ray particles with the galaxy. Radio frequency radiation due to radiative collisions between protons and electrons in interstellar gas gives much too weak a flux, and that from the Cherenkov effect of relativistic particles passing through hydrogen could only account for the observed radio flux under extremely improbable conditions of low temperature ($\leqslant 0{\cdot}01$°K) and ion density (proportion of ionized atom $\leqslant 10^{-4}$). Ginsburg (1951) has shown that the radio noise could only be produced by the interaction of cosmic rays with a general galactic magnetic field of 10^{-6} gauss, if the flux of electrons of energy $\approx 10^9$ ev in the galaxy were some three times the proton flux observed in the primary cosmic rays. However, it has now been shown by Gold (1952) that the polarization of starlight, which was thought to be the strongest experimental evidence for the existence of such galactic fields, can be explained by other means. It is therefore uncertain whether such general fields exist in the galaxy, and it is of interest to examine the interaction between cosmic rays and regions of local field concentration. Ginsburg (1951) and Alfven and Herlofson (1950) have concluded that such regions would have to be assumed very different from our own solar system ; but this is to be expected, since the observed radio noise requires the existence of sources very much stronger than the sun.

The most favourable assumption is that such regions are themselves the source of cosmic rays. In want of a non-electromagnetic theory of cosmic-ray acceleration, this seems indeed very probable. Kwal (1951)

---

* Communicated by the Author.

has considered the case of a flux of high energy protons in a stellar envelope with a field of the order 10^3 gauss, and has concluded that this might explain the solar contribution to the radio noise. If a comparable flux of fast electrons were supposed to accompany the protons, the energy flux of galactic radio noise could also be explained in this way; but there would remain the difficulties:

(*a*) that the observed radio sources do not coincide with bright visible objects; and

(*b*) that the ionization density in such regions would almost certainly be high enough to give rise to a strong circular polarization (cf. Ryle 1950) which is not observed in the galactic radio noise.

It seems at least possible that cosmic-ray acceleration would take place in regions of comparatively low density such, for instance, as might be associated with nova shells or with condensations of matter in the early stages of star formation. It is of special interest to consider the production of radio noise in such regions since the identification by Bolton, Stanley and Slee (1949) of a radio source with the seat of a super nova explosion, the Crab nebula. We shall therefore consider what properties must be postulated for the regions so that the production in them of the observed cosmic-ray flux would simultaneously give rise to the galactic radio noise.

§ 1. Postulated Source Regions

If the local magnetic fields were in thermodynamic equilibrium with the thermal motions of the matter, they might be large; but in the absence of any complete theory of such fields we shall make the much more stringent assumption that they are so restricted that the radius of gyration of electrons in thermal motion is large compared to their mean free path for collisions involving the transfer of a large fraction of their energy (cf. Hoyle 1951). This leads to the approximate relation

$$H \leqslant 4\pi c e^3 m^{1/2} (\tfrac{3}{2} kT)^{-3/2} N,$$

where T is the temperature, N the particle density and e and m the charge and mass of an electron. Thus if T is expressed in °K, then to order of magnitude

$$H \leqslant 10^{-12} N \left(\frac{T}{10^4}\right)^{-3/2}. \qquad \ldots\ldots (1)$$

Most of the observed radio noise sources subtend angles less than 6–8′ at the earth (though exceptions do occur (Bracewell 1952)), and at least some are at distances not less than 10^{18} cm (Smith 1951). If many of them are within our galaxy, they are presumably at distances comparable with interstellar distances, and may thus have linear dimensions $D \leqslant 10^{15}$–10^{16} cm. For charged particles to be accelerated over a long path within the regions we require a mean free path for the collision of energetic particles, $\lambda \ll D$, and a radius of gyration $R \ll D$. These conditions could be satisfied, for particles of energy $10^8 < E < 10^{15}$ ev, by putting $H \geqslant 10^{-3}$ g and $N \leqslant 10^{11}$ cm^{-3}.

Leaving unspecified the precise mechanism of particle acceleration, but only assuming it to be electromagnetic in nature, we must assume that the region would contain a flux of both protons and electrons of high energy. These would only be strictly bound within the region on rather special assumptions, but the tendency for charged particles to escape might well be small. The predominant mode of escape would then be as the uncharged products of collisions—neutrons and γ quanta. The quanta would subsequently nearly all escape from the galaxy without interaction, but those neutrons with $E<10^{15}$ ev would have a proper time for traversing the thickness of the galaxy long compared to their half-life for β decay, and would thus give rise to a cosmic-ray proton flux. Neutrons of energy $E=10^{9\cdot5}$ ev would travel only about 10^{14} cm during a proper time equal to their half-life and would thus seldom escape from the accelerating regions. These assumptions would therefore lead naturally to the observed low energy cut-off in the cosmic-ray spectrum by a mechanism entirely different from that proposed by Unsöld (1951), which would produce a flattening of the energy spectrum, rather than a cut-off, at low energies. The decay electrons would in general receive only a fraction of the neutron energy of the order of the ratio of the masses of electron and proton, and would therefore not contribute appreciably to the observed cosmic-ray flux.

Since it is known (Perlow and Kissinger 1951) that quanta (at least those of low energy) form not more than a few per cent of the cosmic-ray flux, we must suppose that the mean path of a charged particle in the galaxy is much longer than that of a γ quantum. We must, however, assume in any case that the proton paths are very much curved in the galaxy to account for the observed high degree of isotropy in cosmic rays.

Since most of the cosmic-ray energy flux is carried by particles of $E<10^{11\cdot5}$ ev, and the radius of gyration of a particle of this energy in a field of 10^{-12} gauss is $R\approx10^{21}$ cm, which is comparable with the thickness of the galaxy, we need not assume any galactic field in excess of that required by relation (1) in order to ensure this for all but the higher energy particles. If the most energetic cosmic-ray particles have a galactic origin, it is difficult to explain their isotropy without a large general galactic field.

§ 2. The Interaction of Electrons with the Field

The energy of the electron flux will be partly radiated into the galaxy as γ quanta, of energy comparable to the electron energies, due to collisions with nuclei, and to a less extent as low energy quanta due to interaction with the field, some of which will fall in the radio noise frequencies. The latter process is described by the theory developed by Vladimirskii (1948) and Schwinger (1949). Thus the rate of energy radiation along the path of the electron is

$$-\frac{dE}{dx}=\frac{2}{3}\left(\frac{e^2}{mc^2}\right)^2\left(\frac{E}{mc^2}\right)^2H^2, \quad \ldots\ldots \quad (2)$$

where H is the component of the magnetic field perpendicular to the path (which we shall assume to be of the same order as $|H|$). Most of the radiation is at frequencies of order

$$\nu_1 = \frac{1}{2\pi}\frac{eH}{mc}\left(\frac{E}{mc^2}\right)^2 \quad . \quad . \quad . \quad . \quad . \quad . \quad . \quad . \quad (3)$$

and the spectrum is roughly as shown in fig. 1 (which is plotted from figures given by Vladimirskii (1948)), the intensity varying with $(\nu/\nu_1)^{1/3}$ for $\nu \ll \nu_1$.

The ratio of the total low-frequency radiation flux to the γ flux from electrons of energy E is

$$\frac{W(H)}{W(\gamma)} = -\frac{dE}{dx}\frac{\lambda}{E} = \frac{2}{3}\left(\frac{e}{mc^2}\right)^4 EH^2\lambda, \quad . \quad . \quad . \quad . \quad . \quad (4)$$

Fig. 1

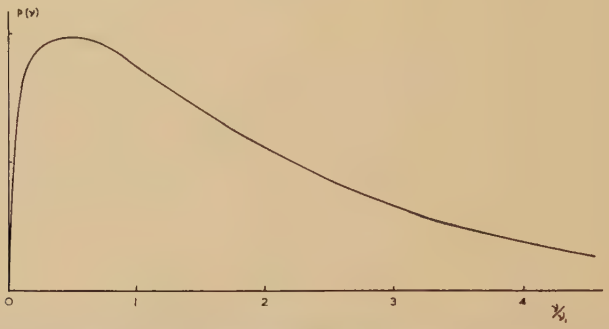

The spectrum ($p(\nu)$) of electromagnetic radiation emitted by an electron moving in a magnetic field.

where λ is the mean free path for energy loss by radiative collision. The fraction of $W(H)$, $[W(R)]/[W(H)]$, which lies in the frequencies $2\times10^7<\nu<10^8$, can be obtained by integrating fig. 1, and from this we can find $f(E)=[W(R)]/[W(\gamma)]$. For a fixed value of ν_1, $[W(R)]/[W(H)]$ and E^2H are constant, and, using eqn. (4), we can thus obtain a general relation between f and E for all values of H and λ by plotting $f\lambda^{-1}H^{-3/2}$ against $H^{1/2}E$. This is shown in fig. 2, in which the units are cm, gauss and electron volts.

The observed ratio of flux of radio noise to cosmic-ray γ component will correspond to the value of f averaged over the energy spectrum of the electron flux within the sources. This spectrum is not known, for it cannot be assumed to be the same as the observed spectrum of primary cosmic rays, but it is plausible to assume that it is a steeply decreasing function of E. If, then, we consider only those electrons of such energy that $H^{1/2}E>10^{6\cdot1}$, we may assume that a large fraction will have energies such that $10^{6\cdot1}<H^{1/2}E<10^{8\cdot1}$. In this case, from fig. 2, the observed ratio, F, will be given by

$$0\cdot5<\frac{F}{\lambda H^{3/2}}\times10^{19}<1\cdot6,$$

and we may, without much error, put

$$F\approx10^{-19}\lambda H^{3/2}. \quad . \quad . \quad . \quad . \quad . \quad . \quad . \quad . \quad (5)$$

For hydrogen λ is of order $10^{26}N^{-1}$ cm, so that, if H has the maximum value allowed by relation 1,

$$F \approx 10^{-2}N^{1/2}T^{-9/4}. \quad \ldots\ldots\ldots \quad (6)$$

The observed value of this ratio is of order 3×10^{-4}, if we take the γ component to contain 0·1% of the energy of primary cosmic rays (Perlow and Kissinger 1951); thus we must put

$$T^{9/2}N^{-1} \approx 10^{3}. \quad \ldots\ldots\ldots \quad (7)$$

If, for example, we suppose $N=10^{9}$, then we require $T \approx 10^{2\cdot7}$ °K, which is lower than the accepted value for interstellar gas (10^{4} °K), but not improbable if the region were able to radiate thermal energy through the presence of even small quantities of dust. In this case we should have to assume the order of magnitude of $H \approx 10^{-1}$ gauss, and the lower energy limit of the electron flux contributing to the radio noise would be $E \approx 4$ MeV. Most of the resultant γ quantum energies would thus be in the range investigated by Perlow and Kissinger (1951).

Fig. 2

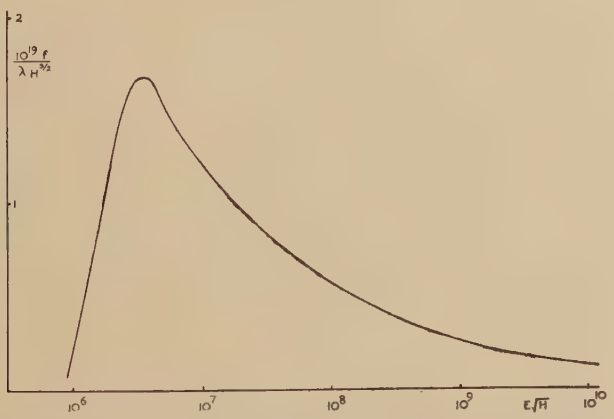

The relation between electron energy and the ratio of its radiation loss at radio noise frequencies to that as γ quanta.

The frequency spectrum of the radio noise could only be deduced if both the energy spectrum of the electron flux and the variation both of the flux and of H throughout the source regions were known. In the absence of this knowledge it is only worth while to show that it would not be grossly dissimilar from the observed spectrum.

If we assume uniform flux and field, take the very rough approximation for the spectrum of fig. 1,

$$p(\nu) \sim \nu^{1/3} \quad \text{for} \quad \nu<\nu_1$$
$$p(\nu) = 0 \quad \text{for} \quad \nu>\nu_1,$$

and assume the energy spectrum of the electrons to be

$$N(E) \sim E^{-\alpha},$$

then a straightforward integration leads to the noise spectrum

$$I(\nu) \sim \nu^{\left(1-\frac{\alpha}{2}\right)}.$$

If the electron spectrum is similar to that of primary cosmic rays $2<a<2{\cdot}5$ and $-0{\cdot}5>(1-a/2)>-0{\cdot}75$, which is compatible with the observed spectrum (Ryle 1950).

§ 3. Conclusion

These expressions must be regarded as very approximate, but they serve to show that we should expect considerable variation of source strength with temperature and a smaller variation with density. The observation that the few discrete radio noise sources at present identified with extra-galactic nebuli (Hanbury-Brown and Hazard 1952) show some tendency to be associated with those of low optical brightness may thus favour the assumption of an inverse relation between magnetic field and temperature, such as we have assumed.

It is clear that even if the magnetic fields produced by the random motion of matter are much less than would be required by equipartition of energy, plausible conditions can still be postulated in which the production of cosmic rays by an electromagnetic process would lead naturally to the observed radio noise flux. If such a mechanism is indeed an important source of radio noise, the γ component of primary cosmic rays should show the same marked anisotropy as that of the galactic radio noise. More experimental evidence on the magnitude, spectrum and direction of this component would be very desirable.

The presence of nuclei heavier than protons in the primary cosmic-ray flux could not be explained by the escape mechanism discussed above. If such nuclei were accelerated in regions similar to those proposed they would have to escape as charged particles. It would probably be an over-simplification, however, to assume that all cosmic rays are produced in similar sources.

Acknowledgment

I wish to thank Mr. T. Gold and Mr. S. G. F. Frank for many discussions and the administrators of the University of Cambridge Clerk-Maxwell Scholarship Fund for financial support.

References

Alfven, H., and Herlofson, N. 1950, *Phys. Rev.*, **78**, 616.
Bolton, J. G., Stanley, G. J., and Slee, O. B., 1949, *Nature, Lond.*, **164**, 101.
Bracewell, R., 1952, *Observatory*, **72**, 27.
Ginsburg, V. L., 1951, *Doklady Akad. Nauk. S.S.S.R.*, **76**, 377.
Gold, T., 1952, *Nature, Lond.*, **169**, 322.
Hanbury-Brown, R., and Hazard, C., 1952, *Phil. Mag.*, **43**, 137.
Hoyle, F., 1951, *Proceedings of the Conference on the Dynamics of Ionised Media*, London (April.).
Kwal, B., 1951, *J. Phys. et Rad.*, **12**, 66.
Perlow, G. J., and Kissinger, C. W., 1951, *Phys. Rev.*, **81**, 552, and **84**, 572.
Ryle, M., 1950, *Rep. Prog. Phys.*, **13**, 184.
Schwinger, J., 1949, *Phys. Rev.*, **75**, 1912.
Smith, F. G., 1951, *Nature, Lond.*, **168**, 962.
Unsöld, A., 1951, *Phys. Rev.*, **82**, 857.
Vladimirskii, V. V., 1948, *J. Exp. and Theor. Phys.*, **18**, 392.

LXXXI. *Further Aspects of the Trident Process*

By J. E. Hooper, D. T. King,* and A. H. Morrish†
H. H. Wills Physical Laboratory, University of Bristol ‡

[Received May 6, 1952]

Abstract

The division of energy between the secondary particles in the direct production of electron pairs by fast electrons is discussed, and experimental results are compared with the Bhabha theory. The angular separations of the tracks of the secondary particles are considered. An event attributed to pair production by a fast meson is described.

§1. Introduction

A trident has been defined (Powell 1949) as an event, observed in an electron sensitive photographic emulsion, in which an electron pair is created on the path of a relativistic charged particle, presumably by its interaction with an atomic nucleus. Observations of these events have been made in a number of laboratories (Occhialini 1949 ; Bradt, Kaplon and Peters 1950). It has been shown (Hooper, King and Morrish 1951 a) that the great majority of tridents are initiated by fast electrons and that they represent a distinct process and are not due to the chance conversion of a *bremsstrahlung* γ-ray close to the track of the parent particle. In the majority of reported measurements it has been proved that, within the limits of experimental error, a balance of energy exists between the primary and the secondary particles.

Bhabha (1935) has considered the theory of the process, and has shown that a close relationship exists between pair production by a fast ($\beta \sim 1$) charged particle and pair creation by a photon. A Fourier analysis may be made of the field of the incident particle, so that the components are considered as a spectrum of photons. v. Weizsäcker (1934) has shown that the form of this spectrum is given approximately by $1/h\nu$. Bhabha considers the materialization of these photons in the Coulomb field of a stationary particle, and thus evaluates the trident cross section by the use of the theory of Bethe and Heitler (1934). This treatment leads to an expression for the differential cross section of the form

$$dQ = f(Z_1, Z_2, E_-, E_+, B)\, dE_- \,.\, dE_+ \quad . \quad . \quad . \quad . \quad . \quad . \quad (1)$$

where $Z_1 e$ and $Z_2 e$ are the charges of the moving and stationary particles and E_-, E_+ are respectively the energies of the created electron and

* Now at the Office of Naval Research, Washington, D.C.
† Now at the University of British Columbia, Vancouver, B.C.
‡ Communicated by Professor C. F. Powell, F.R.S.

positron. B represents the relativistic factor $[1-(v^2/c^2)]^{-1/2}$ for the incident particle. Equation (1) holds for values of E_-, E_+ within the limits :

$$m_e c^2 \ll E_-,\ E_+ \ll \text{primary energy}.$$

Integration of (1) with respect to E_-, E_+ leads to an expression which, provided the condition

$$B < 2{\cdot}137\,.\,Z^{-1/3}. \quad . \quad . \quad . \quad . \quad . \quad . \quad . \quad . \quad (2)$$

is satisfied, shows that the cross section varies approximately as the cube of $\log_e B$. For values of B exceeding those given by (2) the effects of screening by the atomic electrons must be considered, and Bhabha (1935) taking these into account, derives the more complicated form given by eqn. (47) in his paper. This, however, leads to a variation not markedly different from that given by the simple cubed logarithm relation.

It has already been shown (Hooper *et al.* 1951 a) that the experimental results are compatible with this variation of cross section, but it has not been possible to distinguish between various more detailed theories (e.g. Racah 1937 ; Ravenhall 1950).

§ 2. Energy Division in Tridents

It is notable that in more than 90% of the tridents observed, one of the secondary particles carries away more than half the primary energy ; in more than 50% of the tridents over two thirds of the primary energy is carried away by one of the secondaries. It was suggested that this unequal energy division might reduce the otherwise large effect of the trident process in the early development of electromagnetic cascades (Hooper *et al.* 1951 b).

Integration of (1) over all energies E_+, of the positron leads to an expression which shows that the probability of the electron having an energy E_-, independent of the value of E_+, is approximately proportional to $1/E_-$. Since (1) is symmetric in E_- and E_+, a corresponding relation holds for E_+, and therefore a distribution in energy of the created electrons would, for a particular primary energy, also be of hyperbolic form.

An important feature of these experiments is our inability to distinguish the created electrons with certainty among the secondary particles. Even if the charge carried by each particle was measured with a powerful magnetic field (Dilworth, Goldsack, Goldschmidt-Clermont, and Levy 1950), it would be possible to do no more than identify one of the three secondaries as a created particle.

The distribution of the energies of the created electrons, predicted by Bhabha, suggests that in the majority of events the two created particles are those of lowest energy. In this work we have designated the secondary particle energies E_1, E_2, and E_3, in order of decreasing magnitude, so that E_2 and E_3 are taken, by convention, to represent the materialization of a ' virtual ' photon.

Our measurements have been made on 56 tridents which occurred in plates exposed to the cosmic radiation ; thus the energy of the primary particles may lie between 60 MeV and 100 BeV. Nevertheless, a distribution of the values of E/E_T, where E_T is the primary energy, should be hyperbolic, of the form $E_T/E-1$. A histogram on which the values of both E_2/E_T and E_3/E_T are plotted is shown in fig. 1. It may be seen that for the lower values of $E_{2,3}/E_T$ the histogram is in satisfactory agreement with the hyperbolic curve, which is a normalized plot of the function $E_T/E-1$. It is clear, however, that on account of our convention in designating the created particles, the histogram cannot extend beyond $E_{2,3}/E_T=0{\cdot}5$.

Fig. 1

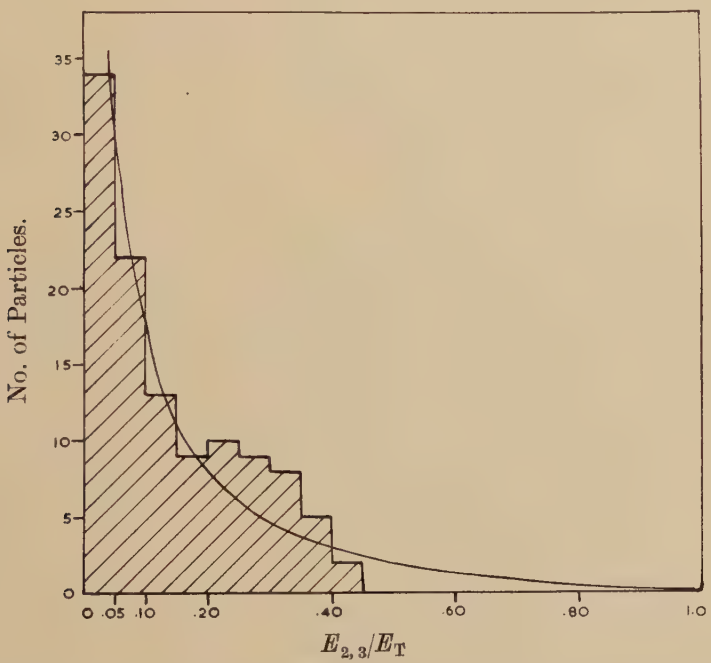

The distribution in values of both E_2/E_T and E_3/E_T. The smooth curve represents the function $E_T/E-1$ drawn to enclose an area equal to that of the histogram.

According to the theory, the secondary particle of highest energy is, in a small proportion of the tridents, one of the created electrons. If we were, in fact, able to identify the created pair particles among the secondaries we might reasonably expect better agreement of the histogram with the theoretical curve.

In fig. 2 we have plotted the distribution of the values of $(E_2+E_3)/E_T$ for all the measured tridents. A recent detailed calculation by Ott (1952) on the basis of the theory of Bhabha predicts that such a distribution has a maximum when the energy of the created pair is about 2 MeV, whatever the

energy of the primary electron. For higher energies of the created pair, the distribution is again approximately hyperbolic, as would be expected. As our primary energies are all greater than 60 Mev, the maximum in the curve which Ott predicts does not suffice to explain the departure of the histogram from the hyperbolic form. We are unable to attribute this result to the use of our convention, although it may be due to poor statistics or a failure to observe those tridents in which the created pair is of very low energy.*

Fig. 2

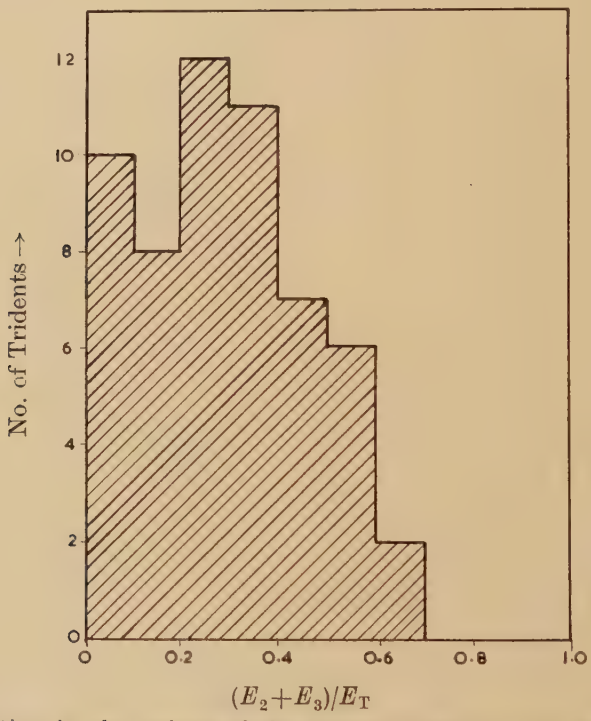

The distribution in the values of the quantity $(E_2+E_3)/E_T$ for each of 56 tridents.

Our results in fig. 1 indicate that in the production of tridents by electrons one of the created pair particles will be, in about 10% of the events, the secondary particle of greatest energy. This figure agrees roughly with that given by the Bhabha theory. A more accurate check on the theory will be possible when the new high energy electron accelerators come into use.

---

* *Note added in proof* :—Ott has recently informed us that he has compared the experimental distribution shown in fig. 1 with a curve deduced from a more detailed theoretical treatment. He states that this comparison also suggests that a considerable number of tridents with very low energy secondaries have not been observed.

§3. Angular Separation in Tridents

Bhabha shows further that, with electron pairs directly created by an electron, the angular separations of the secondary particles with respect to the primary direction are of the order $m_e c^2/E_-$, and $m_e c^2/E_+$ respectively. On the other hand, in electron pairs created by heavier particles, the angular separation is of the order of $1/B$, depending on the energy of the primary particle. The cross section for pair creation by mesons or protons is small compared with that by electrons.

The small angular separations observed for secondary particles in tridents confirm the earlier conclusion (Hooper *et al.* 1951 a) that the great majority of these events are caused by electrons. There are only four events in which the angular separation of one of the secondary particles is of the order of 5°, but in these examples we have found that the energy of the particle concerned was less than 10 MeV, not very large in relation to $m_e c^2$. A similar event, described by Occhialini (1949) may be explained in this way. We therefore consider that our observations lend strong support to the Bhabha theory.

Fig. 3

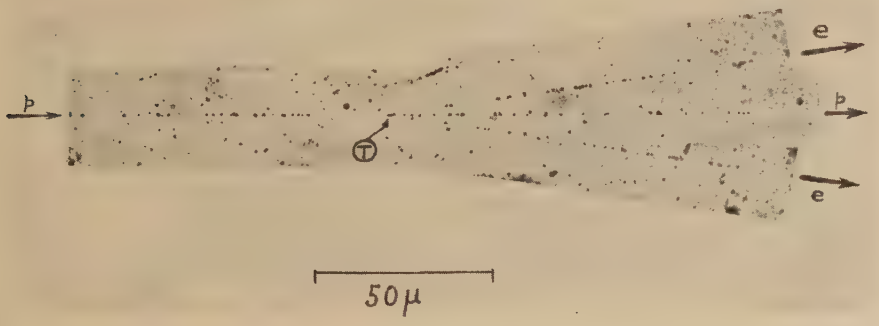

A photomosaic of an event in which a singly charged particle (track *pp*) appears to produce an electron pair (*ee*) at T. It is probable that the incident particle was a meson.

In conclusion we describe in detail a trident which is remarkable in several respects. This event is shown in fig. 3. The grain densities in all the tracks have the minimum value; scattering measurements on the track of the incident particle *p* indicate a primary energy of about 1200 MeV and there is no measurable angular deviation at T in *pp*. The two tracks marked *e* are each of energy about 50 MeV, so that it is reasonable to assume that *ee* represent a created electron pair.

The notable features of the event are the wide angle and the symmetry in both angle and energy of the secondary particles. We note that for this example the condition

$$m_e c^2 \ll E_-,\ E_+ \ll \text{primary energy}$$

is valid, irrespective of the mass assumed for the incident particle.

The magnitude of the separation angles ($8\frac{1}{4}^{c}$ each) is consistent with the view that the primary particle is a π or μ meson, for which the value of B is about 8.

It is significant that in the observations on the 5 mm track of the primary particle there is no evidence, such as radiative energy loss, which would conflict with this interpretation.

Acknowledgments

In the course of these investigations we have enjoyed discussions with Dr. R. H. Dalitz, and Mr. K. Gottstein, who have brought several points to our attention. We are further indebted to Professor C. F. Powell, F.R.S. for his continued interest. One of us (A.H.M.) wishes to acknowledge a maintenance grant from the N.R.C. of Canada. The work forms part of a programme supported by D.S.I.R. to which one of us (J.E.H.) is indebted for a maintenance grant.

References

Bethe, H., and Heitler, W., 1934, *Proc. Roy. Soc.* A, **146,** 83.
Bhabha, H. J., 1935, *Proc. Roy. Soc.* A, **152,** 559.
Bradt, H. L., Kaplon, J., and Peters, B., 1950, *Helv. Phys. Acta*, **23,** 24.
Dilworth, C. C., Goldsack, S. J., Goldschmidt-Clermont, Y., and Levy, F., 1950, *Phil. Mag.*, **41,** 1042.
Hooper, J. E., King, D. T., and Morrish, A. H., 1951 a, *Phil. Mag.*, **42,** 304 ; 1951 b, *Can. Journ. Physics*, **29,** 545.
Occhialini, G. P. S., 1949, *Nuovo Cim. Supp.*, **6,** 413.
Ott, K., 1952, private communication.
Powell, C. F., 1949, *Nuovo Cim. Supp.*, **6,** 379.
Racah, G., 1937, *Nuovo Cim.*, **14,** 93.
Ravenhall, D. G., 1950, *Proc. Phys. Soc.* A, **63,** 1177.
v. Weizsäcker, K. F., 1934, *Z. Physik*, **88,** 612.

LXXXII. *The Binding Energy of the Thomas–Fermi Atom*

By J. M. C. Scott
Cavendish Laboratory, Cambridge*

[Received May 19, 1952]

Abstract

The Thomas–Fermi statistical model of the atom leads to the formula $20{\cdot}92\,Z^{7/3}$ ev for the total binding energy of an atom with atomic number Z, but this formula gives values which are too high by roughly 20%. The actual binding energies increase quite smoothly with increasing Z, which suggests the existence of a more appropriate formula.

The reasons for the discrepancy are explained and a new theoretical formula derived. This is compared with spectroscopic and self-consistent field data and is found to agree within 1 or 2%. Some uncertainty remains about the relativistic correction for heavy atoms.

§1. Introduction

The Thomas–Fermi statistical model of the atom leads to the formula $20{\cdot}92\,Z^{1/3}$ ev for the total binding energy of an atom with atomic number Z. It is known that the values given by this formula are some 20 or 30% higher than the experimental binding energies derived from spectroscopy. The actual binding energies of light atoms are found to increase very smoothly almost exactly as $Z^{7/3}$, but with a different constant (Young 1929, Allard 1948):

$$W \doteqdot 15{\cdot}73\,Z^{7/3} \text{ ev}. \quad . \quad . \quad . \quad . \quad . \quad . \quad . \quad (1)$$

A different empirical formula has been proposed by Foldy (1951), which is equivalent to

$$W \doteqdot 13{\cdot}60\,Z^{12/5} \text{ ev}, \quad . \quad . \quad . \quad . \quad . \quad . \quad . \quad (2)$$

and which is designed to represent the properties of heavier atoms better.

The purpose of this paper is to explain the reasons for the discrepancy, and to derive a better theoretical formula. This will be shown to be in good agreement with the data.

The failure of the ordinary theoretical formula (due essentially to Milne 1927) can be explained as follows. If one seeks to account for the total binding energy W of an atom within 1 or 2% by a statistical model, it is evidently necessary to make sure that no terms are neglected which are larger in order of magnitude than $1/Z$ times the total energy. There are actually two such terms: one arises from a boundary effect, and is of the order Z^2 and the other is due to exchange and is of the order $Z^{5/3}$.

* Communicated by the Author.

It will be shown that these terms, which have different signs, combine to produce a variation roughly as $Z^{7/3}$ for light atoms (but with a reduced coefficient), in agreement with the data of Young and Allard, and a variation roughly as $Z^{12/5}$ for heavier atoms, in agreement with Foldy's data.

§2. Preliminaries

2.1. *Notation*

All quantities will be expressed in Hartree's atomic units, unless otherwise specified. Following substantially the notation of Schiff (1949) and Condon and Shortley (1935), the electrostatic potential at a distance r from the nucleus is expressed as a fraction $\chi(x)$ of the potential due to the nucleus itself, where $r=bx$; b is a scale factor proportional to the extent of the main part of the charge distribution:

$$b=(9\pi^2/128Z)^{1/3}=0{\cdot}88534\,Z^{-1/3}. \quad . \quad . \quad . \quad . \quad . \quad (3)$$

The total binding energy is denoted by W, and the electrostatic potential at the nucleus due to the electrons only is denoted by $-v$. The symbol v will be used in this sense throughout the present paper.

2.2. *Nature of the Statistical Method*

In the statistical method, it is convenient to think of a fictitious or purely mathematical problem, in which Z is very large, say a million, so that even $Z^{1/3}$ is large, and the terms of any series in descending powers of $Z^{1/3}$ can be clearly separated. The solutions of a non-relativistic wave equation are envisaged, with magnetic effects omitted (i.e. $c\to\infty$, $\alpha\to 0$). The consideration of such an idealized limit helps to clarify the procedure, in the present work just as in the original Thomas–Fermi calculation, despite the air of unreality which it creates.

2.3. *Connection between W and the Electrostatic Potential of the Electrons*

Of the various ways of calculating the binding energy, perhaps the easiest is to relate it to the electrostatic potential $-v$ at the nucleus due to the charge distribution of the electrons. The argument consists in considering the effect of increasing the nuclear charge by a small amount δZ. This change may be regarded as a perturbing field $V(r)=-\delta Z/r$. According to standard perturbation theory, the change in the energy of the ground state is given by an integral containing the perturbing potential and the unperturbed wave functions:

$$\int \psi^* V\psi = -\delta Z \int |\psi|^2/r.$$

But this is equal to the potential at the origin due to a charge-density $-\delta Z|\psi|^2$, and is equal to $-v$ defined earlier. Thus

$$\frac{dW}{dZ}=v. \quad . \quad . \quad . \quad . \quad . \quad . \quad . \quad . \quad . \quad (4)$$

The energy of any electrons which have to be added on the outside of the atom to keep it electrically neutral has been here neglected, but the correction is O(1) which is smaller than any terms which need be retained in the subsequent calculations.

The usual formula for the binding energy is obtained by noting that

$$v=\lim_{r\to 0}(Z/r)(1-\chi)$$
$$=-(Z/b)\cdot\chi'(0). \quad \ldots\ldots\ldots \quad (5)$$

Here b is given by (3), and the derivative $-\chi'(0)$ is Baker's constant

$$-\chi'(0)=B=1{\cdot}5881. \quad \ldots\ldots\ldots \quad (6)$$

This leads to the usually-quoted formulae

$$v=1{\cdot}794\,Z^{4/3} \quad \ldots\ldots\ldots \quad (7)$$

(Lamb 1951, Mack 1950) and, using (4),

$$W=0{\cdot}769\,Z^{7/3}$$
$$=20{\cdot}92\,Z^{7/3}\text{ electron volts.} \quad \ldots\ldots\ldots \quad (8)$$

The latter formula was first given by Milne (1927), but with a numerical inaccuracy which was corrected by subsequent writers, e.g. Baker (1930).

Those corrections which are larger than $1/Z$ times the main term (7) or (8), as regards order of magnitude, will now be investigated.

§3. The Boundary Effect

The boundary effect, which will be considered next, is perhaps most familiar for the case of independent particles confined in a large cubical box (volume L^3). In the zero-order approximation there are $L^3.\frac{4}{3}\pi P^3/h^3$ single-particle wave functions with momentum less than P; and this can be equated to the number N of particles when one particle is assigned to each state. The next approximation, which is easily obtained, corresponds physically to the fact that the density of particles is considerably reduced in the region near the boundary within a distance of say a quarter of the wavelength of the fastest particle, while at interior points the density of particles must be increased by a factor $1+O(N^{-1/3})$ so as to compensate.

In the present application, there are two important differences. First, the boundary which concerns us most is a point instead of a surface. Although the zero-order (Thomas–Fermi) formulae give an electron-density which tends to infinity at the nucleus, it can be shown that the necessary boundary corrections reduce the number of electrons in the boundary region by a finite amount (finite as $Z\to\infty$), and that the density elsewhere is increased only by a factor $1+O(Z^{-1})$, which is negligible for the purpose of the present calculations. Secondly, the field is singular, so that a finite error in the number of electrons in the boundary region (radius $O(1/Z)$, or roughly the K-shell region) causes an error of the order of Z^2 in the binding energy, that is to say a fraction $1/Z^{1/3}$ of the total binding energy, which cannot be ignored in practice.

To calculate this correction quantitatively, the true effect of the K and L shells will be compared with that which is implied by the statistical model. It turns out that hydrogen wavefunctions may be used because the field in the boundary region is sufficiently nearly a Coulomb potential. In the idealized Thomas–Fermi model, the total number of electrons with energy less than $-E$, within a spherical shell of thickness dr, is easily shown to be

$$\frac{Z}{b^3}\left(\frac{\chi}{x}-\frac{bE}{Z}\right)^{3/2} r^2\,dr. \qquad . \quad . \quad . \quad . \quad . \quad . \quad . \quad . \quad (9)$$

Since a shell of charge Q contributes an amount Q/r to the potential $(-v)$ at the nucleus, the electrons with energy less than $-E$ ought to contribute an amount

$$\frac{Z}{b}\int\left\{\chi(x)-\frac{Ebx}{Z}\right\}^{3/2} x^{-1/2}\,dx \qquad . \quad . \quad . \quad . \quad . \quad (10)$$

to the potential $-v$ at the nucleus.

Now choose E so that there are just two electrons beyond this energy according to the statistical model. The contribution to v is found to be

$$2\,.\,3^{1/3}\,.\,Z.$$

The actual potential due to the two K-electrons on the other hand is (minus) $2Z$ atomic units. Thus the value of $-v$ obtained statistically needs to be increased by an amount

$$2Z(3^{1/3}-1)=0{\cdot}88Z.$$

(In deriving this result χ has been replaced by 1, but the percentage errors thereby committed are of the order of $Z^{-2/3}$, which is within the accuracy aimed at.)

If the eight L-electrons are included as well, a similar calculation shows that the discrepancy for the first ten electrons is

$$2Z(15^{1/3}-2)=0{\cdot}93Z.$$

In the idealized problem in which Z is so enormous that many shells of tightly-bound electrons can be taken into account in this way, the complete boundary correction to be applied to v is

$$-2Z\lim_{n\to\infty}\{[\tfrac{1}{2}n(n+1)(2n+1)]^{1/3}-n\}=-Z.$$

The corresponding correction to be applied to the total binding energy W is found from (4) and is

$$-\tfrac{1}{2}Z^2. \qquad . \quad . \quad . \quad . \quad . \quad . \quad . \quad . \quad (11)$$

It is negative because the statistical model allows too great a density of electrons very close to the nucleus.

(It may be remarked that the *number* of electrons of energy $<-E$ in a Coulomb field is given by the statistical method as well as can reasonably be expected ; it is in v that it gives a systematic error.)

§4. The Exchange Effect

The exchange energy, that is to say the contribution to the total energy which appears in the form of exchange integrals when we construct an approximate wave function out of combinations of one-particle wave functions with the correct symmetry properties, tends to lower the energy of the ground state. Exchange is disregarded in the Thomas–Fermi model, which corresponds to the original Hartree equations rather than to the Hartree–Fock equations. Its effect in a statistical model has been discussed by Dirac (1930).

It will not be necessary to report our calculations in detail, as a textbook has since appeared (Corson 1951) which covers most of the essential points. It should, however, be added that it is *not* necessary to abandon the Thomas–Fermi distribution and calculate a new distribution allowing for exchange (this in any case leads to serious difficulties in the peripheral region of the atom). The reason is that the effect of exchange is to modify the density distribution by a fraction $O(Z^{-\frac{2}{3}})$, except at the extreme outside of the atom which does not affect the total energy appreciably; and the energy may be calculated from the unperturbed density-distribution with only a second-order error provided that an appropriate method is used, as is discussed in the usual accounts of variational methods.

The result (cf. Corson 1951, eqn. (9.48), p. 169) is a positive contribution to the binding energy W, of magnitude

$$\frac{4bZ^2}{\pi^2}\int_0^\infty \chi^2\,dx, \quad . \quad . \quad . \quad . \quad . \quad . \quad . \quad . \quad (12)$$

where b is given by (3), and the integral has the value

$$\int_0^\infty \chi^2\,dx = 0{\cdot}616. \quad . \quad . \quad . \quad . \quad . \quad . \quad . \quad (13)$$

(It was calculated from the table of Bush and Caldwell (1931), which is only accurate to $\frac{1}{2}\%$.)*

§5. Results

Collecting the results, it is found from (8), (11), (12) and (13) that the total binding energy of an atom of atomic number Z, in the non-relativistic approximation, is

$$W = 0{\cdot}7687Z^{7/3} - \tfrac{1}{2}Z^2 + 0{\cdot}221Z^{5/3} + O(Z^{4/3}) \quad . \quad . \quad . \quad (14\,a)$$

in Hartree units, or in electron volts:

$$20{\cdot}92Z^{7/3} - 13{\cdot}60Z^2 + 6{\cdot}01Z^{5/3} + O(Z^{4/3})\ \text{ev}. \quad . \quad . \quad . \quad (14\,b)$$

For the potential at the nucleus due to the electrostatic field of the electrons, we find

$$v = 1{\cdot}7937Z^{4/3} - Z + 0{\cdot}368Z^{2/3} + O(Z^{1/3}). \quad . \quad . \quad . \quad . \quad (15)$$

---

* *Note added in proof:* The constant (13) is equal to 0·61543.

§ 6. Discussion

6.1. *Comparison with Observation*

For the first twenty elements or so, much accurate data on ionization energies has been accumulated by spectroscopists, even for the high stages of ionization which concern us here (Moore 1949). The last two electrons (K shell) constitute a special case, and the energy required to remove them has been obtained from the very accurate formula of Hylleraas (1930), which being non-relativistic is more directly comparable with the present results than are the actual observations (which indeed do not extend beyond fluorine); the relativistic correction (see e.g. Bethe (1933), p. 383) need not be considered at this stage. For the L shell, the values reported in the literature extend as far as phosphorus ($Z=15$); and though in some cases they are extrapolations by the spectroscopists, they are quite accurate enough for the present purpose. With heavier elements, the energy needed to remove the whole L shell (ignoring relativity) may be taken from the semi-empirical formula

$$(Z-S)^2+C. \quad . \quad . \quad . \quad . \quad . \quad . \quad . \quad . \quad (16)$$

Here S has the theoretical value $4+69/256-430/2187=4{\cdot}073$; and the value of C is about $-0{\cdot}2$, based on the sum of values from a study of the higher ionization potentials in each of the eight iso-electronic sequences (cf. Scott 1952). For the M shell, the last-mentioned method has been used to supply the ionization potentials of vanadium IX, X and XI; the other values used are observational.

Table 1. Total 'Non-relativistic' Binding Energy

$Z=$	6 C	9 F	13 Al	18 A	23 V
K shell	32·4	75·5	161·0	313	515
L shell	5·4	24·2	79·5	194	358
M shell			1·9	21	72
Total	37·8	99·7	242·4	528	945
Calc'd (eqn. 14)	36·7	97·6	236·9	518	933
Calc'd (T–F–M)	50·3	129·5	305·5	653	1156

The binding energies W, measured or estimated in this way, which should be quite reliable, are compared in table 1 with the Thomas–Fermi–Milne formula (8) and with the new formula (14). It is seen that the error decreases smoothly from 3% at carbon to 1·3% at vanadium. Since the formula is theoretically only accurate to 1 part in Z, this is surprisingly close agreement.

6.2. *Comparison with Self-consistent Field Data*

For the heavier elements, although there are no relevant experimental data, it is possible to check the formulae against the results of

self-consistent field computations. As the data beyond copper ($Z=29$) do not include the effect of exchange, they have been adjusted by means of the semi-empirical formula

$$0{\cdot}369Z^{2/3}-0{\cdot}64Z^{1/3} \quad . \quad . \quad . \quad . \quad . \quad . \quad . \quad (17)$$

which represents the difference between the Hartree–Fock and the original Hartree values satisfactorily in those cases in which both are known ; the correction amounts to 4 units for mercury (one would not expect it to be as large as the full ' exchange term ' for the reasons given by Slater 1951). The first coefficient in (17) is the theoretical constant used in (15).

A representative selection of self-consistent field data is given in table 2, based on Dickinson's table, for comparison with the values given by (15) and those obtained from the older formula (7) which corresponds to the one-term Thomas–Fermi–Milne formula (8). The agreement is within 1%, which again is better than we have any right to expect from a calculation accurate to 1 part in Z.

Table 2. Values of v

Z	Calculated (T–F–M)	Calculated (eqn. 15)	*S–C* field
7	24·02	18·37	18·32
9	33·58	26·18	26·12
11	43·88	34·71	35·43
18	84·61	69·15	69·67
20	97·38	80·10	80·20
26	138·16	115·40	115·35
30	167·2	140·8	140·9
33	189·9	160·7	162·0
74	557	490	494
80	618	545	547

6.3. *Comparison with Empirical Formulae*

Besides making the foregoing comparisons, which provide a check of (14) and (15), it is interesting to examine the power laws which have been advocated, and which represent the available information fairly successfully. From the present point of view, the question is : what power law would most nearly coincide with (14) and (15) ?

Foldy (1951) has plotted the available values of log v against log Z, and obtained a power law $v \propto Z^n$ to represent the data between $Z=4$ and $Z=80$, with an exponent $n=1{\cdot}4$. The relation (15) is of course not a simple power law, but it is natural to inquire what the gradient of a

log-log plot of this kind would be when log Z lies in this region. Taking the geometric mean of 4 and 80, $Z=18$, as a representative value, it is found that

$$\frac{d\,(\log v)}{d\,(\log Z)}=\frac{4}{3}+0{\cdot}186Z^{-1/3}-0{\cdot}033Z^{-2/3}$$
$$=1{\cdot}399. \quad . \quad . \quad . \quad . \quad . \quad . \quad . \quad . \quad . \quad . \quad . \quad (18)$$

Thus v varies approximately as the (7/5)th power of Z in this region. This empirical law ought in fact to be rather good, except for the heaviest elements; and with them, although it may deviate from the theoretical relation (15), both relations will require appreciable relativity corrections.

The success of the 7/3 power law (1) for light elements arises from the fact that the deviation produced by the second term in (14) is partly compensated in this range by the effect of the third term, and it seems that the neglected fourth term acts in the opposite sense too. Thus, over a limited range, the combined effect of these terms is nearly a constant fraction of the main term. The coefficient will evidently be about 15 or 16 ev, e.g. if we put $Z=8$ we find

$$W/Z^{7/3}=20{\cdot}92-\tfrac{1}{2}\times 13{\cdot}60+\tfrac{1}{4}\times 6{\cdot}01=15{\cdot}62 \text{ ev} \quad . \quad . \quad . \quad (19)$$

to be compared with 15·68 (Young 1929), 15·73 (Allard 1948) or 15·6 (Condon and Shortley 1935) for the elements He to F. But for the very lightest elements the statistical method is so inappropriate that any success it has must be ascribed mainly to chance. And for the medium and heavy elements (1) is certainly wrong.

§ 7. Relativity and Magnetic Effects

Relativity effects of all kinds have been disregarded so far. Though this simplification has no serious consequences for $Z<30$, these effects are quite important for heavy elements. It would be a difficult task to calculate them accurately. A straightforward extension of Thomas' statistical method (Vallarta and Rosen 1932) is inapplicable to our present problem, because most of the correction originates in the region close to the nucleus where the statistical method is vitiated by the 'boundary effect', and, in fact, such methods would give an infinite binding energy. Moreover, the interaction between the electrons is not wholly electrostatic.

The relativistic correction to the energy required to strip off the last two electrons is, however, accurately known, and the correction for stripping off all the others is only of the same order of magnitude. We have made rough numerical estimates of the necessary correction to W in various ways, and find that our results can be conveniently represented by the approximate expression

$$W_R-W_{NR}=4\times 10^{-6}Z^{9/2} \quad . \quad . \quad . \quad . \quad . \quad . \quad (20)$$

in atomic units. It amounts to a fraction of a unit as far as phosphorus, and increases from about 15 at Cu to two or three thousand at U. The error in the total binding energy resulting from neglecting relativity is roughly $(Z/30)^2\%$.

§8. Conclusion

The total binding energy of an atom neglecting relativity effects is given by (14), with an error which is in principle of the order of magnitude of 1 part in Z, and which seems in fact to be about 1 part in $4Z$. An estimate of the relativity correction is given by (20). The failure of the currently-quoted formula is due partly to the shortcomings of the statistical model in the region nearest the nucleus, and partly to the effect of exchange.

References

Allard, G., 1948, *J. de Phys. et Rad.*, **9,** 225.
Baker, E. B., 1930, *Phys. Rev.*, **36,** 630.
Bethe, H. A., 1933, *Handbuch d. Physik*, **24/2** (Berlin).
Bush, V., and Caldwell, S. H., 1931, *Phys. Rev.*, **38,** 1898.
Condon, E. U., and Shortley, G. H., 1935, *Theory of Atomic Spectra* (Cambridge).
Corson, E. M., 1951, *Perturbation Methods* (Blackie, London), Chap. 9.
Dickinson, W. C., 1950, *Phys. Rev.*, **80,** 563.
Dirac, P. A. M., 1930, *Proc. Camb. Phil. Soc.*, **26,** 376.
Foldy, L. L., 1951, *Phys. Rev.*, **83,** 397.
Hylleraas, E. A., 1940, *Zeits. f. Phys.*, **65,** 209.
Lamb, W. E., 1941, *Phys. Rev.*, **60,** 817.
Mack, J. E., 1950, *Rev. Mod. Phys.*, **22,** 64 (esp. p. 70).
Milne, E. A., 1927, *Proc. Camb. Phil. Soc.*, **23,** 794.
Moore, C. E., 1949, *Atomic Energy Levels*, Vol. I (U.S. Bureau of Standards).
Schiff, L. I., 1949, *Quantum Mechanics* (New York), p. 273.
Scott, J. M. C., 1952, to be published.
Slater, J. C., 1951, *Phys. Rev.*, **81,** 385.
Thomas, L. H., 1926, *Proc. Camb. Phil. Soc.*, **23,** 542.
Vallarta, M. S., and Rosen, N., 1932, *Phys. Rev.*, **41,** 708.
Young, L. A., 1929, *Phys. Rev.*, **34,** 1226.

LXXXIII. *A New Calculation of Some Properties of Metallic Beryllium*

By B. Donovan
Department of Physics, The University of Sheffield*

[Received March 11, 1952, revised May 6, 1952]

Summary

A quantum mechanical calculation of the lattice constant, compressibility, cohesive energy and work function of metallic beryllium is carried out, using an extension of the cellular method of Wigner and Seitz. Wave functions and energies corresponding to the lowest electronic state in the metal are obtained by numerical integration of the Schrödinger equation, and the ion-core field used is of the Hartree type. The Fermi energy is evaluated by determining the effective electronic mass according to the method devised by Bardeen. Free-electron values are used for the exchange and correlation energies; it is pointed out that the corrections to these two terms may tend to cancel each other. The energy of the valence electrons in the free atom is obtained from the calculations of Hartree, together with the correlation energy. With the exception of the work function, the final results agree very satisfactorily with experiment and compare favourably with the values obtained by more elaborate methods.

§1. Introduction

The quantum theory of metals, as formulated in the cellular approximation of Wigner and Seitz (1933, 1934), has proved eminently successful in the calculation of the cohesive energies of the monovalent metals but as yet has not been applied extensively to metals of higher valency. The first comparable calculation for a polyvalent metal was carried out by Herring and Hill (1940) for beryllium; these authors determined directly the energies at a number of points in k-space and thus obtained the density of states and the mean Fermi energy. More recently, a simpler method, related more directly to the Wigner–Seitz treatment, has been applied by Raimes (1950) to magnesium.

The present paper contains the results of a new calculation for beryllium, similar to that of Raimes, undertaken with the object of ascertaining whether a simpler treatment than that of Herring and Hill would be satisfactory in this case, and whether reasonable results could be obtained without taking explicit account of the zone boundaries. Furthermore it was hoped that additional evidence could be obtained

* Communicated by Professor W. Sucksmith, F.R.S.

regarding Raimes' estimate of the correlation energy in the free atom, which consists of taking a proportion of the total energy of the valence electrons or of the Coulomb interaction energy.

A brief note summarizing the results of the present calculation has already been published (Donovan 1951).

§ 2. Calculation of Wave Functions

Metallic beryllium has a close-packed hexagonal structure, and we shall assume that it is a reasonable approximation to replace the atomic polyhedron for this lattice by a sphere of equal volume. In constructing a self-consistent field in the metal we neglect exchange interaction between the valence and core electrons ; this will be neglected also when considering the free atom. Moreover, in the derivation of the total energy of the metal, exchange and van der Waals interactions between the ion-cores are neglected.*

The self-consistent field we shall use is based on the fact that the probability of two electrons with parallel spins being in the same atomic cell is very small. Thus for a given electron the potential field may be expressed as the sum of the ion-core field and that due to the charge distribution, within the cell, of all the electrons with opposite spin (cf. Raimes, *loc. cit.*, eqn. (3)). The ion-core field was taken from the Hartree calculation for Be^{++} (Hartree and Hartree 1935 a), assuming that the ion-core remains unchanged in the metal.

The wave function ψ_0 corresponding to the lowest electronic state, and the eigenvalue ϵ_0 of the appropriate Schrödinger equation, may be obtained by the iterative process of numerical integration described by Raimes (*loc. cit.*). This procedure was carried out for eight values of the radius r_s of the atomic sphere and the resulting curve for ϵ_0 is shown in fig. 3. The general form of the wave functions may be seen from fig. 1, which represents ψ_0 for $r_s=2{\cdot}30$ Bohr units. This wave function is normalized according to the equation

$$\int_0^{r_s} r^2\psi_0^2\, dr=1.$$

§ 3. Total Energy in the Metal

On the basis of the assumptions mentioned in § 2, the total energy of the valence electrons in the metal may be calculated according to the one-electron approximation. As a consequence of the particular potential used the resulting expression does not include a separate term for the Coulomb energy (cf. Raimes, *loc. cit.*) and the total energy, expressed in rydbergs per electron, is given by

$$E=\epsilon_0+3{\cdot}508\frac{\alpha(r_s)}{r_s^{\,2}}-\frac{1{\cdot}154}{r_s}-\frac{0{\cdot}576}{0{\cdot}79r_s+5{\cdot}1}. \quad \ldots \quad (1)$$

* The validity of this assumption has been verified by Herring and Hill (*loc. cit.*).

In this expression α is the effective mass parameter, i.e. the ratio of the actual electronic mass to the effective mass near the centre of the Brillouin zone. The second, third and fourth terms in (1) represent respectively the Fermi, exchange and correlation energies.

In writing the Fermi energy as the product of α and the free-electron value we are tacitly assuming that all the electrons have the same effective mass and we are thus ignoring the effect of the zone boundaries. Using the method devised by Bardeen (1938) the value of α was determined for every value of r_s and the resulting curve is shown in fig. 2. The variation with r_s closely resembles that for lithium and Bardeen's values for this case are plotted in fig. 2 for comparison.

Fig. 1

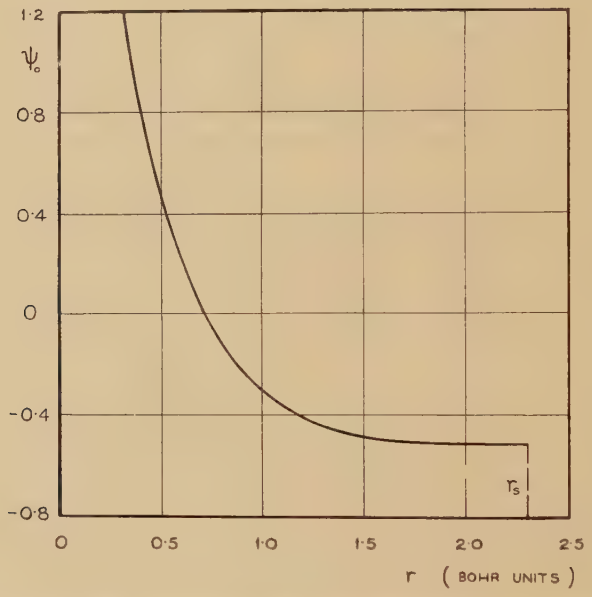

Wave function for lowest electronic state, corresponding to $r_s = 2{\cdot}30$ Bohr units.

Herring and Hill (*loc. cit.*) calculated values of α for three values of r_s, as indicated in fig. 2, and it is interesting that their value of 0·616 for $r_s = 2{\cdot}37$ is reproduced exactly by the present work. However a curve drawn through the three points would lie slightly above our fig. 2 for $r_s < 2{\cdot}37$ and considerably below for $r_s > 2{\cdot}37$. In this connection it should be pointed out that in the calculations of Herring and Hill the same potential (that for $r_s = 2{\cdot}37$) was used in all three cases whereas in the present treatment each integration for α was carried out with the potential function appropriate to the particular value of r_s.

As indicated in (1) free-electron formulae are used for the exchange and correlation energies, discussed respectively by Bloch (1929) and Wigner (1934). Tentative suggestions for modifying the free-electron

formulae have been put forward (Herring and Hill, *loc. cit.*, Herring 1951) but, on applying these to the present calculation, it is found that the corrections to the exchange and correlation energies cancel each other in such a way as to leave the sum of these terms virtually the same as for free electrons.

The values of E obtained from (1) are plotted in fig. 3. If the free-electron expression be used for the Fermi energy the values of the total energy do not lead to results with quantitative significance. This

Fig. 2

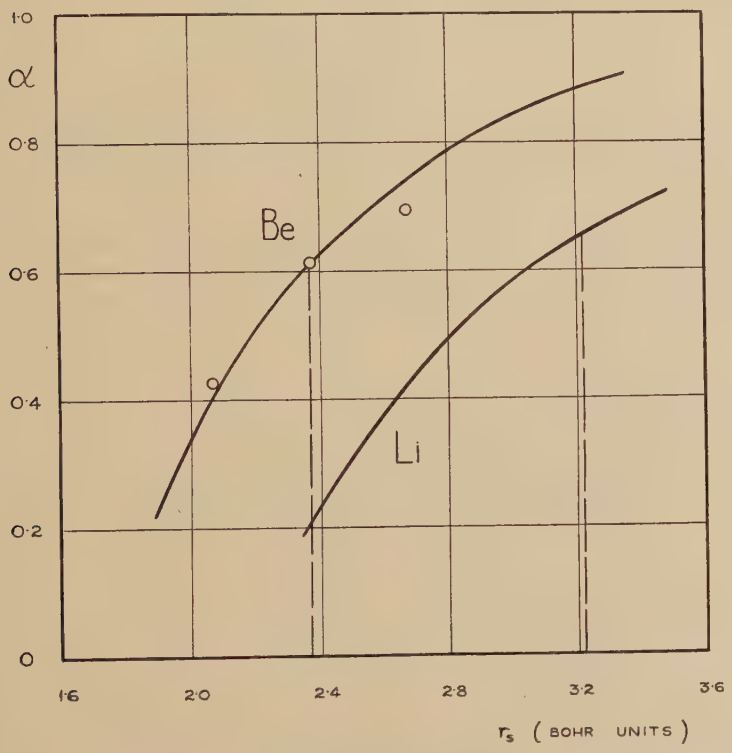

Effective mass parameter for beryllium and lithium. The circles represent the values calculated by Herring and Hill. The broken vertical lines indicate the observed lattice constants.

behaviour is in contrast to that for magnesium, for which Raimes obtained better agreement with experiment by using the free-electron value for the Fermi energy.

§4. Total Energy in the Free Atom

For the free neutral atom the appropriate data may be obtained from the calculations of Hartree and Hartree (1935 a, b). Since we are neglecting exchange interaction between the valence and core electrons

both in the metal and in the free atom, we require firstly the energy of the valence electrons according to the Hartree approximation. This is −0·940 rydbergs per electron (line *a* in fig. 3).

Since the two valence electrons have opposite spins there will be no exchange energy, but some cognisance must be taken of the correlation energy. This is a measure of the error involved in the use of one-electron wave functions and should therefore be given by the difference between the experimental and the Fock values of the total energy. For the 2*s* electrons the correlation energy can be estimated only in an indirect manner and the position is unsatisfactory in view of the discrepancies between the various estimates.

Fig. 3

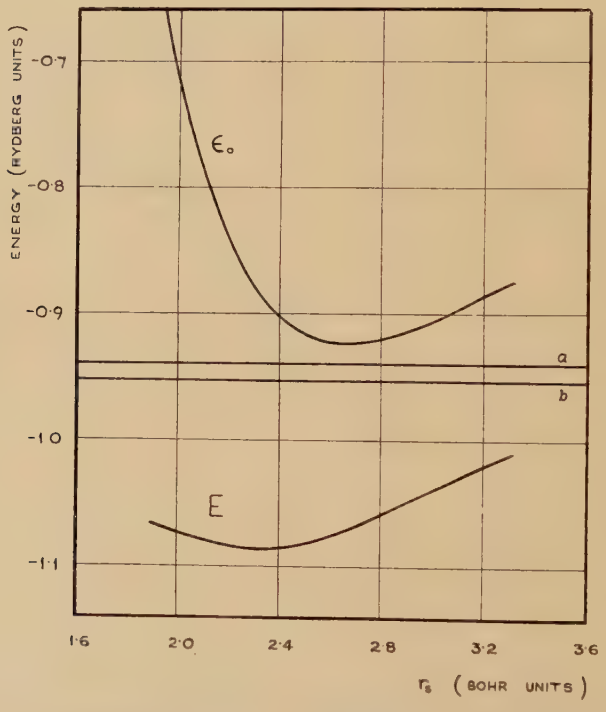

Eigenvalue of lowest electronic state and total energy in the metal. The lines *a* and *b* represent respectively the total energy in the free atom with and without correlation energy.

Raimes (*loc. cit.*) has suggested that the correlation energy might be estimated by taking a definite proportion of the observed total energy or of the Coulomb energy for the relevant electrons. He obtained the numerical factors from the helium atom, for which the total correlation energy is known to be −0·076 rydbergs. On this basis the correlation energy is estimated by multiplying the observed total energy by 0·013 or

the Coulomb energy by −0·037. For beryllium both methods give the same result, namely, −0·013 rydbergs per electron. If this value be accepted the total energy in the free atom is −0·953 rydbergs per electron and this is indicated by line *b* in fig. 3.

However, an estimate of −0·05 rydbergs per electron for the correlation energy has been given by Seitz (1940, p. 248) and it is difficult to reconcile Raimes' suggestion with the available data for beryllium. In particular, it leads to a much larger correlation for the 1*s* electrons than for the 2*s* electrons, which is extremely unlikely in view of the fact that the total correlation energy in Be is more than double that in Be^{++}.

§ 5. Results and Discussion

The equilibrium lattice constant, compressibility and cohesive energy may be determined by the usual methods and the results are set out in table 1, together with the experimental values and those obtained by Herring and Hill. In the latter case extreme values are quoted where various methods were employed in the calculations. The experimental value for the lattice constant may be deduced from the measurements of Gordon (1949) and the experimental compressibility has been given by Bridgman (1932).

Table 1

	Lattice Constant (Bohr units)	Compressibility ($cm^2/kg \times 10^7$)	Cohesive Energy (κ cal/mole)	Work Function (volts)
Present Calculation	2·34	8·0	84	−0·3
Herring and Hill	2·23 ; 2·57	7·5 ; 11·3	53	−1·9
Experimental	2·36 (0° c)	7·8 (30° c)	75	3·9

The cohesive energy is given by the difference in energy between line *b* and the minimum of *E* in fig. 3 and the rather high value obtained tends to strengthen the view that the correlation energy has been under-estimated by Raimes' method. If the correlation energy is taken to be −0·05 rydbergs per electron, as mentioned in § 4, the binding energy is 61 κ cal/mole. Herring and Hill used the experimental value for the energy of the valence electrons which, as they admitted, is too large and leads to a value of the cohesive energy which is much too low.

Finally, a rough value for the work function may be obtained using the formulation of Herring and Nichols (1949, p. 230). The value given in table 1, which excludes the contribution due to the surface double layer, was derived from the value of *E* at the calculated lattice constant.

Comparison with the observed value (Mann and DuBridge 1937) shows that the disagreement, though smaller than that found by Herring and Hill, is still too large to be explained by the double layer term.

With the exception of the work function, the calculated values obtained in the present work are in good agreement with experiment and are certainly no less satisfactory than those of Herring and Hill. However, it must be emphasized that in the present application, it is necessary to consider variations only in the *size* of the atomic polyhedron ; the form of the cell remains unaltered. In view of the neglect of the zone boundaries the present method would be of little value in problems involving a distortion of the atomic polyhedron.

The author wishes to express grateful thanks to Professor A. G. Walker and to Mr. G. H. Jowett for placing at his disposal a Marchant electric calculating machine, on which the numerical work was carried out. The author is also indebted to Dr. S. Raimes, of Imperial College, London, for helpful conversations.

References

Bardeen, J., 1938, *J. Chem. Phys.*, **6,** 367.
Bloch, F., 1929, *Zeits. f. Phys.*, **57,** 545.
Bridgman, P. W., 1932, *Proc. Amer. Acad. Arts and Sciences*, **68,** 27.
Donovan, B., 1951, *Nature, Lond.*, **168,** 836.
Gordon, P., 1949, *J. App. Phys.*, **20,** 908.
Hartree, D. R. and W., 1935 a, *Proc. Roy. Soc.* A, **149,** 210 ; 1935 b, *Ibid.*, **150,** 9.
Herring, C., 1951, *Phys. Rev.*, **82,** 282.
Herring, C., and Hill, A. G., 1940, *Phys. Rev.*, **58,** 132.
Herring, C., and Nichols, M. H., 1949, *Rev. Mod. Phys.*, **21,** 185.
Mann, M. M., and DuBridge, L. A., 1937, *Phys. Rev.*, **51,** 120.
Raimes, S., 1950, *Phil. Mag.*, **41,** 568.
Seitz, F., 1940, *Modern Theory of Solids* (New York : McGraw-Hill).
Wigner, E., 1934. *Phys. Rev.*, **46,** 1002.
Wigner, E., and Seitz, F., 1933, *Phys. Rev.*, **43,** 804 ; 1934, *Ibid.*, **46,** 509.

LXXXIV. *The Investigation of Soft Radiations from* ^{239}Pu *and* ^{233}U *with a Proportional Counter* *

By D. West, J. K. Dawson and C. J. Mandleberg
Atomic Energy Research Establishment, Harwell †

[Received April 21, 1952]

Abstract

Soft electromagnetic radiations from ^{239}Pu and ^{233}U have been investigated with a proportional counter filled with krypton or xenon.

^{239}Pu emits the L x-radiation of uranium with an intensity of $(4\pm1)\times10^{-2}$ L x-rays per α particle. The L x-radiation arises as a result of the internal conversion of γ rays. Residual unconverted gamma rays with energies of $52{\cdot}0\pm0{\cdot}3$ kev and $38{\cdot}5\pm0{\cdot}4$ kev are emitted. The intensities of these gamma rays are 7×10^{-5} and 2×10^{-5} quanta per α particle respectively. K x-rays are emitted with an intensity of about 2×10^{-5} quanta per α particle.

A gamma radiation of energy equal to $45{\cdot}0\pm0{\cdot}3$ kev is ascribed to ^{238}Pu or ^{240}Pu.

^{233}U emits the L x-radiation of thorium with an intensity of $(4\pm1)\times10^{-2}$ L rays per α particle. Gamma radiations of energies $42{\cdot}8\pm0{\cdot}3$ kev and $56{\cdot}1\pm0{\cdot}4$ kev are present with intensities of 5×10^{-4} and 10^{-4} quanta per α particle respectively.

§ 1. Introduction

Fine structure is present in the energy spectrum of α particles from many of the natural α particle emitters. The fine structure groups arise from transitions to excited states of the daughter nucleus and so their α particles are of lower energy than those which arise from the transition to the ground state. The detection of fine structure in the α particle energy spectrum itself is often difficult due to the small energy differences involved and to the usually weak intensity of the fine structure components. In these cases the radiations emitted from the excited states of the daughter nucleus following the emission of an α particle are often more readily detectable and provide much more accurate values of the energy levels of the residual nucleus than does a direct measurement of the α particle spectrum.

* Some of the results obtained with plutonium have already been briefly reported (West and Dawson 1951).

† Communicated by the Authors.

The proportional counter is a very convenient instrument for investigating γ radiations in the energy region up to about 100 kev. Filled with krypton or xenon, such counters have a high efficiency for detecting γ radiations; moreover the great majority of the γ radiation detected is absorbed in the gas of the counter by the photo-electric process, so that the size of pulse produced in the counter is directly proportional to the total energy of the γ radiation. (Hanna, Kirkwood and Pontecorvo 1949.)

Soft radiations from ^{239}Pu were first investigated by Ghiorso (1944) by an absorption method. Rosenblum, Valadares and Goldschmidt (1950) recently reported the presence of fine structure in the α particle energy spectrum of ^{239}Pu. They observed a low energy group of alpha particles differing in energy by about 50 kev from the main group. The present work was undertaken to examine the radiations from the excited state of ^{235}U which results from the emission of a low energy group of α particles by ^{239}Pu. The method is of general application and results obtained with ^{233}U are also described.

§ 2. Apparatus and Method

The proportional counter was made of soft glass 1 mm thick with an aquadag cathode on the outside (Maze 1946). Its diameter was 5 cm and the active length was 34 cm. It was fitted with a tungsten central wire of diameter 0·005″. Half way along the counter two thin mica windows (0·0038 cm thickness) were incorporated at opposite ends of a diameter to admit very soft radiations. The counter was filled to about 55 cm of mercury pressure with a mixture of krypton (or xenon) and 10% methane. Pulses from the counter were amplified by a head amplifier and linear amplifier, the output of which was fed into a 30 channel pulse analyser whose channels were 1 volt wide.

Energy calibrations of the counter were carried out with characteristic K x-radiation from K capture bodies (Rothwell and West 1950). Calibration runs were taken immediately before and after the measurement with the radiation under investigation to eliminate the effects of any slight drifts in the apparatus. Any lack of linearity in the amplifier and the associated electronic equipment was eliminated by calibrating the apparatus with artificial pulses from a pulse generator. The size of pulse fed into the apparatus could be varied by accurately known amounts and a curve of output pulse size versus input pulse size was plotted. All pulse sizes are then referred by means of this calibration graph to the output of the pulse generator which was known to be linear.

Strong α particle sources excite the characteristic x-rays of materials which they strike (Curie and Joliot 1931). For this reason sources were allowed in contact only with light elements whose characteristic x-rays are very soft. Where a thin source was required it was deposited on aluminium; stronger sources consisted of solid material contained in thin glass tubes.

§ 3. Efficiency of the Counter for γ Radiations

In the absence of any escape of photo-electrons from the gas into the walls of the counter, the efficiency of the counter can be calculated from the geometry and the photo-electric absorption coefficient of the counter gas for the γ radiation. The loss of photo-electrons due to wall effect was investigated by varying the pressure of krypton in the counter. Uncollimated sources of ^{153}Gd (41·4 kev), ^{241}Am (60 kev) and ^{140}Tm (85 kev) were counted in a standard position in contact with the outside wall of the counter. A typical pulse size distribution from ^{153}Gd is shown in fig. 1. The ' escape ' peaks having an energy 12·7 kev below

Fig. 1

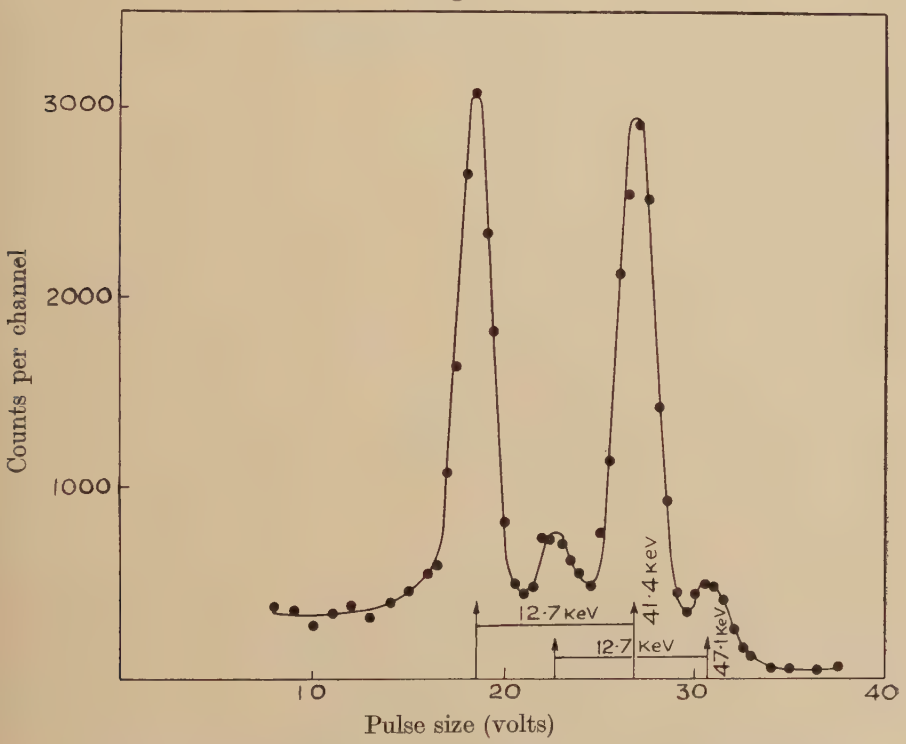

K x-rays from a calibration source (^{153}Gd) in a krypton-filled counter.

that of the peaks corresponding to the full energy of the radiations is characteristic of krypton (West and Rothwell 1950). The escape peak occurs as a result of the escape of the K x-radiation of krypton (12·7 kev) from the counter following photo-electric absorption in the K shell.

The counting rate at a given pressure of gas was measured for each of the sources by evaluating the areas under the ' escape ' and full energy peaks in the pulse size distributions. The mean free path for photo-electric absorption is large compared with the counter dimensions at the energies and pressures in question, so the number of quanta absorbed is

proportional to the pressure of krypton in the counter. The counting rate per unit pressure is therefore a measure of the efficiency of detecting an absorbed quantum. The pressure of krypton could not be made large enough to obtain the saturation values for each radiation corresponding to no escape of photo-electrons. Instead the counter was placed in a magnetic field of 6000 gauss parallel to its axis (West and Rothwell 1950) and in these conditions it was assumed that the amount of escape was negligible. The counting rate per unit pressure of krypton is normalized to unity in the presence of the magnetic field. The curve of efficiency of detection of an absorbed quantum versus pressure of krypton is shown in fig. 2.

Fig. 2

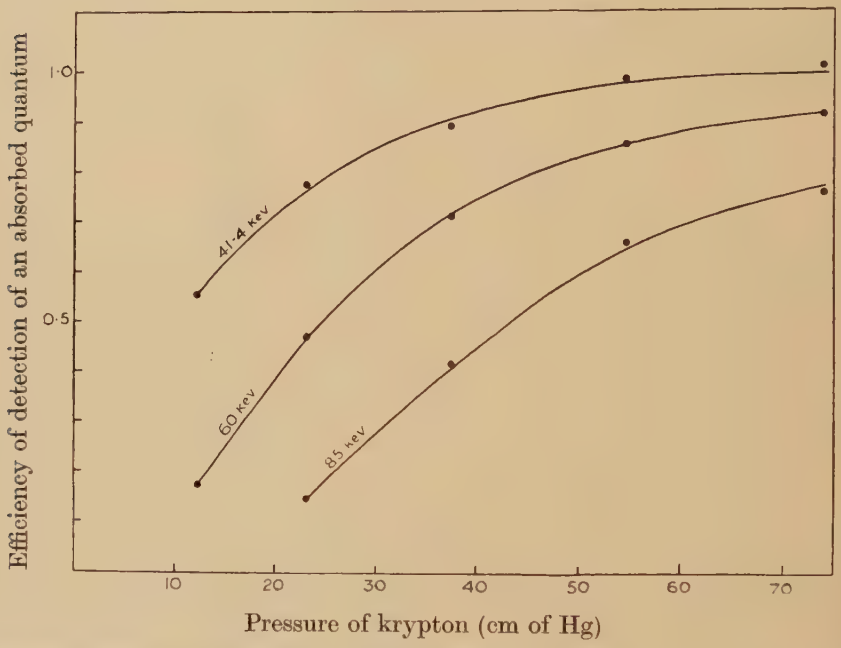

Measured efficiency of detection of an absorbed γ ray in a 5·0 cm diameter krypton filled counter.

It was noticed that even when as much as 50% escape occurred there was no appreciable broadening of the peaks in the distribution. The photo-electron follows a tortuous path and the wall effect sets in when any part of the track grazes the counter wall and not when the end of its track just reaches the wall as is the case with particles following a rectilinear path. With soft electrons, therefore, the onset of wall effect is characterized by an immediate large diminution of pulse size which removes this pulse completely away from the region of the peak. The fact that a narrow peak is obtained is therefore no indication that the wall effect is small.

The amount of escape in a krypton filled counter at these energies is mainly a property of the energy of the photo-electron removed from the K shell. It is possible, therefore, to make an approximate calculation of the escape in other gases for radiations which give the same energies of photo-electron as those measured in krypton. It is assumed that the effective range of the photo-electron is inversely proportional to the number of electrons per c.c. in the gas. This assumption will result in an underestimation of the efficiency for gases of atomic number greater than krypton and an overestimation for gases of smaller atomic number. The derived curves for argon and xenon are shown in fig. 3.

Fig. 3

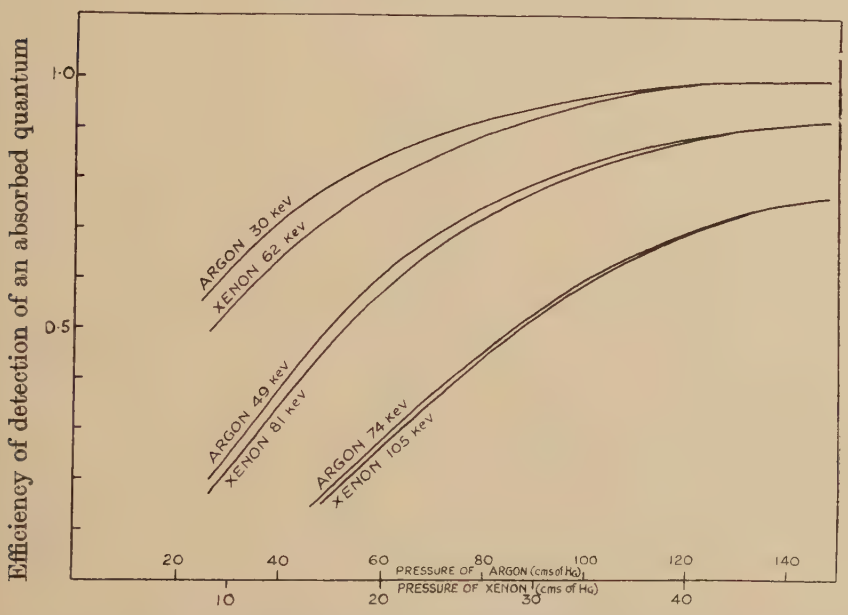

Approximate curves (derived from measurements in krypton) showing efficiency of detection of an absorbed γ ray in a 5 cm diameter counter filled with argon or xenon.

§ 4. Measurements with ^{239}Pu

The L X-radiation

A source of 66 micrograms of ^{239}Pu was deposited on aluminium and covered with a thin film of ' Zapon ' lacquer. It was placed close to one of the windows of a counter which contained krypton and the pulse distribution measured. The distribution obtained is shown in fig. 4. It consists of three peaks which are characteristic of atomic L x-radiation. The peaks correspond to the α, β and γ groups of L x-ray lines. The energies of the groups were measured from calibrations of the counter with 20·2 kev x-rays from a ^{103}Pd K-capture source (17 days half-life).

The escape peaks from the L x-radiation shown in fig. 4 are shown in fig. 5. There is no escape peak from the L_α radiation which must therefore have an energy less than 14·3 kev (the K binding energy of krypton). The energy of the escape peaks was measured by calibrating the counter with 8·07 kev x-rays from ^{65}Zn (250 days). The energies of the L_β and L_γ radiations could then be obtained by adding 12·7 kev in each case. The percentage accuracy of the determination is thereby improved. Several independent measurements were made; the results are given in table 1 which includes the energies of the L radiations of uranium and plutonium for comparison.

Fig. 4

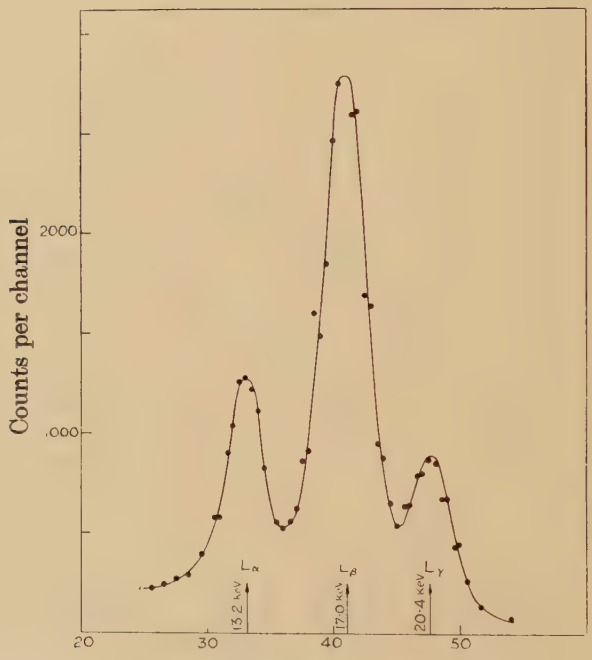

L x-radiation from ^{239}Pu.

Table 1*

	L_α	L_β	L_γ
Experimental values (kev)	13·2±0·3	17·0±0·2	20·4±0·2
Energies of uranium L x-rays (kev)	13·6	16·9	20·2
Energies of plutonium L x-rays (kev)	14·2	17·9	21·4

* The L x-ray spectrum is complex and consists of many individual lines which are not resolved by the proportional counter technique. The energy values quoted are the mean energies of the more prominent lines within each group. The values for plutonium are obtained by extrapolation.

It is evident from table 1 that the radiation is the L x-radiation of uranium. An estimate of its intensity was obtained by measuring the counting rate in each group of L rays when the counter was exposed to a collimated beam of the radiation. The efficiency of the counter was estimated from the geometry and the known absorption coefficients of krypton for the individual radiations. The measured intensity was 4×10^{-2} L rays per α particle with an estimated uncertainty of $\pm1\times10^{-2}$. The L_α, L_β and L_γ radiations are present in the ratios 1·0 : 1·5 : 0·3 respectively.

Fig. 5

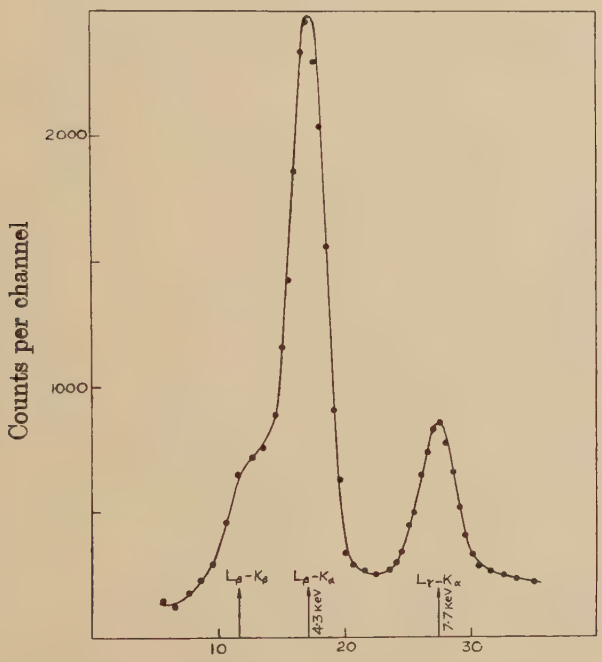

'Escape' peaks of the L x-radiation from ^{239}Pu in a krypton filled counter.

§ 5. Soft Gamma Radiations

Very much stronger sources of ^{239}Pu were needed for studying the soft gamma radiations. Sources several milligrams in weight were used. Each source was placed in contact with the glass wall of the counter instead of over the window to reduce the intensity of L x-radiation detected. Measurements were first carried out using a counter containing krypton. The pulse size distribution is shown in fig. 6. The energies of the radiations were determined after the counter had been calibrated with characteristic x-rays of energy 41·4 kev from ^{153}Gd (half-life 155 days). The interpretation of the pulse size distribution shown in fig. 6 is complicated by the presence of the escape peaks. The peak A at

52·3±0·4 kev energy represents the total energy of one radiation since there is no comparable peak at 52·3+12·7=65 kev. The escape peak from this radiation should give rise to a peak of about equal intensity at 39·6 kev. The peak B at 38·4±0·4 kev energy is too large to be entirely due to the escape peak of the 52·3 kev radiation. A radiation of energy close to 38·4 kev must be present as well. The energy of this second radiation, however, cannot be determined accurately due to its accidental coincidence with the escape peak. The weaker radiations consist of peak C at 59·2±0·5 kev, whose escape peak lies at 46·5 kev.

Fig. 6

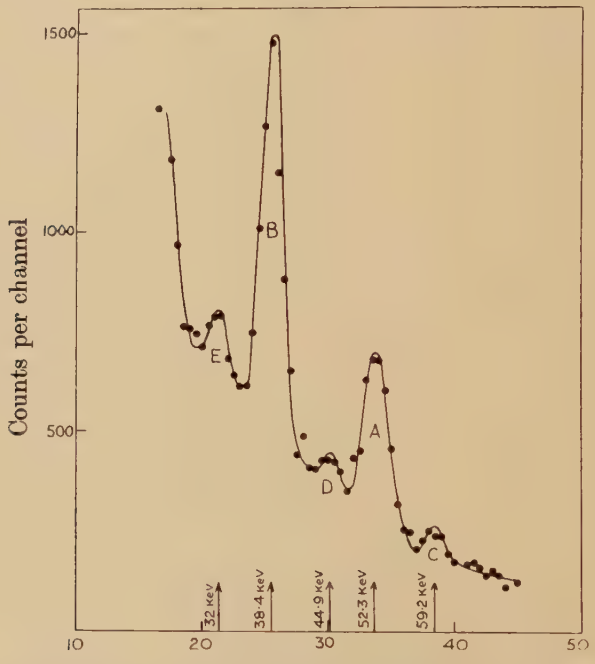

Gamma radiations from plutonium detected with a krypton filled counter.

It is not possible from these measurements alone to decide whether the peak at 44·9±0·4 kev (peak D) can be accounted for entirely as an escape peak, in which case peak E at 32 kev represents another radiation ; or alternatively, whether a radiation of about 44·9 kev energy is present as well, having its escape peak at 32 kev. To avoid the uncertainties due to escape peaks a counter containing xenon was used. With xenon the escape peak is 29·7 kev below the main peak, so that considerably less confusion is possible.

The pulse size distribution with a xenon filled counter is shown in fig. 7. The two more prominent radiations, peaks A and B are now seen unambiguously. Their energies are 51·8±0·4 kev and 38·5±0·4 kev.

Additional radiations at $60{\cdot}3 \pm 0{\cdot}4$ kev (peak C) and at $45{\cdot}1 \pm 0{\cdot}4$ kev (peak D) are also present. The peak E at $69{\cdot}2 \pm 0{\cdot}4$ kev was investigated using a larger source of ^{239}Pu. It was shown to be the escape peak of a weak radiation of energy equal to 101 kev. An even weaker radiation of energy 115 kev was also present. The energies of the K_α and K_β radiations of uranium are 96·9 kev and 111 kev while those of plutonium are 101 kev and 115 kev respectively. This radiation is therefore almost certainly K radiation, but the measurements made were not sufficiently precise for deciding to which of these two elements the radiation belongs.

Fig. 7

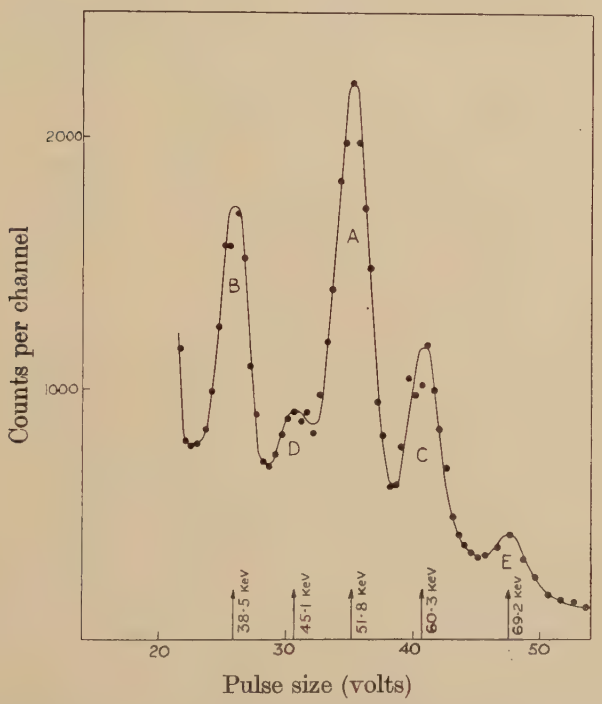

Gamma radiations from plutonium detected with a xenon filled counter.

The plutonium samples that were used had all been carefully purified to remove fission products. As an additional check that the weak radiations observed were not due to fission products, one of the samples that had been measured was put through an additional cycle of repurification from fission products. The process was expected to reduce the amount of fission products present by at least a factor of ten. After this additional purification process the sample again gave the same γ rays in about the same intensities. In addition we have now observed the radiations with several different samples of plutonium. There is therefore a strong indication that the radiations are not due to fission products.

There remains the possibility that some of the radiations are due to other isotopes of plutonium or transuranic elements which are known to be produced at the same time as plutonium. Accordingly the γ radiations from two samples of plutonium of different isotopic constitutions were compared. The samples contained ^{238}Pu, ^{240}Pu and ^{241}Pu in small amounts in addition to ^{239}Pu. The percentage by weight of ^{240}Pu was about one half as much in sample I as in sample II. Much smaller percentages of ^{238}Pu and ^{241}Pu were present. Sample I contained about one third as much ^{238}Pu and about one fifth as much ^{241}Pu as sample II.

The γ-ray spectrum from sample II showed an enormously increased amount of the radiation of 60·3 kev energy (peak C in fig. 7) relative to the other radiations. This radiation was shown to be due to ^{241}Am—the daughter of ^{241}Pu ($\sim$10 years half-life) which is also present in the samples. The americium was removed by a chemical oxidation and

Fig. 8

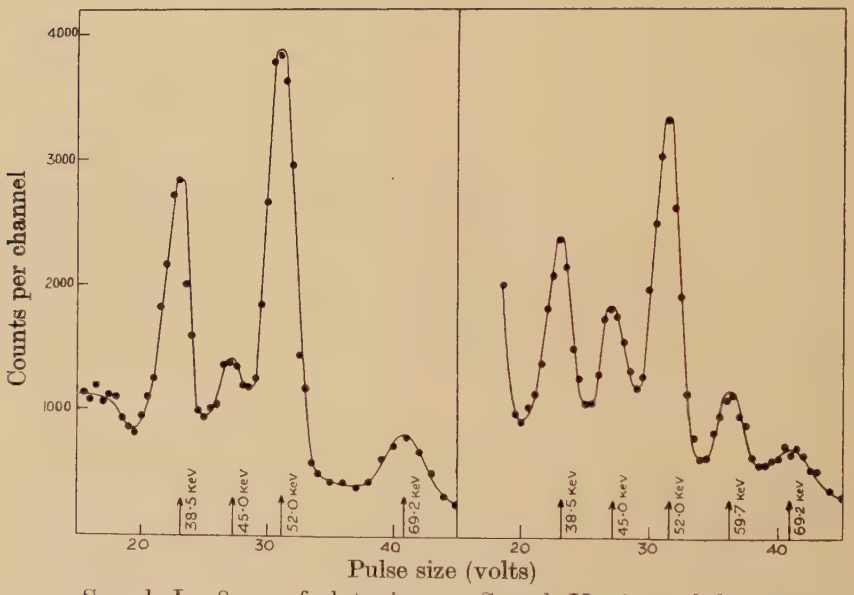

Sample I : 8 mg of plutonium. Containing small percentages of ^{240}Pu, ^{239}Pu and ^{241}Pu.

Sample II : 6 mg of plutonium. Containing larger percentages of ^{240}Pu, ^{238}Pu and ^{241}Pu.

Comparison of gamma ray spectra from samples of plutonium of different isotopic constitutions.

precipitation cycle. Both samples were treated in this way and measurements made as soon as possible after the chemical separation to avoid the growth of further amounts of ^{241}Am.

The γ-ray spectra from an 8 mg source of sample I and a 6 mg source of sample II are shown in fig. 8. The γ-rays of energy 52·0 kev and 38·5 kev are present in both samples in nearly the same intensities and are therefore due to ^{239}Pu.

The $45{\cdot}0 \pm 0{\cdot}3$ kev radiation is about twice as intense in sample II as in sample I and is therefore due to ^{240}Pu or possibly ^{238}Pu. The intensities of the radiations from ^{239}Pu were estimated from the efficiencies of the counter for the two radiations. The mean track length of γ rays in the counter was calculated for a point source on the wall of the counter. The mean value was $0{\cdot}92 \times$(diameter of the counter) for γ rays entering the counter.

Measurements with both krypton and xenon counter fillings were used in deriving the energies and intensities. The final results are contained in table 2.

Table 2. Radiations from ^{239}Pu

Radiation	Estimated intensity per α particle
Uranium L x-rays	$4 \pm 1 \times 10^{-2}$
$52{\cdot}0 \pm 0{\cdot}3$ kev gamma ray	7×10^{-5}
$38{\cdot}5 \pm 0{\cdot}4$ kev gamma ray	2×10^{-5}
K x-rays	2×10^{-5}

§ 6. Origin of the L x-Radiation

The L x-radiation could arise in the following ways :—

(1) As a result of excitation produced by the passage of an alpha particle through the electron shell of an atom.

(2) As a result of orbital electron capture by the nucleus.

(3) As a result of internal conversion of a nuclear γ ray in the L shell.

We can exclude process (1) on the following grounds : since the radiation is characteristic L radiation of uranium it cannot arise from the passage of α-particles through the plutonium of the source. It could conceivably arise as a result of the excitation of the electron shell of its parent atom by an α-particle during its emission. This process would be a universal property of α emitters. Investigations so far (Rubinson and Bernstein 1951) suggest that the intensity of L radiation produced by this process is very much weaker than that observed here. Process (2) is energetically impossible for ^{239}Pu since ^{239}Np is β^--active. It is concluded, therefore, that the L radiation arises as a result of the internal conversion in the L shell of a γ-ray which follows the α-particle emission from ^{239}Pu. This conclusion is supported by the results of Albouy and Teillac (1951) using photographic plates who found soft conversion electrons from ^{239}Pu having an intensity of 0·16 conversion electrons per α particle. The energies corresponded to those of the L conversion electrons of a γ-ray of energy equal to about 50 kev. The weak intensity of γ rays observed here compared with that of the L rays or conversion

electrons means that there is a high degree of internal conversion (conversion coefficient ~ 1000). Some further experiments were performed to see whether the excited state of ^{235}U in question was long lived. A chemical separation of the uranium daughter of plutonium was carried out by solvent extraction. The uranium fraction was then deposited on an aluminium foil and the latter placed near the window of the proportional counter. No L rays were detected and this enabled the half-life of the transition to be set at less than two minutes. In a further experiment, coincidences between α particles detected by a geiger counter and L rays detected by the proportional counter were measured, using a

Fig. 9

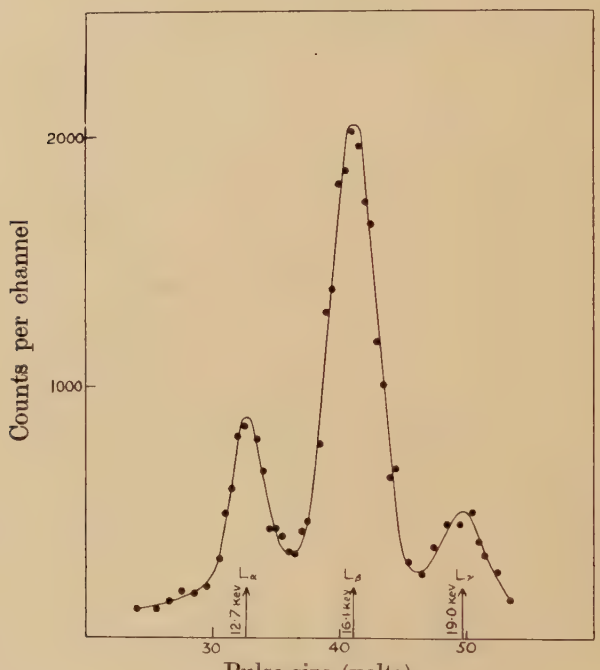

L x-radiation from ^{233}U.

coincidence resolving time of 4 microseconds. The number of coincidences observed agreed with that calculated if it was assumed that all the L rays observed were in coincidence with α particles. It is concluded that the half-life of the excited state of ^{235}U which gives rise to the L radiation is less than 4 microseconds.

§ 7. Measurements with ^{233}U

Studier (1947) has reported soft radiations from ^{233}U. It was therefore decided to investigate this isotope with the proportional counter technique.

A source containing 1·9 mg of ^{233}U was deposited on aluminium. L x-radiation was observed from this source by means of a krypton filled counter. The pulse size distribution is shown in fig. 9. The energies of

the peaks were measured in a similar manner to that described for plutonium.

The results are given in table 3.

Table 3

Experimental values (kev)	$12{\cdot}7 \pm 0{\cdot}2$	$16{\cdot}1 \pm 0{\cdot}2$	$19{\cdot}0 \pm 0{\cdot}2$
Energies of thorium L rays (kev)	12·9	15·9	19·0
Energies of uranium L rays (kev)	13·6	16·9	20·2
Relative intensities	1·0	1·8	0·3

The L rays are evidently those of thorium, the daughter element in the decay of ^{233}U. The overall intensity was estimated as $(4 \pm 1) \times 10^{-2}$ which is closely similar to the intensity obtained with plutonium.

Fig. 10

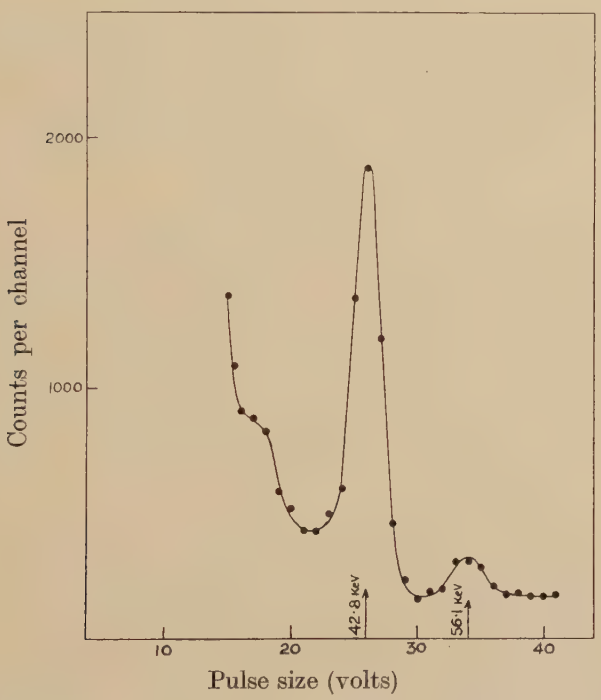

Gamma radiations from ^{233}U in a xenon-filled counter.

Soft γ radiations were looked for with counters containing krypton and xenon. The pulse size distribution obtained with a xenon counter is shown in fig. 10. The prominent radiation at $42{\cdot}8 \pm 0{\cdot}3$ kev is more intense than the radiations observed from plutonium, but is again very much weaker than the L radiation. The results of the measurements with ^{233}U are given in table 4.

By an argument very similar to that used in the discussion on plutonium it can be shown that the L radiation from ^{233}U must arise from the internal conversion of a γ ray which follows the α particle emission.

Only the weak γ radiations listed in table 4 were found in the energy region up to 120 kev. A converted γ radiation in this energy region must be responsible for the L radiation, since if the γ radiation were of energy greater than 120 kev K x-radiation of comparable intensity to that of the L radiation would have been observed. The γ radiation responsible for the L radiation must therefore be highly internally converted.

Table 4

Energy of Radiations from ^{233}U	Estimated intensity per α particle
(Thorium L x-rays)	$4\pm1\times10^{-2}$
$42{\cdot}8\pm0{\cdot}3$ kev	5×10^{-4}
$56{\cdot}1\pm0{\cdot}4$ kev	1×10^{-4}

§8. Conclusions

Proportional counters are very suitable for investigating γ radiations in the region up to 100 kev. The presence of fine structure in α particle spectra can be revealed by the presence of L radiation arising from the internal conversion of soft γ rays. The degree of conversion is often very high, so that only weak unconverted γ radiation is emitted.

Acknowledgments

The authors wish to thank Dr. R. Hurst and Mr. W. J. Whitehouse for helpful discussions, Miss R. M. Elliott and Mr. A. J. Walter for assistance in the purification of the plutonium and Dr. J. Milsted for preparing the ^{233}U source. Thanks are also due to Mr. C. D. Florida who developed the 30 channel pulse analyser and for maintaining the instrument. Acknowledgment is made to the Director, Atomic Energy Research Establishment, for permission to publish this work.

References

Albouy, G., and Teillac, J., 1951, *Comptes Rendus*, **232**, 326.
Curie, I., and Joliot, F., 1931, *J. Phys. Radium*, **2**, 20.
Ghiorso, A., 1944, *Plutonium Project Report* CK 1511.
Hanna, G. C., Kirkwood, D. H. W., and Pontecorvo, B., 1949, *Phys. Rev.*, **75**, 985.
Maze, R., 1946, *J. Phys. Radium*, **6**, 164.
Rosenblum, S., Valadares, M., and Goldschmidt, B., 1950, *C. R. Acad. Sci. Paris*, **230**, 638.
Rothwell, P., and West, D., 1950, *Proc. Phys. Soc.*, **63**, 541.
Rubinson, W., and Bernstein, W., 1951, *Phys. Rev.*, **82**, 334.
Studier, M. H., 1947, *Plutonium Project Report*, CB 3793.
West, D., and Dawson, J. K., 1951, *Proc. Phys. Soc.*, **64**, 586.
West, D., and Rothwell, P., 1950, *Phil. Mag.*, **41**, 873.

LXXXV. *Theoretical Results on High Energy Nuclear Collisions in Light and Heavy Elements*

By H. Messel and R. B. Potts
University of Adelaide, South Australia
and
C. B. A. McCusker
Dublin Institute for Advanced Studies, Ireland*

[Received May 12, 1952]

Summary

Cascade theories appropriate to the various schemes of plural production of mesons suggested by Heitler and Janossy (and one by us) are developed. A set of master diffusion equations are set up which contain the various schemes as special cases. Their exact solution is given and detailed numerical results are presented for one of the schemes. These are presented in a form suitable for direct comparison with those obtained experimentally using photographic plate techniques. It is suggested, now that the detailed numerical results are available, that a recomparison be made between theory and experimental results previously obtained, in order to see whether the scheme considered does or does not agree with experimental observations. Results are presented in tabular form both for light and heavy elements and for mesons as well as protons.

§1. Introduction

In a series of papers (Camerini *et al.* 1951 a, b, 1952) under the general title of ' Nuclear Transmutations produced by Cosmic Ray Particles of Great Energy ', the Bristol group published experimental results relating to well over 15,000 nuclear disintegrations. Their data is by far the most extensive to appear to date. From a detailed analysis of this data it was hoped to throw some light upon the fundamental processes involved in high energy nucleon-nucleon and nucleon-nucleus collisions. In particular it was hoped to give a satisfactory answer to the highly controversial question : Are mesons produced in high energy nucleon-nucleon collisions according to the multiple or plural theory of meson production ? The Bristol group concluded that their results could be explained in terms of either the multiple theory with secondary generation of mesons, or the plural theory assuming many body collisions. They were, however, seriously handicapped in carrying out their analysis because of the absence, at that time, of detailed numerical results based on the plural theory.

* Communicated by Professor C. F. Powell, F.R.S.

Heitler and Janossy (1949, 1950) and Terraux (1951) have carried out limited calculations based on the plural theory, but these rested fundamentally upon the dubious postulate that successive collisions within the nucleus could be treated as statistically independent events. Furthermore their treatment did not take the cascade character of the process fully into account. Detailed theoretical results based upon the various theories of meson production are essential for the experimentalist if he is to make an adequate comparison between his experimental observations and the predictions of theory. We shall develop in this paper the cascade theories appropriate to a number of schemes of meson production proposed by Heitler and Janossy (1949, 1950) and give detailed numerical results for one of these. A further scheme, suggested by the recent experimental results of Lock and Yekutieli (1952) will also be developed.

The purpose of this paper will not be to attempt to prove or disprove either the plural or multiple theory of meson production, but rather to present detailed results which will provide the basis for future comparison between theory and experiment.

§2. Meson-Nucleon and Meson-Nucleus Interactions

In the original theory of Heitler and Janossy (1949) it was assumed :—

(*a*) Every high energy nucleon-nucleon collision leads to the creation of one and only one meson.

(*b*) The primary nucleon makes on the average more than one collision in traversing the nucleus (the effect of recoil nucleons was neglected).

(*c*) The mesons produced are simply emitted without any interaction with the nucleons of the nucleus in which they were created.

Later Heitler and Janossy (1950) and Terraux (1951) endeavoured to include the effect of recoil nucleons (hereafter referred to as scheme HJ(1)) and at the same time suggested two further possible theoretical schemes for the production of penetrating showers by nucleons and π-mesons. In the one scheme it was postulated that a π-meson gives a large fraction of its energy to a nucleon inside a nucleus and that the nucleon then gives rise to a penetrating shower via the cascade process (referred to as HJ(2)). In the other scheme it was suggested that the π-mesons may give rise to penetrating showers by a multiple process in which the primary meson ' splits ' up into several mesons (referred to as HJ(3)).

Recent experimental results of Camerini *et al.* (1952) suggest that the mesons suffer only small fractional energy losses in emerging from the nucleus in which they were created. At the same time strong evidence was given which supports the view that an isolated meson suffers a large energy loss in traversing nuclear matter and can, when in collision with a nucleus, lead to the production of further mesons. The collision cross section for meson-nucleus collisions was shown to be geometric or very nearly so. These authors suggested that the apparent discrepancy

between the results might be resolved by assuming that only a few high energy mesons are in general created in primary collisions and that these mesons undergo multiplication in subsequent meson-nucleon collisions. Rosser and Swift (1951) have put forward evidence supporting this view. These authors exposed photographic plate emulsions both above and below 30 cm of lead, at an altitude of 9000 feet, and found that for showers with 2 or more ' shower particles ' the ratio of charged to neutral primaries is greater for the showers observed beneath the lead than for those above. They concluded that it was necessary to postulate an interaction of the mesons with nuclear matter whereby further mesons were created. The two schemes proposed by Heitler and Janossy were considered and it was concluded that only the second scheme, that of meson splitting, might account for their results. Lock and Yekutieli (1952), in a preliminary study of nuclear disintegrations produced by π-mesons in the energy range 0·05 to 1·1 Bev, have arrived at a similar conclusion. They also argue that a low energy primary meson may make on the average 2 to 3 collisions within the nucleus.

One is tempted to deduce from the results of Lock and Yekutieli that *very high energy mesons* cascade within a nucleus in a manner entirely analogous to that for nucleons. We therefore now postulate that the mesons interact with nucleons, and that for high energies each meson-nucleon collision gives rise to two mesons and one nucleon, thus

(A) meson+nucleon→meson+meson+nucleon

(B) nucleon+nucleon→nucleon+nucleon+meson.

The mesons and nucleons created may cascade within the nucleus and in dispersed matter. It is further assumed that for the high energies considered the cross sections for processes A and B are equal. This assumption is probably an oversimplification of the physical reality but some support is given to it by the complete symmetry of the cross section for process B. In a paper by Messel (1951 a) it was shown that the best possible choice of $F(\eta_1, \eta_2)$, the cross section for process B, was a function symmetrical with respect to the η_1, η_2 and η_m, the meson energy. This choice of $F(\eta_1, \eta_2)$ yields average values of η_1, η_2 and η_m which are equal : $\eta_1=\eta_2=\eta_m=\frac{1}{3}$. It is reasonable to draw an analogy between A and B and hence to use the same cross section for both processes. It is interesting to note that process B has been observed in laboratory experiments, but process A has not, perhaps because only low π-meson bombarding energies are at present available. In process B it is further assumed that one and only one meson is created in each nucleon-nucleon collision.

§3. Mixed Nucleon-Meson Cascades

We now give a set of master equations for the average number of nucleons and the average number of mesons at a depth x in homogeneous nuclear matter, for the various schemes of shower production proposed by Heitler and Janossy and by us (MPM). Let $n^{(j)}(E, x)\,dE$ be the average number

of nucleons with energies in the interval E, dE at depth x collision units in homogeneous nuclear matter, due to a primary particle (j). When $j=1$, the primary particle is a nucleon, when $j=2$, a meson. Let $\pi^{(j)}(E, x)$ represent the corresponding quantity for π-mesons. The master equations are then given by

$$\left\{\frac{\partial}{\partial x}+1\right\}n^{(j)}(E,x)=\int_E^\infty n^{(j)}(E',x)\,\bar{F}(E/E')dE'/E' + \int_E^\infty \pi^{(j)}(E',x)\;k(E/E')dE'/E', \quad . . . . . (1)$$

$$\left\{\frac{\partial}{\partial x}+q\right\}\pi^{(j)}(E,x)=\tfrac{1}{2}\int_E^\infty n^{(j)}(E',x)\bar{F}(E/E')dE'/E' + \int_E^\infty \pi^{(j)}(E',x)\;l(E/E')dE'/E', \quad . . . . . (2)$$

where

$$\bar{F}(\eta_1)=\int\{F(\eta_1,\eta_2)+F(\eta_2,\eta_1)\}d\eta_2 \quad . . . . . (3)$$

and q, $k(E/E')$ and $l(E/E')$ are to be chosen according to the scheme considered.

The solutions for the average number of nucleons $N^{(j)}(E)$ and the average number of π-mesons $\pi^{(j)}(E)$ with energies greater than E emitted from a nucleus, are obtained from (1) and (2) by making use of Laplace–Mellin transforms and averaging over all possible path lengths through the nucleus. The results are left in convenient matrix form:

$$\begin{bmatrix}N^{(1)}(E) & N^{(2)}(E)\\ \pi^{(1)}(E) & \pi^{(2)}(E)\end{bmatrix}=\boldsymbol{I}_1\left\{\frac{V[D_A\lambda_1(s)]}{\lambda_2(s)-\lambda_1(s)}\begin{bmatrix}q-\lambda_1(s)-l(s) & k(s)\\ W(0,s) & \alpha(s)-\lambda_1(s)\end{bmatrix} + \frac{V[D_A\lambda_2(s)]}{\lambda_1(s)-\lambda_2(s)}\begin{bmatrix}q-\lambda_2(s)-l(s) & k(s)\\ W(0,s) & \alpha(s)-\lambda_2(s)\end{bmatrix}\right\}, \quad . . . . . (4)$$

where

$$\begin{matrix}\lambda_1(s)\\ \lambda_2(s)\end{matrix}=\tfrac{1}{2}\{q+\alpha(s)-l(s)\}\pm[\tfrac{1}{4}\{q+\alpha(s)-l(s)\}^2 + k(s)W(0,s)-\alpha(s)\{q-l(s)\}]^{1/2} \quad . . . . . (5)$$

$$\boldsymbol{I}_1=\frac{1}{2\pi i}\int_{s_0-i\infty}^{s_0+i\infty}(E_0/E)^s\,ds/s \quad . . . . . (6)$$

$$\alpha(s)=1-2W(0,s) \quad . . . . . (7)$$

$$W(r,s)=\int_0^1\int_0^{1-\eta_1}\eta_2^r\eta_1^s F(\eta_1,\eta_2)\,d\eta_1,d\eta_2 \quad . . . . (8)$$

$$V[D_A\lambda_1(s)]=2\frac{1-\{1+D_A\lambda_1(s)\}\exp[-D_A\lambda_1(s)]}{[D_A\lambda_1(s)]^2} \quad . . . (9)$$

and D_A is the average number of collisions suffered by a particle in making a diametrical passage through a nucleus of atomic weight A. Furthermore,

$$l(s)=\int_0^1 (E/E')^s l(E/E')\,dE/E', \quad . \quad . \quad . \quad . \quad . \quad (10)$$

and

$$k(s)=\int_0^1 (E/E')^s k(E/E')\,dE/E'. \quad . \quad . \quad . \quad . \quad . \quad (11)$$

The values of q, $k(E/E')$ and $l(E/E')$ are given in table 1 for the various schemes considered.

Table 1

Scheme	q	$k(E/E')$	$l(E/E')$
HJ(1)*	0	0	0
HJ(2)	1	k'=constant	k'
MPM	1	$\frac{1}{2}\overline{F}(E/E')$	$\overline{F}(E/E')$

In table 2 the values of $l(s)$, $k(s)$, $\lambda_1(s)$ and $\lambda_2(s)$ are tabulated for the three schemes.

Table 2

	$l(s)$	$k(s)$	$\lambda_1(s)$	$\lambda_2(s)$
HJ(1)	0	0	$\alpha(s)$	0
HJ(2)	$k'/(s+1)$	$k'/(s+1)$	$\{1-W(0,s)-k'/2(s+1)\}$ $+\{W^2(0,s)+(k')^2/4(s+1)^2\}^{1/2}$	$\{1-W(0,s)-k'/2(s+1)\}$ $-\{W^2(0,s)+(k')^2/4(s+1)^2\}^{1/2}$
MPM	$2W(0,s)$	$W(0,s)$	$1-W(0,s)$	$1-3W(0,s)$

§4. Results

We have carried out detailed calculations for the scheme HJ(1) using eqns. (4) and (5). The explicit form of the cross section $F(\eta_1,\eta_2)=120\eta_1\eta_2(1-\eta_1-\eta_2)$ for inelastic nucleon-nucleon collisions is taken from the work of Messel (1951 a), where it was shown that its use allowed one to account adequately for the development of the nucleon component of the cosmic radiation in the atmosphere. The results of the calculation are presented in tables 3 and 4. For the light elements carbon, nitrogen and oxygen an average value of $D_A=3{\cdot}7$ was used ; for the heavy elements silver and bromine the value $D_A=6{\cdot}8$ was chosen.

* Clementel (1950) has also obtained a solution for this scheme for a set of special boundary conditions. The solution for the nucleons has been obtained previously by Messel (1951 b) in his treatment of the more general problem of a nucleon cascade developing in the atmosphere.

Table 3. Theoretical Results for High Energy Nucleon-nucleus Collisions in Light Elements (Carbon, Nitrogen and Oxygen) based on the Plural Theory of Meson Production

E_0 BeV	P_1	P_2	P_3	Π_1	Π_2	Π_3	n_s	$\Pi+P$	$P_3+\Pi_3$	Π_3/n_s	P_3/n_s	$\frac{\Pi+P}{n_s}$	Π_1/n_s	$P_2/\Pi+P$
1	0·15	0·09	0·06	0·64	0·54	0·10	0·79	0·63	0·16	0·13	0·076	0·79	0·81	0·14
2	0·27	0·17	0·10	1·04	0·84	0·20	1·31	1·01	0·30	0·15	0·076	0·77	0·79	0·17
3	0·37	0·24	0·13	1·32	1·02	0·30	1·69	1·26	0·43	0·18	0·076	0·74	0·78	0·19
5	0·54	0·38	0·16	1·72	1·23	0·49	2·26	1·61	0·65	0·22	0·071	0·71	0·76	0·24
7	0·68	0·49	0·19	2·04	1·38	0·66	2·72	1·87	0·85	0·24	0·070	0·69	0·75	0·26
10	0·85	0·63	0·22	2·34	1·44	0·90	3·19	2·07	1·12	0·28	0·069	0·65	0·73	0·30
12	0·94	0·71	0·23	2·50	1·46	1·04	3·44	2·17	1·27	0·30	0·067	0·63	0·73	0·33
15	1·06	0·81	0·25	2·72	1·50	1·22	3·78	2·31	1·47	0·32	0·066	0·61	0·72	0·35
20	1·22	0·96	0·26	3·00	1·56	1·44	4·22	2·52	1·70	0·34	0·064	0·60	0·71	0·38
30	1·44	1·15	0·29	3·48	1·78	1·70	4·92	2·93	1·99	0·34	0·059	0·60	0·71	0·39
50	1·77	1·44	0·33	3·98	2·25	1·73	5·75	3·69	2·16	0·30	0·057	0·64	0·69	0·39
100	2·34	1·98	0·36	4·68	2·90	1·78	7·02	4·88	2·24	0·25	0·051	0·70	0·67	0·41
200	2·92	2·55	0·37	5·30	3·55	1·75	8·22	6·10	2·12	0·21	0·045	0·74	0·65	0·41
300	3·19	2·80	0·39	5·70	3·99	1·71	8·89	6·79	2·10	0·19	0·044	0·77	0·64	0·41
500	3·57	3·20	0·37	6·19	4·53	1·66	9·76	7·73	2·03	0·17	0·038	0·79	0·62	0·41
1000	4·12	3·75	0·37	6·75	5·16	1·59	10·87	8·91	1·96	0·15	0·034	0·82	0·62	0·42
1500	4·42	4·07	0·35	7·20	5·65	1·55	11·62	9·72	1·90	0·13	0·030	0·84	0·62	0·42
2000	4·62	4·28	0·34	7·45	5·90	1·55	12·07	10·18	1·89	0·13	0·028	0·84	0·62	0·42

Table 4. Theoretical Results for High Energy Nucleon-nucleus Collisions in Heavy Elements (Silver and Bromine) based on the Plural Theory of Meson Production

E_0 BeV	P_1	P_2	P_3	Π_1	Π_2	Π_3	n_s	$\Pi+P$	$P_3+\Pi_3$	Π_3/n_s	P_3/n_s	$\frac{\Pi+P}{n_s}$	Π_1/n_s	$P_2/\Pi+P$
1	0·060	0·035	0·025	0·63	0·10	0·53	0·69	0·13	0·56	0·77	0·04	0·19	0·91	0·26
2	0·12	0·068	0·048	1·18	1·18	1·00	1·30	1·25	1·05	0·77	0·04	0·19	0·91	0·26
3	0·17	0·10	0·067	1·66	0·30	1·36	1·83	0·40	1·43	0·74	0·04	0·22	0·91	0·25
5	0·27	0·17	0·10	2·38	0·53	1·85	2·65	0·70	1·95	0·70	0·04	0·26	0·90	0·24
7	0·37	0·24	0·13	2·95	0·77	2·18	3·32	1·01	2·31	0·66	0·04	0·30	0·89	0·24
10	0·49	0·32	0·17	3·66	1·10	2·56	4·15	1·42	2·73	0·62	0·04	0·34	0·88	0·23
12	0·57	0·38	0·19	4·06	1·27	2·79	4·63	1·65	2·98	0·60	0·04	0·36	0·88	0·23
15	0·68	0·47	0·21	4·58	1·52	3·06	5·26	1·99	3·27	0·58	0·04	0·38	0·87	0·24
20	0·83	0·59	0·24	5·30	1·90	3·40	6·13	2·49	3·64	0·55	0·04	0·41	0·86	0·24
30	1·12	0·80	0·32	6·47	2·52	3·95	7·59	3·32	4·27	0·52	0·04	0·44	0·85	0·24
50	1·57	1·14	0·43	8·17	3·40	4·77	9·74	4·54	5·20	0·49	0·04	0·47	0·84	0·25
100	2·47	1·82	0·65	10·94	5·02	5·92	13·41	6·84	6·57	0·44	0·04	0·52	0·82	0·26
200	3·58	2·80	0·78	14·24	6·94	7·30	17·82	9·74	8·08	0·41	0·04	0·55	0·80	0·28
300	4·45	3·55	0·90	16·47	8·45	8·02	20·92	12·00	8·92	0·38	0·04	0·58	0·79	0·30
500	5·45	4·35	1·10	19·40	10·40	9·00	24·85	14·75	10·10	0·36	0·04	0·60	0·78	0·30
1000	7·52	6·02	1·50	24·10	13·75	10·35	31·62	19·77	11·85	0·33	0·05	0·62	0·76	0·30
1500	9·18	7·36	1·82	26·95	15·85	11·10	36·13	23·21	12·92	0·31	0·05	0·64	0·75	0·32
2000	10·60	8·50	2·10	29·20	17·40	11·80	39·80	25·90	13·90	0·30	0·05	0·65	0·73	0·33

It will be noted that in both table 3 and 4 primary nucleon energies as low as 1 BeV were considered. In the energy region $E_0=1$ to 5 BeV, the occurrence of elastic nucleon-nucleon collisions is important, so that our calculations will actually give an overestimate of the number of shower particles in this energy region. When using the tables, this point should be kept in mind.

The symbols in the various columns denote the following (we assumed that one half of the nucleons were protons and two-thirds of the mesons to be charged) :

P_1=average number of protons with kinetic energy greater than 500 MeV.

P_2=average number of protons with kinetic energy greater than 800 MeV.

$P_3=P_1-P_2$=average number of identifiable protons among the shower particles.

Π_1=average number of charged π-mesons with kinetic energy greater than 80 MeV.

Π_2=average number of charged π-mesons with kinetic energies greater than 1 100 MeV.

$\Pi_3=\Pi_1-\Pi_2$=average number of identifiable charged π-mesons among the shower particles.

$n_s=\Pi_1+P_1$=average number of shower particles.

$\Pi+P=\Pi_2+P_2$=average number of shower particles which cannot be identified as protons or mesons because of their high energies.

Π_3+P_3=average number of identifiable protons and charged mesons among the shower particles.

In fig. 1 we have plotted the number of shower particles n_s against the primary energy E_0 both for the light and heavy elements. In fig. 2 we give the curves for the mean square angular deviation of the shower protons (P_1) from the direction of motion of the incident nucleon plotted against n_s. It is likely that the angular deviation for high energy mesons (Π_2) is very similar to that for P_1. These results were taken from a paper in preparation by Chartres and Messel which used the theory recently developed by Messel and Green (1952 a, b).

§5. Discussion

Even a casual glance at tables 3 and 4 reveals some rather surprising differences between the results for light and heavy nuclei. Though in both cases the ratio of charged π-mesons to the total number of shower particles is very high, varying from 90% to 62% depending upon the energy, the behaviour of the various components $(\Pi+P)/n_s$, Π_3/n_s is very different in the two cases. For instance for the light elements the $\Pi+P$ particles constitute from 79 to 84% and the identifiable mesons from 13 to 34 to 13% of the shower particles, depending upon the energy range considered.

This behaviour in the case of the heavy elements is completely reversed, the $\Pi+P$ particles now only constituting from 19 to 65% of the shower particles and the identifiable charged mesons from 77 to 30%. It is, further, interesting to note that in the case of the heavy elements there is a steady increase in the proportion of $\Pi+P$ particles as the number of shower particles increases whereas for the light elements this proportion at first decreases and then increases again with increasing n_s. Also for any given n_s the proportion of $\Pi+P$ particles is always greater in the case of the light elements than in the heavy.

Fig. 1

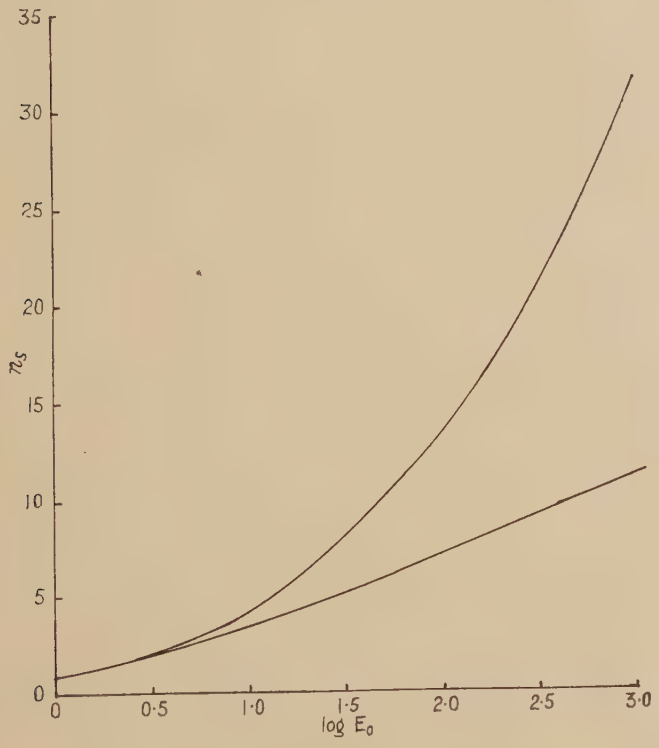

Plot of the average number of shower particles n_s against log E_0, where E_0 is the primary energy measured in Bev. The top curve is for the heavy elements silver and bromine; the bottom curve for the light elements carbon, oxygen and nitrogen.

The proportion of protons among the $\Pi+P$ particles in the case of both heavy and light elements is astonishingly low and in no case does it increase above 40%. In the case of the light elements the saturation effect to be expected for high energies is readily seen; for heavy elements the flattening out of the n_s versus E_0 curve is much slower.

In order to make an adequate comparison between theory and experiment it will be necessary to apply appropriate weight factors to the results

for heavy and light elements according to the proportions of these elements in the photographic emulsion concerned. We have carried out this procedure roughly and made a comparison with the Bristol group results. The most surprising conclusion of this comparison has been that we were unable to find any great discrepancy between the theoretical results here predicted and the experimental results. Unfortunately, however, the comparison can only be made at a few points and it would be interesting if the experimental results could be compared again with the HJ(1) theory now that detailed results predicted by this theory are available.

Fig. 2

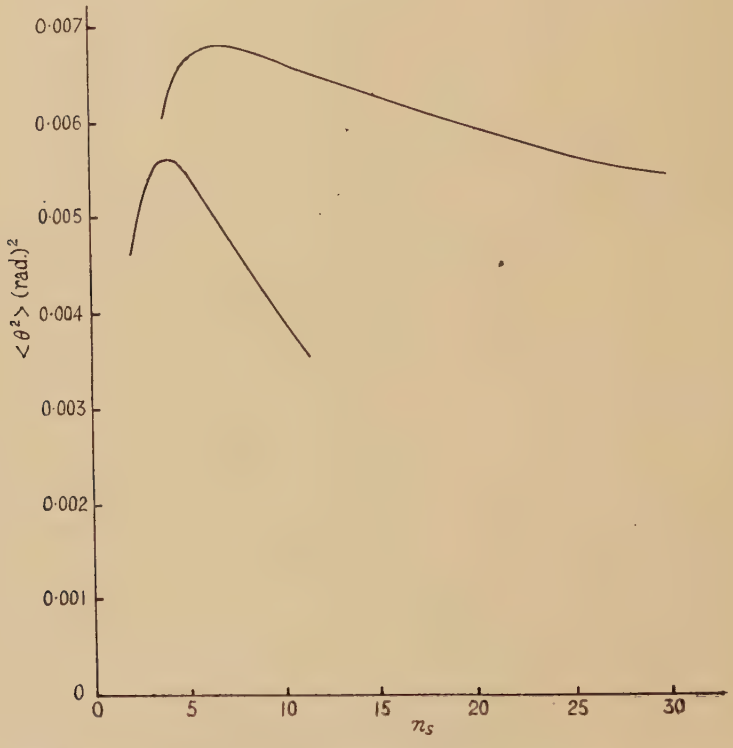

Plot of the mean square angle of emission $<\theta^2>$ of proton shower particles (P_1), resulting from a nucleon-nucleus collision, against the average number of shower particles n_s. The top curve is for the heavy elements silver and bromine ; the bottom curve for the light elements carbon, oxygen and nitrogen.

We mention briefly one point which seems to be in disagreement with experimental observation, namely, the very low proportion of identifiable protons and high proportion of $\Pi+P$ particles. This discrepancy, if real, would be removed in the HJ(2) and MPM models. Calculations are at present being carried out for the HJ(2) model and results will be made available shortly.

References

Camerini, U., Davies, J. H., Fowler, P. H., Franzinetti, C., Muirhead, H., Lock, W. O., Perkins, D. H., and Yekutieli, G., 1951 a, *Phil. Mag.*, **42,** 1241.

Camerini, U., Davies, J. H., Franzinetti, C., Lock, W. O., Perkins, D. H., and Yekutieli, G., 1951 b, *Phil. Mag.*, **42,** 1261.

Camerini, U., Lock, W. O., and Perkins, D. H., 1952, *Progress in Cosmic Ray Physics* (North-Holland Publishing Co., Amsterdam).

Clementel, E., 1950, *Nuovo Cim.*, **7,** 109.

Heitler, W., and Janossy, L., 1949, *Proc. Phys. Soc.* A, **62,** 374 ; 1950, *Helv. Phys. Acta*, **23,** 417.

Lock, W. O., and Yekutieli, G., 1952, *Phil. Mag.*, **43,** 231.

Messel, H., 1951 a, *Proc. Phys. Soc.* A, **64,** 726 ; 1951 b, *Comm. Dublin Inst. Advanced Studies*, **7**.

Messel, H., and Green, H. S., 1952 a, *Proc. Phys. Soc.* A, **65,** 245 ; 1952 b, *Phys. Rev.* (in press).

Rosser, W. G. V., and Swift, M. W., 1951, *Phil. Mag.*, **42,** 856.

Terraux, C., 1951, *Helv. Phys. Acta*, **24,** 551.

LXXXVI. *The Electrical Resistance of Magnesium, Aluminium, Molybdenum, Cobalt and Tungsten at Low Temperatures*

By J. G. Thomas and E. Mendoza
H. H. Wills Physical Laboratory, University of Bristol*

[Received April 17, 1952]

Abstract

This paper describes further results concerning the minimum of electrical resistance of metals at low temperatures. Some magnesium wires, known to contain 0·01 atomic per cent of iron, exhibited definite minima ; the magnetoresistance and the susceptibility were, however, independent of temperature. It therefore appears that though the minimum in zero field may well be an effect due to the presence of impurity atoms, the mechanism is not that of scattering of conduction electrons by unfilled electronic d-shells in these impurity atoms. Measurements on a dilute alloy of manganese in aluminium confirmed the filling of the d-shells of the transition metal by the multivalent solvent.

The resistance of each of several samples of molybdenum went through a minimum rising to a constant value below about 0·1° K. A superconducting impurity ($T_c \sim 0{\cdot}4°$ K, $H_0 \sim 30$ gauss), unidentified but probably a compound, could be produced by annealing. Samples of cobalt (hexagonal close-packed with traces of face-centred cubic) and tungsten showed no anomalies or superconductivity down to the region of 0·06° K.

§1. Introduction

In a previous paper (Mendoza and Thomas 1951) the authors described measurements of the electrical resistance of specimens of gold, silver and copper at low temperatures (i.e. from 4·2° K down to the region of 0·06° K). The resistance of most specimens of these metals was found to increase with decreasing temperature, implying the existence of a minimum in the resistance–temperature curve, whereas present-day theory demands a constant residual resistance in this region. Some of the specimens exhibited normal magnetoresistive effects (i.e. they obeyed Kohler's rule) while others behaved abnormally.

Similar behaviour in these and other metals has been extensively studied ; to the list of references in the previous paper may be added the following : Rorschach and Herlin (1951) demonstrated that the effect is still present in magnesium even when the resistance is measured without attaching leads to the specimen ; Serin (1951) found that the resistance of a specimen of gold in the helium range is independent of measuring current

* Communicated by Dr. L. C. Jackson.

over a range from 3 mA to 4 A. The measurements of Friedberg, Estermann and Goldman (1952) of the specific heat of magnesium seem to eliminate the possibility that the resistive mechanism is like that in a semi-conductor. The work of MacDonald and Templeton (1951) on gold containing added amounts of copper and nickel, and of Gerritsen and Linde (1951) and Gerritsen (1951) on gold, silver and copper contaminated with manganese, tend to concentrate attention on the role of specific impurity atoms in producing the effect; the results of MacDonald (1951 b), whose curves for copper from different sources are different in shape, may imply a similar mechanism. Gerritsen and Korringa (1951) have proposed a model to explain the results of Gerritsen and Linde; other more general theories have been described by MacDonald (1951 a), who relates the anomaly in zero field to anomalous magnetoresistance effects, and by Klemens (1951) in terms of the quantum theory of electrical resistance carried to a higher approximation.

The present paper describes measurements on 'pure' magnesium, molybdenum, cobalt and tungsten, and on aluminium both 'pure' and contaminated with small amounts of manganese. The apparatus and methods of measurement have been described in our previous paper.

§2. Results and Discussion—Magnesium

All specimens used came from a batch of 0·125 mm diameter wire drawn by Johnson Matthey from their rod (Lab. No. 1848). A spectrographic analysis of the rod revealed the presence of Mn, Fe, Si, Cu, Ag, Pb, Al, Ca and Na, the lines being either faintly visible or very faintly visible. Chemical analysis of the material have the following results: Fe 0·013%, Mn 0·0023%, Pb 0·0013%, Cu, Al, Ag not detected. The estimated purity of the material was greater than 99·98%.

Most of the experiments were done with the current and potential leads attached with screw contacts.*

Resistance Measurements in Zero Magnetic Field

A striking feature observable in the results is the great variation of the resistance–temperature curves from specimen to specimen cut from the same piece of wire. If the cause of the increase of resistance at low

* Of the curves taken with soft-soldered leads, we may mention specimen Mg 1 which showed an extremely large increase of resistance with decreasing temperature. The wire was annealed for three hours at 300° C *in vacuo*; T_{min} above 20° K; if R_0=resistance at 273° K, resistance below 20° K given approximately by $R/R_0=10^{-2}$ (10·5—24/T), i.e. 0·117 at 20° K, 0·165 at 4° K, 0·265 at 1·5° K; magnetoresistance positive at 4·2° K, negative at 1·5° K. Later the wire was accidentally broken and the recoverable part was tested again; with soft-soldered leads there was then found only a small increase with decreasing temperature, with the minimum at about 4° K. These results may be due either to the irreproducibility of contacts soft-soldered to magnesium, or to the presence of a portion of the wire of high resistance and anomalous properties somewhere in the part which was broken off.

temperatures is in fact the presence of certain types of impurity atoms, this may mean that the impurities were distributed unevenly along the length of the wire.

Table 1 gives the values of T_{min}, the temperature of the minimum, and R_{min}, the value of the resistance at that temperature, both for our specimens and those of others whose published data quotes these values. There does not seem to be a universal curve connecting these two parameters, at least for small values of R_{min}, though there is a general trend linking larger T_{min} with larger R_{min}. In terms of the 'contamination' theory of the origin of the minima, this may be taken to imply that no single impurity was predominant in all specimens. (This is in contrast to the results for gold, where the existence of a single T_{min}–R_{min} curve for specimens of widely differing origins may imply that one impurity—probably silver—was predominant in very many specimens.)

Table 1

$10^3 \times R_{min}/R_0$	T_{min} (° K)	Reference
(~100	Above 25	Present work : Mg 1)
53	Above 20	Meissner and Voigt (1930)
32	About 7	,, ,, ,, ,,
44	16	Rorschach and Herlin (1951)
16	5	Present work : Mg 2
15·7	0·7	,, ,, Mg 5
8	2	,, ,, Mg 4
7·5	5	,, ,, Mg 3

Of our specimens, Mg 2 was not annealed ; all others were annealed *in vacuo* for three hours at 300° C.

A feature of all curves for magnesium in zero field is that the rate of rise of resistance increases with decreasing temperature down to the lowest temperatures investigated (0·06° K).

Magnetoresistance Measurements

The results of many magnetoresistance experiments in transverse fields are contained in fig. 1, a reduced Kohler diagram, using a Debye Θ of 300° K. (The discrepancy with the curve given by Justi (1948) shown dotted, seems to be real, and not entirely due to the use of a different Debye Θ.) It is seen that over a considerable range of temperature—0·2° K to 4·2° K—all specimens give results which are normal to within experimental accuracy.

Susceptibility Measurements

By a small modification of the Sucksmith balance, we were able to measure the susceptibility of a rod of the magnesium from room temperature down to 1·2° K. The accuracy was about 5% at all temperatures. Little disturbance due to the de Haas–van Alphen effect was expected as

the applied field was inhomogeneous. The absolute value of susceptibility was $+0{\cdot}25\times10^{-6}$ per gram and within experimental error there was no change with temperature. Selwood (1943) quotes the same figure as the best value at room temperature.

Discussion

These results concerning the magnetoresistance and the susceptibility are of interest because the specimen was known to contain 0·06 atomic per cent of iron and 0·01 atomic per cent of manganese. The behaviour is in marked contrast to that of alloys of the noble metals containing

Fig. 1

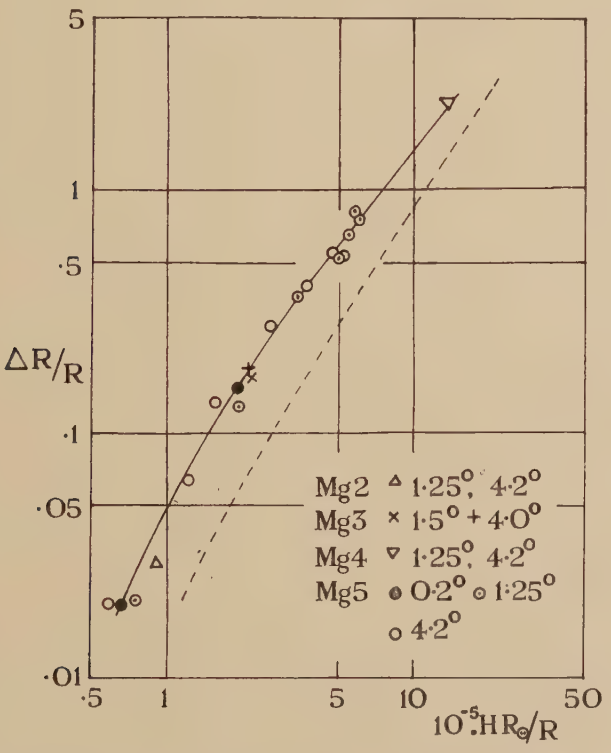

comparable concentrations of iron and manganese ; these are known to have abnormal magnetoresistance effects (Nakhimovich 1941, Gerritsen and Linde 1951) and to have paramagnetic susceptibilities which vary strongly with temperature (Nakhimovich 1941, and see Néel 1940 and Constant 1945 for further references). To explain the results for the contaminated noble metals it is postulated that even in solution the transitional elements still have their d-shells incompletely filled. But it is also known that when transition metals are dissolved in metals of valency greater than unity, the d-shells may be filled up, when the atoms lose their transitional structure ; this has been deduced from the limits of solubility (Raynor 1949). The resulting alloys should then be expected to have

much more normal magnetic properties. Our measurements may therefore be interpreted to mean that this filling of the positive holes in the d-shells occurs when iron and manganese are dissolved in magnesium.* Since however the resistance of our specimens in zero field exhibit pronounced minima, it seems that scattering of the conduction electrons by the unfilled d-shells of the impurity atoms—the mechanism dealt with by Gerritsen and Korringa—is not also responsible for the minimum effect in magnesium.

§3. Results and Discussion—Aluminium and Aluminium-Manganese

Measurements in Zero Magnetic Field

Some ' super-pure ' aluminium (99·995%) was drawn through steel dies to a diameter of 0·3 mm. The specimens were annealed at 300° C for two hours *in vacuo*. As the resistance was rather low our measurements were confined to the helium range. The residual resistance was found to be constant to 1 part in 10^3 throughout this temperature range ($R/R_0 = 2{\cdot}89 \times 10^{-3}$ for Al 1, $2{\cdot}57 \times 10^{-3}$ for Al 2). Of previous results for aluminium (see our previous paper for references), some have shown slight minima.

In order to test the statement made in the last section—that a multivalent element containing a small proportion of transition element as impurity may have a normal magnetoresistance—a carefully homogenized alloy of aluminium with 0·05% (i.e. 0·10 atomic per cent) of manganese was prepared. In zero field it was found to have a resistance which was constant to 1 part in 10^3 from 4·2° K to 1·3° K ($R/R_0 = 15{\cdot}5 \times 10^{-3}$ for Al 3, $15{\cdot}4 \times 10^{-3}$ for Al 4). Matthiessen's rule was obeyed—that is, the difference between the specific resistance of the alloy and the pure metal was the same at room temperature as at helium temperature.

Magnetoresistance Measurements

The magnetoresistive behaviour of the aluminium and of the alloy with manganese was found to be normal from 4·2° K down to 1·3° K; transverse fields up to 1 500 gauss were used. The results are represented in the reduced Kohler diagram, fig. 2, which uses a Debye Θ of 395° K. (Justi's curve, shown dotted, uses the same value.) Thus the alloy behaved as if the d-shells of the manganese were completely filled by electrons donated by the aluminium.

§4. The Origin of the Minimum of Resistance

We may assemble the following data : (*a*) the results of MacDonald and Templeton on the minimum shown by gold wires containing copper (and with them, the possibility mentioned above that silver in gold can also

* In connection with the work on silver-manganese alloys, it may be of interest to remark that the curves given by Schulze (1941), for liquid air temperatures and above, indicate that the addition of tin, in concentrations comparable with that of the manganese, can remove the maxima from the resistance–temperature curves. Here the tin seems to act as an electron donor to the manganese.

produce a minimum) ; (*b*) the present authors' observations on a gold wire with a minimum but with normal magnetoresistance ; (*c*) the above data on magnesium. These seem to show that, if the minimum is indeed an effect due to the presence of impurity atoms, it can be produced even by impurities which one has hitherto represented by models of a very simple kind. In dealing with the data on solutions of the transition metals in noble metals, quite complicated structures can plausibly be attributed to the impurity atoms, and these can be made to account for the experimental results. At present, however, it seems that comparable methods cannot be applied to such systems as, say, dilute solutions of copper in gold or of iron in magnesium.

Fig. 2

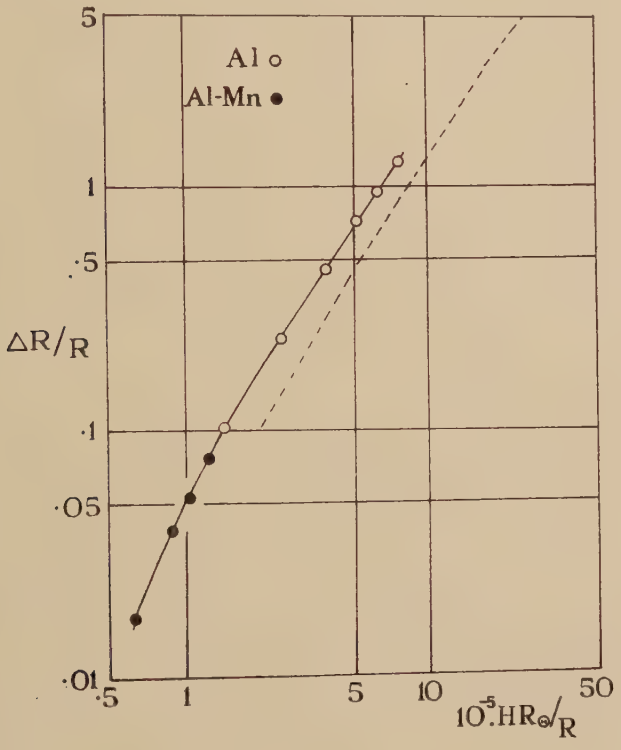

§5. Results and Discussion—Molybdenum

All specimens were obtained from the B.T.H. Co. Ltd., in the form of polycrystalline wires, some of them 0·10 mm in diameter, others 0·025 mm. The principal impurities were quoted as O 0·113%, Fe 0·008% and SiO_2 0·015%, together with spectrographic traces of Ni and Cr. The resistance of the best specimen was lower than any previously recorded except that of Justi and Foroud (1939) ; but as their specimen was a single crystal and ours a polycrystalline wire, the chemical impurity contents of the two specimens were probably about the same.

Leads were attached by silver soldering using a nichrome soldering bit.

Resistance Measurements

The results for several specimens are shown in fig. 3. Details of the specimens and of the measuring conditions are as follows : Specimen Mo 3 : diameter 0·025 mm, no heat treatment, measuring current 0·06 and 0·1 mA. Specimen Mo 4 : next to Mo 3 on the reel of wire ; with no heat treatment gave a curve close to that for Mo 3. Later annealed for two hours in a vacuum better than 10^{-5} mm Hg, most of the wire being at 800° C, with some ' hot spots ' at 1 200° C ; measuring current 0·2 mA for the lower branch of the curve. The fall of resistance was later realized to have been due to the presence of small amounts of a superconducting impurity ; the curve was taken again in the presence of a magnetic field of 30 gauss using 0·2 mA measuring current ; the upper branch was then obtained. The superconducting impurity will be dealt with later. Specimen Mo 2 : diameter 0·1 mm, no heat treatment, measuring current 0·3 mA with check points in the helium range using 3 mA. During part of the work in the helium range, measuring conditions were not good. Specimen Mo 1 : diameter 0·1 mm, no heat treatment, measuring current 0·3 mA. Specimen Mo 5 : diameter 0·1 mm, annealed at a uniform temperature of 1 500° C for two hours in a vacuum better than 10^{-5} mm Hg ; measuring current 0·3 mA for the lower branch—which went to zero resistance—the upper branch being taken partly in zero magnetic field using 3 mA measuring current, partly in fields up to 30 gauss using 0·2 mA measuring current.

A notable feature of the curves for the normal metal is the constancy of resistance at the lowest temperatures. This is thought not to be a spurious effect for the following reasons : The flattening was observed under conditions where, with other metals, the resistance was found still to rise with decreasing temperature. Further, the curves were reproduced within close limits using a range of measuring currents, and the flattening is therefore not thought to be an effect due to poor thermal contact between the salt and the wire. Lastly, whereas most of the points above 0·05° K were obtained by demagnetizing to the region of 0·05° K and allowing the specimen to warm up slowly, others were obtained by direct demagnetization from fields less than the maximum available ; both sets of points gave consistent results and showed that no appreciable persistent temperature inhomogeneities (which might have produced errors) were present in the salt.

A further feature is that over a considerable range of temperature the resistance varies exponentially with decreasing temperature. None of the curves given by Gerritsen and Linde exhibits either the flattening over the 2 : 1 temperature range or the exponential variation.

It may be noted that Meissner and Voigt (1930) found an increase of resistance at low temperatures, Steiner and Fünfer (1936) found none.

The Superconducting Component

The curves for Mo 4 and Mo 5 showed that a superconducting component was present. The superconductivity could be destroyed either by applying

Fig. 3

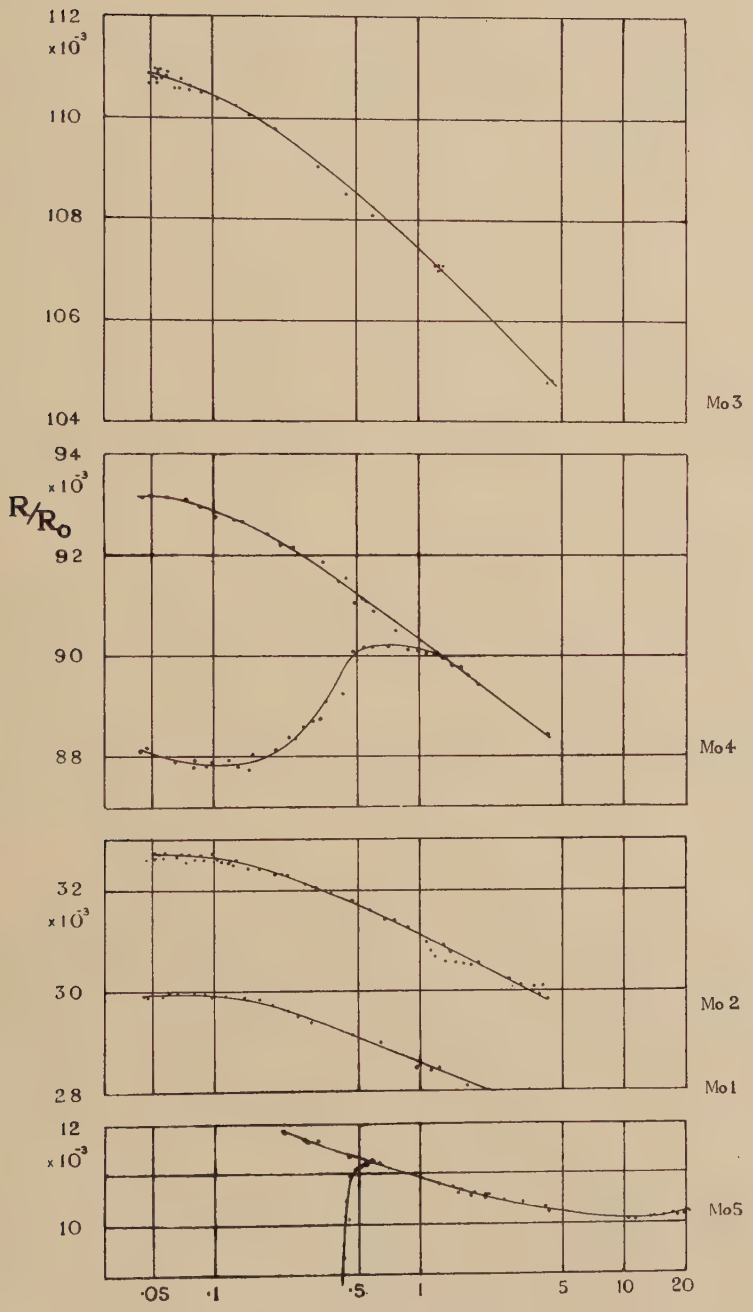
112
x10⁻³
110
108
106
104
Mo3
94
x10⁻³
R/R₀
92
90
88
Mo4
32
x10⁻³
30
28
Mo 2
Mo1
12
x10⁻³
10
Mo5
·05
·1
·5
1
5
10
20
Temperature (deg. absolute)

a transverse magnetic field or by passing a current of a few milliamps through the wire. At 0·3° K the values were 18 gauss to restore half resistance and 26 gauss to restore full resistance with 0·3 mA current; with no external field 3 mA restored full resistance. Comparison of these two effects suggested that the superconductor was in the form of fine filaments and this was in accord with the great breadth of the transition in zero field. Presumably the filaments were continuous in Mo 5 but not continuous in Mo 4.

The superconductor was only present in those wires which had been annealed. It has not been possible so far to identify the impurity, but X-ray examination of Mo 5 and a length of unannealed wire did confirm the presence of a second component in Mo 5. Since the position of molybdenum in the periodic table suggests that it might be a superconductor, it is relevant to enquire whether the annealing above 1 200° C could have produced another crystalline modification. The X-ray work of Edwards, Speiser and Johnston (1951) eliminates this possibility, however. It appears therefore that the superconductor must be a compound of some sort; for previous work on the superconductivity of molybdenum see Shoenberg (1940).

Magnetoresistance Experiments

Specimen Mo 3 was abnormal in its magnetoresistive behaviour; at 4·2° K the effect was small and positive, at 1·2° K the value of $\Delta R/R$ went through a maximum with increasing field, then fell to zero and became negative at high fields. All other specimens followed Kohler's rule in transverse fields, as may be seen from the reduced Kohler diagram, fig. 4, using $\Theta=450°$ K. The discrepancy with the curve given by Justi (1948) may be due to the use of a different value of Θ.

§6. Results for Cobalt and Tungsten

Cobalt

Cobalt wire 99·95% pure was drawn for us by New Metals and Chemicals Ltd., to a diameter of 0·13 mm. For an unannealed sample, which was very springy, the value of R/R_0 was 0·162 at 4·2° K, 0·160 at 1·20° K, remaining at that value down to 0·10° K. For a specimen annealed for three hours at 1 000° C *in vacuo*, the value was determined as 0·0302 from 4·2° K down to 1·36° K, and 0·0303 from 1·20° K down to 0·06° K. It may be noted that both of the specimens of Meissner and Voigt (1930) showed definite minima.

An X-ray examination of the untreated wire showed a hexagonal close-packed structure; the heat treated wire contained also a small amount of face-centred cubic structure, so that the absence of superconductivity for both these modifications has been shown down to 0·06° K.

The magnetoresistance effect was the same at 4·2° K as at 1·2° K, showing a marked saturation; but since in these experiments the wire was wound on a vertical cylinder with the field applied horizontally, the field

was partly transverse and partly longitudinal, and there is little quantitative value in the results.

Tungsten

For a single specimen of tungsten wire (supplied by the B.T.H. Co. Ltd., impurities SiO_2 and Al_2O_3 each 0·025% ; prepared by sintering) 0·025 mm diameter, the residual resistance was large ($R/R_0=0·10$) and independent of temperature from 4·2° K down to 0·10° K. Other recent work on the same metal has given similar results (van den Berg 1948).

The magnetoresistance effect was small but normal.

Fig. 4

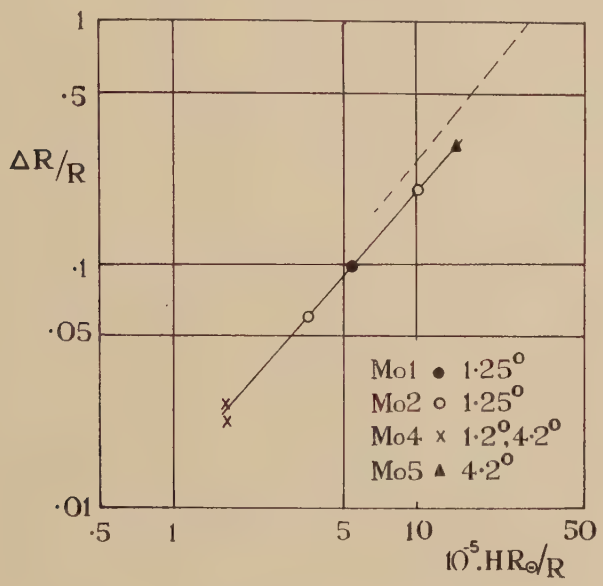

§ 7. Conclusions

In addition to the conclusions presented in § 4 it has also been found that several specimens of molybdenum present further examples of resistance-minima with no correlated magnetic anomalies, within experimental error. The resistance in zero field becomes constant again below an attainable low temperature, whereas the resistance of all the other metals studied continues to rise at the lowest temperatures.

Acknowledgments

The authors acknowledge their indebtedness to Dr. L. C. Jackson for help and advice, to the other members of the Low Temperature Group for assistance during experiments and to Dr. J. Friedel for discussions. The x-ray analyses were kindly carried out by the Research Department of the National Smelting Co., Avonmouth.

One of us (J.G.T.) was in receipt of a grant from the D.S.I.R.

References

Constant, F. W., 1945, *Rev. Mod. Phys.*, **17,** 81.

Edwards, J. W., Speiser, R., and Johnston, H. L., 1951, *J. Appl. Phys.*, **22,** 424.

Friedberg, S. A., Estermann, I., and Goldman, J. E., 1952, *Phys. Rev.* [2], **85,** 375.

Gerritsen, A. N., 1951, *Proc. Internat. Conf. on Low Temperature Physics* (ed. R. Bowers, Oxford), p. 47.

Gerritsen, A. N., and Korringa, J., 1951, *Phys. Rev.* [2], **84,** 604.

Gerritsen, A. N., and Linde, J. O., 1951, *Physica*, **17,** 573, 584.

Justi, E., 1948, *Leitfähigkeit u. Leitungsmechanismus fester Stoffe* (Göttingen : Vandenhoeck & Ruprecht), p. 64.

Justi, E., and Foroud, A., 1939, *Phys. Zeits.*, **40,** 501.

Klemens, P. G., 1951, *Proc. Internat. Conf. on Low Temperature Physics* (ed. R. Bowers, Oxford), p. 40.

MacDonald, D. K. C., 1951 a, *Phil. Mag.* [7], **42,** 756 ; 1951 b, *Proc. Internat. Conf. on Low Temperature Physics* (ed. R. Bowers, Oxford), p. 58.

MacDonald, D. K. C., and Templeton, I. M., 1951, *Phil. Mag.* [7], **42,** 432.

Meissner, W., and Voigt, B., 1930, *Ann. Phys., Lpz.*, **7,** 761.

Mendoza, E., and Thomas, J. G., 1951, *Phil Mag.* [7], **42,** 291.

Nakhimovich, N. M., 1941, *J. Phys., U.S.S.R.*, **5,** 141.

Néel, L., 1940, *Le Magnétisme* (Paris : Inst. Internat. de Coopération Intellectuelle), II, 65.

Raynor, G. V., 1949, *Progress in Metal Physics* (ed. B. Chalmers, London), I, p. 49.

Rorschach, H. E., and Herlin, M. A., 1951, *Phys. Rev.* [2], **81,** 467.

Schulze, A., 1941, *Phys. Zeits.*, **42,** 6, 385.

Selwood, P. W., 1943, *Magnetochemistry* (New York : Interscience Publishers), p. 191.

Serin, B., 1951, private communication.

Shoenberg, D., 1940, *Proc. Camb. Phil. Soc.*, **36,** 84.

Steiner, K., and Fünfer, E., 1936, *Congrès Int. du Froid, La Haye*, **1,** 388.

van den Berg, G. J., 1948, *Physica*, **14,** 111.

LXXXVII. CORRESPONDENCE

Ice Crystals of Spiral Form Grown from the Vapour

By B. J. Mason
Department of Meteorology, Imperial College, London
and
P. G. Owston
I.C.I. Research Fellow, Department of Chemistry, University College, London*

[Received May 13, 1952]

This note describes some ice crystals of unusual spiral form found growing on the cooling pipes of a cold store containing whale-meat. They had been growing for about three and a half years at a constant air temperature of $-10 \pm 0{\cdot}1^\circ$ C.

The crystals have much in common with those described as ' crevasse hoar ' by Seligman (1936), and occur in remarkably light skeletal masses made up of many incomplete hexagonal prisms with ' hopper ' development of both prism faces (rectangular) and basal faces (hexagonal) as shown in figs. 1 and 2 (Plate LX). These seem to have been formed by the addition of rod-like crystals of thickness $\frac{1}{2}$ to 1 mm to the edges of a small central hexagonal prism.

None of the hexagonal basal faces, however, was complete, but showed the spiral formation called ' scrolls ' by Seligman, the outer turns of which exceeded two inches in diameter for the largest crystals. A number of single spirals are shown in fig. 2, and a particularly beautiful and symmetrical double scroll in fig. 3 (Plate LX).

The directions of the crystal axes in different crystals varied and bore no obvious relation to thermal gradients or air currents. X-ray examination showed the rod-like crystals to be mono-crystalline and elongated parallel to one of the crystallographic a axes. The hopper faces are therefore $(10\bar{1}0)$ and (0001).

No crystal was observed with both basal faces developed. Crystals of various spatial orientations were detached and tested for piezo-electric properties by the Giebe–Scheibe method; no indication of these properties was found either before or after light crushing of the crystals to break up any possible twins. Pyro-electric properties were also not found though the apparatus used could detect charges only one-twentieth as strong as those developed by the very weakly polar *s*-triphenyl benzene. Development at one end only of the c axis is therefore not proof that ice possesses a polar structure.

---

* Communicated by the Authors.

Though the crystals are of spiral form and sometimes exhibit pairs of spirals of opposite hand (figs. 2 and 3), this is not an example of crystal growth by spiral dislocations, for the crystals are made up of successive two-dimensional spiral layers, not of one continuous three-dimensional spiral. A possible explanation of the mode of formation is that at an early stage in growth some obstruction—perhaps the support on which it grew—prevented the crystal from completing a hexagonal edge and so initiated the spiralling ; this would be consistent with the occasional occurrence of symmetrical double spirals.

One of us (B. J. M.) wishes to thank the Superintendent of the Low Temperature Research Station, Cambridge, for permission to work in the cold chambers and both authors are indebted to the staffs of their departments for photographic and other assistance.

Reference

Seligman, G., 1936, *Snow Structure and Ski Fields* (London : Macmillan), p. 73.

The Extra Electrical Resistance due to Cold Work and Neutron Irradiation of Platinum

By R. A. Dugdale
Atomic Energy Research Establishment Harwell, Didcot, Berks.*

[Received June 5, 1952]

In a recent paper, Seitz (1952) has put forward the hypothesis that part of the extra resistance brought about by the cold working of metals is due to the creation of vacant lattice sites by moving dislocations. In this connection it seems worth while to report the results of some recent experiments on the annealing of the extra resistance produced in platinum wire by cold work and by neutron bombardment.

Neutron bombardment in a pile may be expected to form localized groups of vacant lattice sites and interstitial atoms, since, in general, a fast neutron on collision with one of the atoms of the lattice will give it sufficient kinetic energy to displace several other nearby atoms (Seitz 1949). On subsequent heating one may expect the vacant lattice sites or the interstitial atoms, or both, to acquire some mobility, leading to one or more of the following processes :—

(1) ' Recombination ' of interstitial atoms and vacancies.

(2) A randomizing of their spatial distribution.

(3) Condensation of vacancies.

(4) Disappearance of vacancies and interstitials at grain boundaries.

---

* Communicated by the Author.

These processes would lead to a reduction in the excess resistance which had been produced by the neutron bombardment. If a part of the excess resistance caused by cold work is due to lattice vacancies, one might expect some similarity in its behaviour on annealing.

The decay of the extra resistance of two irradiated and one cold worked resistor of platinum (each of about 1 Ω) has been followed part of the way when they were heated first to 70° C for 640 hours, and subsequently to 90° C for 336 hours. The resistance was measured at intervals to an accuracy of 1 part in 10^6, after cooling to the triple point of water. The two irradiated resistors had increased in resistance by 0·2% during a three months irradiation at 50° C in the Harwell pile B.E.P.O. The extra resistance of the cold worked resistor amounted initially to about 1·5%. During the two annealing periods about 13% of the extra resistance of the cold worked resistor and one irradiated resistor, and about 17% of the extra resistance of the other irradiated resistor disappeared.

All the resistance decay curves could be fitted to an empirical formula of the type

$$r = A - B \log_{10} (t+\gamma), \quad . \quad . \quad . \quad . \quad . \quad . \quad . \quad . \quad (1)$$

where r is the extra resistance, and A, B, and γ are constants at constant temperature. The fit was good everywhere except in the early stages of the annealing at 70° C, where a small deviation was noticeable. It should be emphasized that this empirical relation between r and t cannot hold indefinitely, and no physical significance can be attached to the constants.

Although it is not known which of the four processes postulated above is the important one at these temperatures, an activation energy can be estimated if we assume

$$\frac{dr}{dt} = f(r)\, e^{-U/kT}. \quad . \quad . \quad . \quad . \quad . \quad . \quad . \quad . \quad (2)$$

The gradient dr/dt can be determined for any value of r from the empirical formula (1). If this is done at the point where the temperature was changed, U can be determined from the equation

$$U = k \log \left[\left(\frac{dr}{dt} \right)_{T_2} \Big/ \left(\frac{dr}{dt} \right)_{T_1} \right] \Big/ \left[\frac{1}{T_1} - \frac{1}{T_2} \right]. \quad . \quad . \quad . \quad (3)$$

This has been done for all three resistors, and the following table shows the values of U obtained, together with the constants A, B, and γ.

Resistor	A ($\mu\Omega$)		B ($\mu\Omega$/hr.)		γ (hrs.)		U (ev)
	70° C	90° C	70° C	90° C	70° C	90° C	
1. Irradiated	2748	3592	182	570	67	250	1·19
2. Irradiated	2582	2913	146	332	56	178	1·19
3. Cold worked	15926	15317	928	1050	36	85	1·20

The agreement in the value of U for the three resistors is noteworthy. This, together with the general similarity in shape of the annealing curves, suggests strongly that the same processes are responsible for the decrease of resistance in the two cases. This supports Seitz's speculation that the increased resistance due to cold work is at least in part due to the creation of lattice vacancies (and perhaps interstitial atoms).

The author's thanks are due to Professor N. F. Mott for drawing his attention to the paper by Seitz, and to Sir John Cockcroft, Director of the A.E.R.E., for permission to publish this note.

References

Seitz, F., 1949, *Crystal Growth* : *A General Discussion of the Faraday Society*, p. 271 ; 1952, *Advances in Physics*, **1**, 43.

LXXXVIII. *Notices of New Books and Periodicals received*

Cloud Chamber Photographs of the Cosmic Radiation. By G. D. Rochester and J. G. Wilson. [Pp. 128.] (London : Pergamon Press Ltd.) £3 10*s*. 0*d*.

An atlas of cloud chamber photographs of various phenomena associated with Cosmic Rays is very welcome. The photographs are collected from laboratories throughout the world, and include a large number that have not been published hitherto. With each photograph there are captions which explain most adequately the main features of the event, and also stress any doubt there may be to the correctness of the interpretation put forward. The first section is devoted to technical features of operation. In the remaining sections the photographs show, in an extremely vivid manner, a wide variety of cosmic ray phenomena ranging from electron cascades to the recently discovered V particles. Such a book is very dependent upon the quality of production ; in this case it is excellent.

The book besides being of great assistance to those who work with cloud chambers should in addition have a very wide appeal, since it depicts many fundamental phenomena clearly. P. H. F.

Low Temperature Physics. By F. E. Simon, N. Kurti, J. F. Allen and K. Mendelssohn. [Pp. 132.] (London: Pergamon Press Ltd.) Price 21*s*.

The four lectures which are reported in this volume are by Professor F. E. Simon (A General Survey), Dr. N. Kurti (The Temperature Range below 1° K), Professor J. F. Allen (Liquid Helium) and Dr. K. Mendelssohn (Superconductivity). The course was given at the Royal Institution in March 1950, but the version for the press contains references to work done as recently as a few months ago.

This book provides an excellent account of the present position in a rapidly changing subject, reviewing its topics against the background of physics as a whole and putting the successes and the difficulties into perspective. It should interest not only specialists in low temperatures, but also workers in the many other branches of physics to which low temperature techniques are being increasingly applied. E. M.

Fig. 4

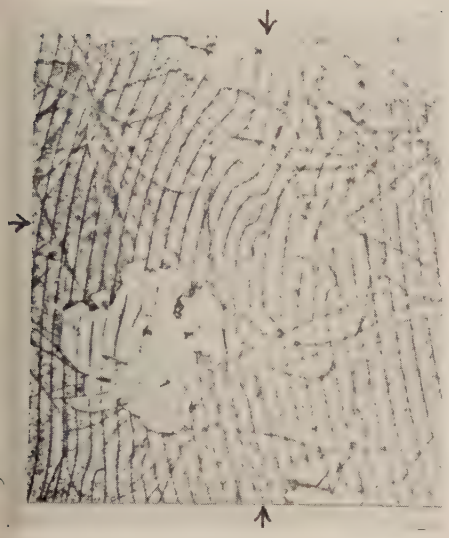

The area of interest lies around the two dislocations near the point of intersection of the arrows. ×500

Fig. 6

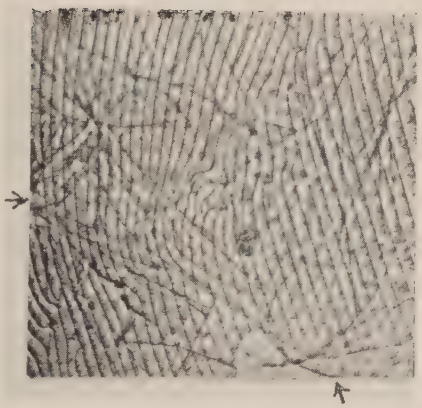

The lower arrow marks the layer edge under discussion, while the horizontal arrow marks the level of the dislocation. ×500

Fig. 8

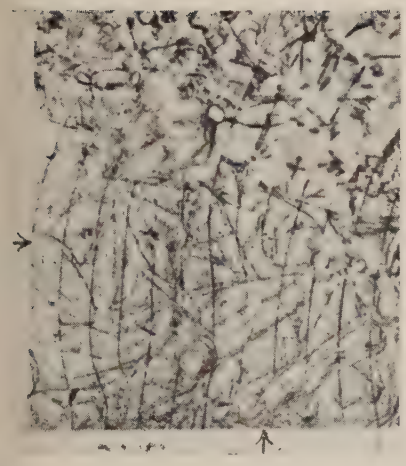

The hook-shaped layer edge lies near the point of intersection of the arrows. ×625

Fig. 9

The right-hand pair of horizontal and vertical arrows mark the hook-shaped layer edge. The left-hand pair of arrows mark the situation shown diagrammatically in fig. 10. ×625

Fig. 11

If the three layer edges which are arrowed are traced upwards it will be found that all three finish with a hook-shape.
×625

Fig. 12

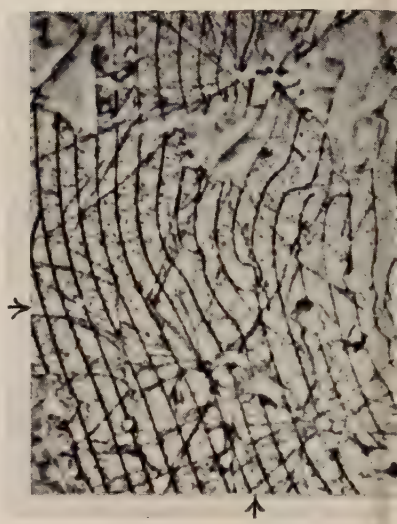

The area around the point of intersec
of the arrows is that under discuss
×

Fig. 14

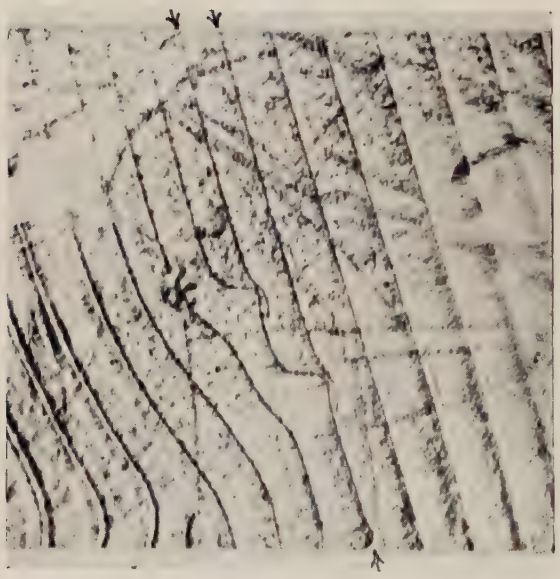

The three layers discussed are marked by arrows. If the two upper layer edges are traced down it will be seen that they end on dislocations.
×1500

Fig. 16

The two twin dislocation loops lie arou
points of intersection of the two ve
arrows with the horizontal arrow.

Fig. 17

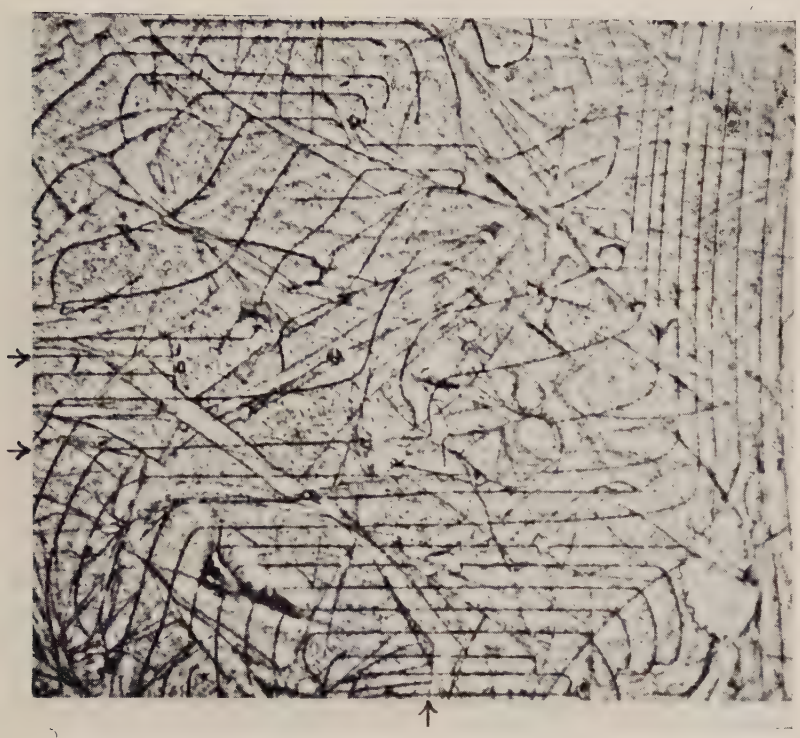

The two layers with short straight edges close to the dislocations lie near the point of intersection of the vertical arrow with the lower horizontal arrow. The higher horizontal arrow marks a layer edge at the termination of which the dislocation has moved upwards. ×625

Fig. 18

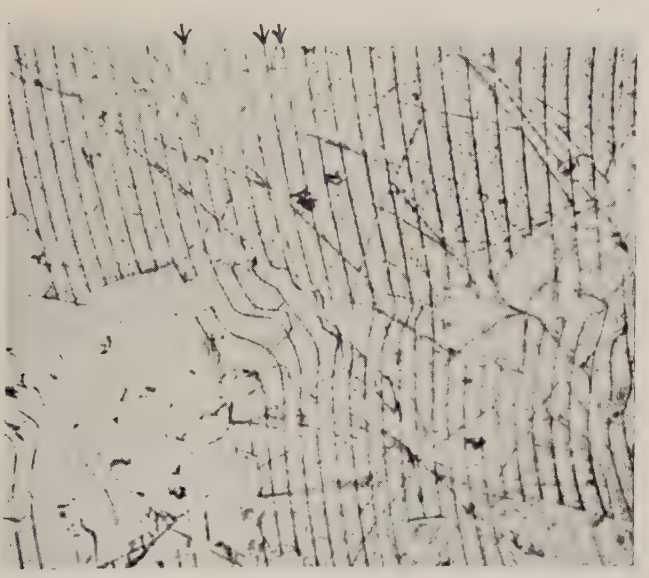

The three dislocations which have moved lie at the termination of the three layer edges which are arrowed. ×625

Fig. 19

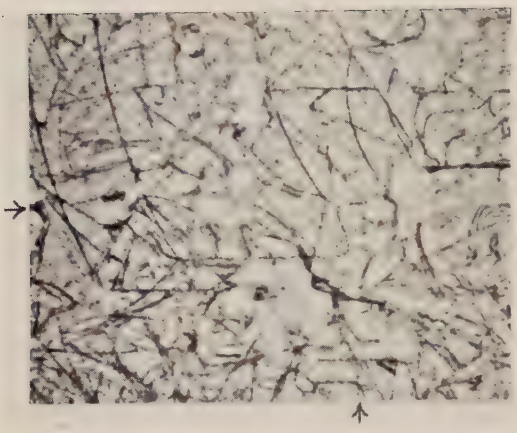

The sections of the layers discussed lie near the point of intersection of the arrows. ×625

Fig. 24

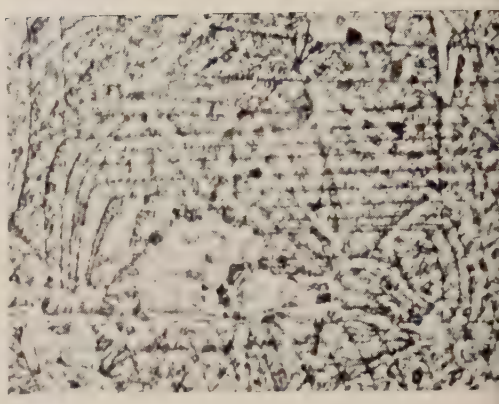

A typical small limited slip-zone.

Fig. 23

The vertical arrows denote the line along which the dislocation has moved, and along which linear kinking can be seen. The horizontal arrows denote the limits of the area in which location has moved. To help in the identification of the area it is shown isolated on the r

Fig. 29

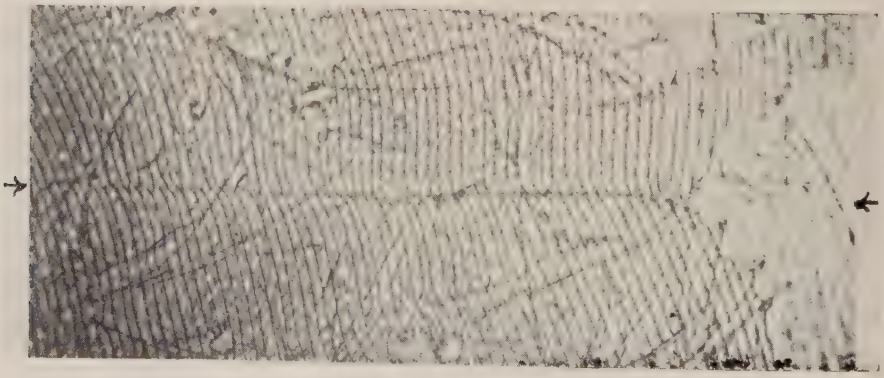

A limited slip-zone, formed just before, or after, growth ceased, in which it is possible to trace the kinking of the outer layers. ×625

Fig. 27

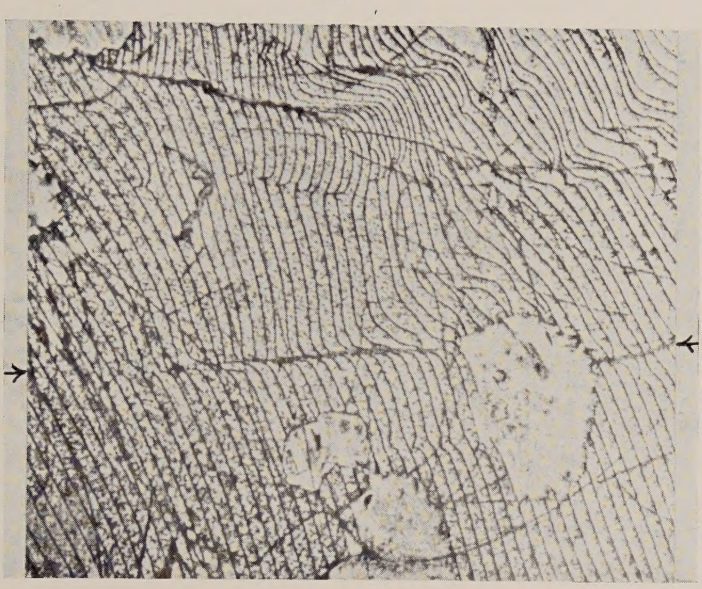

×625

Fig. 28

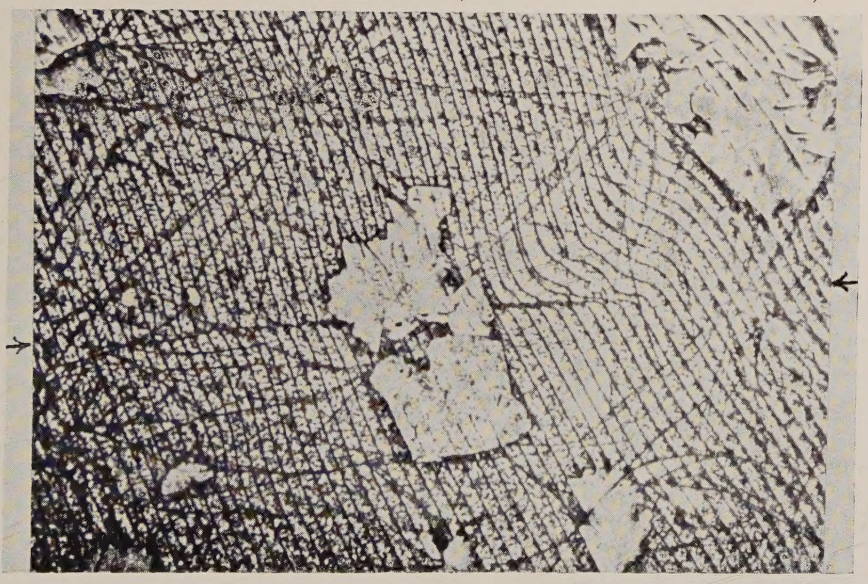

Limited slip-zones, formed just before, or after, growth ceased in which it is possible to trace the kinking of the outer layers. ×625

Fig. 30

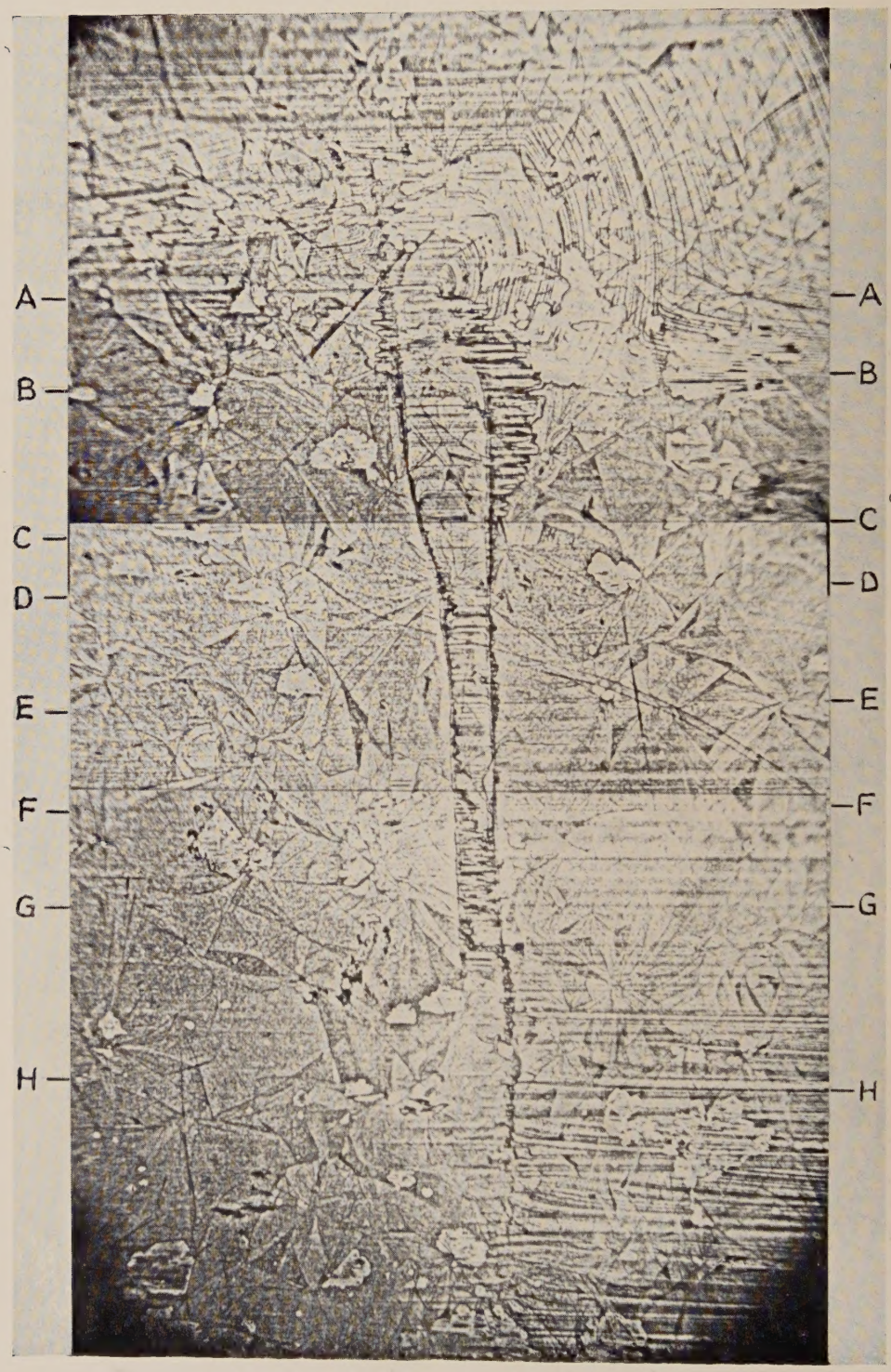

A small-scale mosaic of a complex 'buckled' strip which has probably been produced by the simultaneous action of a number of different dislocation sources. ×250

Fig. 3

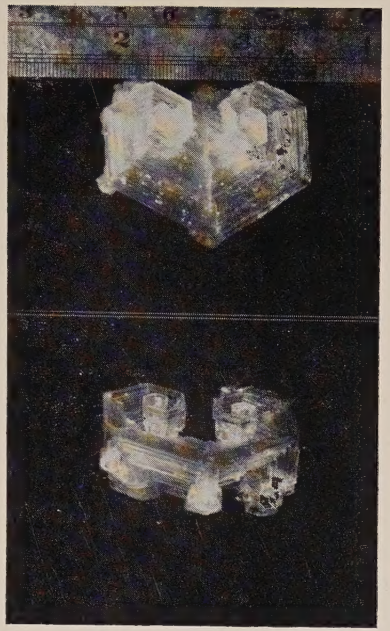

Fig. 2

Fig. 1. A mass of incomplete hexagonal prisms showing 'hopper' development of both basal and prism faces.

Fig. 2. Crystals growing *in situ* on the cooling pipes of the cold chamber. (Outer turns of largest spirals are more than two inches across.)

Fig. 3. Two views of a symmetrical double scroll.